SLAC-377
UCRL-PROP-105579
UC-414
(E)

PEGASYS/Mark II: A Program of Internal Target Physics Using the Mark II Detector at the PEP Storage Ring

The PEGASYS/Mark II Collaboration

November 1990

This work was performed under the auspices of the U.S. Department of Energy by S.L.A.C. under contract number DE-AC03-76SF00515 and by Lawrence Livermore National Laboratory under contract number W-7405-ENG-48. Work also supported by N.S.F grant PHY90-14406.

Printed in the United States of America. Available from the National Technical Information Service, U.S. Department of Commerce, 5285 Port Royal Road, Springfield, Virginia 22161. Price: Printed Copy A07, Microfiche A01

PEGASYS/ Mark II

PEP Gas TArget-Spectrometer **SYS**tem

Collaborating Institutions

American University
University Blaise Pascal (IN2P3)
Georgetown University
Iowa State University
Institute of Theoretical and Experimental Physics, (Moscow)
Lawrence Berkeley Laboratory
Lawrence Livermore National Laboratory
University of Maryland
University of Massachusetts
University of Milan
Ohio University
University of Pennsylvania
Rensselaer Polytechnic Institute
C.E.N. Saclay(CEA/IRF)
Stanford Linear Accelerator Center
Stanford University
Tel Aviv University
University of Virginia
University of Washington
Yerevan Physical Institute

TABLE OF CONTENTS

Section I. ABSTRACT

This document is a proposal to SLAC on behalf of the PEGASYS Collaboration for a program of internal target physics at PEP utilizing the Mark II detector. Having completed its tour of duty at SLC in November, 1990, we propose that the Mark II detector be returned to the PEP storage ring, where it will be used in conjunction with a long gas target for studies of QCD with nucleon and nuclear targets, as well as tests of QED in lepton pair production, and a search for new neutral bosons. We expect that the detector in its new configuration could be commissioned by late 1991 and begin taking data by 1992. This document presents the physics to be accomplished with the Mark II, and describes the minimal changes to the detector that we will need to make it function for internal target experiments. We also show a possible timeline for the project, and indicate the makeup of the collaboration that will carry out the work.

Section II. INTRODUCTION

Project Overview

Original Proposal

The PEGASYS Collaboration, which formed in November, 1986, proposed an experimental program to study multiparticle final states in electron deep inelastic scattering from nucleon and nuclear targets, using electrons of up to 15 GeV in the PEP storage ring. The Collaboration developed a detailed design for a facility consisting of a large-aperture forward spectrometer, a cryogenic gas jet target, and some particle detection capability at backward angles.

The capital construction costs of this facility were estimated to be approximately \$15M, and would have been borne by the DOE Office of Nuclear Physics, SLAC, and the Institute for Theoretical and Experimental Physics in Moscow who would have provided the 600-ton magnet. Construction was estimated to take approximately 3 years after funding.

This project was awarded conceptual approval by both the Nuclear Physics Program Advisory Committee (NPAC), and the High Energy Program Advisory Committee (EPAC) at SLAC in 1989. The project furthermore underwent a technical/budgetary review in January, 1990 which established that the design of each System was sound, and that the budget was correct to within 15%.

Mark II

As the project evolved a factor arose which introduced uncertainty into the future configuration of PEP on the time scale coinciding with the planned commissioning of the PEGASYS facility. This was SLAC's initiative to plan and build a B-Factory in the PEP tunnel. Faced with an uncertain situation for PEP in the latter half of the '90s, the DOE Office of Nuclear Physics suspended review of the PEGASYS proposal in February, 1990.

At the behest of the SLAC Directorate, the PEGASYS collaboration undertook to consider the opportunity posed by the Mark II roll-out from SLC scheduled for December, 1990. The Mark II is a sophisticated detector and a unique SLAC resource that has contributed to major developments in high energy physics at three machines over its long career: SPEAR, PEP and SLC. While the geometry and instrumentation of the Mark II depart sharply from that of the original PEGASYS design, its virtues (wide-angle tracking, calorimetry, hermeticity) were too attractive to ignore. Furthermore, its immediate availability and present working condition make it possible to get a program of internal target experiments into operation quickly.

The Collaboration examined the detector's capability and its potential for fixed target kinematics during the summer of 1990 and concluded that the opportunities for nuclear and high energy physics at PEP with the Mark II were unique and exciting. The Collaboration was polled, and the decision was made to proceed with a proposal to SLAC.

In the interest of getting started as quickly as possible with a minimum of effort and cost, we have decided to take a staged approach. In Stage I we would use the detector essentially 'as is' making only the minimum modifications necessary to implement the internal gas target and construct a usable trigger. Our intention is to use all of the detector elements except the inner vertex chamber and the silicon vertex detector. The sequence of installation is presently under discussion, but for the beginning of Stage I we may concentrate our efforts on a subset of the detector elements that would allow us to get on the air quickly and learn about the environment at PEP while making a start on some portion of the physics program at minimal cost. The expected performance of the existing Mark II equipment, plus our minimal changes for use in fixed target experiments, are described in Section IV.

In Stage II, one or two years after the initial running begins, we plan to make several modest upgrades that should significantly enhance the performance and make the system better matched to the requirements of fixed target experiments. These options are outlined in Section IV.G.

Physics Overview

The main body of this proposal is a series of mini-proposals, given in Chapter III, which describe the physics goals and expected results of particular physics measurements. These discussions all assume that the complete Mark II (minus the vertex detectors) is implemented and that target densities compatible with 12 hour beam lifetime are run for 90 days (corresponding to a luminosity of 3.3×10^{32} nucleon/cm^2/sec per beam for deuterium, or an integrated luminosity of 2.6×10^{39} nucleon/cm^2). Many sections of Chapter III build on discussions given in our Draft Proposal of December 1988 (referred to below as the Blue Book), and the reader may wish to refer to that document for more discussion of the underlying physics ideas, kinematics and definitions, and data from previous experiments. In this proposal we concentrate on displaying the capabilities of the Mark II to make the proposed measurements.

The physics of PEGASYS/Mark II overlaps substantially with that of the original PEGASYS proposal, which was built upon a design with a transverse dipole forward spectrometer. With the Mark II detector 'as is', however, there are two significant differences in capability. First, the solid angle coverage with

tracking and calorimetry is much better than in the original PEGASYS design. Second, the coverage at forward angles for hadrons is much deteriorated (due to the hole in polar angle not covered by the CDC of $\theta = 150$ mr); even for tracks which cross the CDC the resolution is poor at very forward angles. For all except high Q^2 events, one must rely on calorimetry alone (the ECC and SAM) for the electron scattering kinematical variables x, Q^2, ν.

In some cases the measurements proposed in the Blue Book are not much affected by using the Mark II, while in others they are significantly enhanced, primarily by the larger coverage at wide angles. A few measurements are seriously compromised, primarily due to the loss of particles that go in the forward direction, and they are either dropped from consideration or the expectations are reduced in scope. Significant new additions to the proposed physics program for PEGASYS are made possible by the large coverage at wide angles. In sections III.K and III.L we describe a new and exciting possibility for measurements of charm production from the proton and nuclear targets. PEGASYS/Mark II would offer a powerful facility for studying the production mechanisms and decay schemes of charmed baryons produced from the proton. There is also a significant rate for detection of J/ψ particles that can be used to study the production mechanisms from the proton and look for effects due to the nuclear medium using heavier targets. In Section III.M we outline the enhanced capabilities the Mark II offers for studying exclusive strange particle production. Very little is known from previous measurements about such topics as the intrinsic strange quark content of the nucleon, the production mechanisms of strange particles in photon reactions, and the kaon form factor. PEGASYS/Mark II could obtain high quality data bearing on these subjects.

PEGASYS/Mark II offers a unique opportunity to explore the final states in high-energy electron scattering from the proton and from both light and heavy nuclei.

Section III. PHYSICS EXPERIMENTS

This section presents a series of mini-proposals for particular physics experiments. They are presented here in the same order as they were originally presented in our Draft Proposal of December 1988 and not in order of relative priority or feasibility. This list of potential experiments can be roughly categorized into two groups according to technical difficulty. The first group are those that can be accomplished fairly easily with the Mark II in Stage I (the full detector is implemented but without any upgrades). These include measurements of Quark Hadronization, Cumulative Production and Tagged Structure Functions, Higher Twist, the Nuclear Response to Quark Knockout, Exclusive Kaon Production, Search for New Particles Coupling to Leptons, and Bose-Einstein Correlations. The data for all these experiments could be taken without straining the capabilities of the detector or without danger from large backgrounds. For the most part they take advantage of the large acceptance at wide angles and they do not depend critically on resolution in any kinematic variables to see the signal. Many of these experiments could gather data simultaneously in a given run. All of them would produce data that would be dramatically better than any previous experiments and many would produce data that is qualitatively new.

Experiments in the second category are those that are more technically demanding. These include measurements of Nuclear Transparency, Inclusive and Exclusive Virtual Compton Scattering, Precision Internal Bremsstrahlung, J/ψ Production, and Open Charm Production. For those experiments that depend on detecting hard photons, it is not clear now how well the detector will be able to reject the backgrounds from competing electromagnetic processes. In some cases it is not clear whether a clean trigger can be formed. In other cases isolating the signal will depend more critically on the resolutions and on rejecting backgrounds by using the hermeticity of the detector to look for extra particles. Such strategies could work. However, before we can have high confidence in them there will need to be more Monte Carlo studies, and the techniques may have to be refined as we begin to understand what the background conditions are like in the real data. The physics payoff for this effort could be quite high. Measurements of virtual Compton scattering and the production of charmed baryons would be very exciting if further studies confirm the technical feasibility of these experiments.

Beyond Stage I it is clear that many of the proposed measurements would be significantly enhanced if the detector were modified to make better measurements of particles in the forward direction, particularly if scattered electrons could be identified and their kinematics determined with more precision in the area covered by the SAM. While the success of the measurements proposed in the following

sections do not depend on any upgrade, in many cases where it is appropriate we note where such an upgrade would improve or extend the physics yield.

As mentioned above, the physics topics discussed in this document in many cases build upon more detailed pedagogical discussion in the PEGASYS Draft Proposal of 1988 and the Addenda of 1989. These documents are available upon request.

III.A. Quark Hadronization in Deep Inelastic Scattering

One of the major objectives of PEGASYS/Mark II is to use nuclear targets to investigate the complex and poorly-understood process by which a quark ejected from its parent nucleon by deep-inelastic scattering materializes into observable hadrons. Specifically, we will investigate the space-time development of this process by comparing the hadron spectra from heavier targets, such as neon, argon, and xenon, with that from deuterium. The nuclear attenuation of the hadrons will be compared with models of the hadronization process to study the hadronic formation length and the degree to which the pre-hadronic system interacts with the nuclear medium.

A great deal of interest in this problem was stimulated by the pioneering experiment of Osborne *et al.*(Osb78), performed at SLAC with a 20-GeV electron beam. Their results, shown in Fig. 1, show significant attenuation of the hadrons that increases with target mass. In contrast, experiments performed by EMC (Wom86) with muon beams at much higher energies (100-280 GeV) show very little evidence for nuclear attenuation, as shown in Fig. 2. Taken together, these two experiments suggest a picture in which the partonic system generated by deep inelastic scattering initially interacts rather weakly with the nuclear medium; significant nuclear attenuation occurs only after the hadrons are formed. The pronounced difference between the results at low and high energies is ascribed to a dependence of the formation length on ν that is most probably linear due to a time dilation effect. In the range of ν accessed by the EMC experiments, hadronization of the leading particles takes place well outside the nucleus, whereas at the lower energies of the SLAC experiment the formation length is comparable to the nuclear size. Thus experiments at the values of ν available in the proposed experiment at PEP are essential in determining the properties of the formation length.

The goal of PEGASYS/Mark II is therefore to study the hadronization process in the energy regime in which nuclear absorption is significant. We will characterize the absorption as a function of Q^2 and ν, target size, and properties of the produced hadrons such as $z = E_h/\nu$, transverse momentum p_T, and the hadronic species. The earlier SLAC experiment suffered from very coarse binning in the kinematic variables and does not provide very strong constraints on the various proposed models for hadronization. A summary of several of these models and the types of measurements required to test them is contained in the December, 1988, PEGASYS Draft Proposal. New results in the high-energy range will soon be available from the Fermilab Muon Tevatron Experiment (E-665). Our results, together with those from EMC and E-665, will provide a greatly improved basis for understanding the phenomenon of hadronization.

The measurements required for studying hadronization are well suited to the initial phase of PEGASYS/Mark II. The detector components that will be used in these measurements are the drift chamber (DC) and the electromagnetic calorimeters, particularly the end-cap calorimeters (ECC). The range of Q^2 accessible is approximately 3 $(\mathrm{GeV/c})^2$ and above. Lower values of Q^2 would require the small angle monitors (SAM); however, the resolution of the SAM's is too poor to achieve adequate resolution in ν and z. Measurements in the range 1 to 3 $(\mathrm{GeV/c})^2$ would be useful, but must await an upgrade in the small-angle performance of the detector. The useful range of ν available with the present configuration is approximately 5 to 9 GeV, limited on the low end by the resolution in ν and on the high end by electron-pion discrimination.

We have estimated the performance of the detector for making measurements of nuclear absorption by calculating samples of events on a deuterium target as a function of Q^2 and ν with the Lund model, and then propagating the leading hadrons (i.e., those with z >0.5) through a simple model of the Mark II detector. An incident energy of 14.5 GeV was assumed. Passage through at least 4 superlayers was required for the drift chamber. The results were averaged over a target length extending $\pm$120 cm from the center of the detector. It was then assumed that the events take place in a typical medium-weight nucleus (A=64), and that the nuclear transmission is 0.68 (i.e., that 68% of the hadrons survive passage through the nucleus). This value is consistent with the results of the earlier SLAC experiment (Osb78). Seven particle species were studied: $\pi^+, \pi^-, \pi^0, K^+, K^-, K^\circ_S$, and ρ°. The neutral particles were reconstructed from their decay products, either two gammas or a π^+/π^- pair. In the actual experiment, the charged kaons will not be separated from the pions. The event rates were normalized to the assumed running conditions, which were a 90-day run with both e^+ and e^- beams present, at a luminosity corresponding to a 12-hour beam lifetime.

A sample of typical results from this performance study is shown in Figs. 3 and 4. In Fig. 3, the statistical accuracy expected in measuring the nuclear transmission is shown as a function of z. The bin size in z is 0.1; bins in Q^2 and ν are 2 $(\mathrm{GeV/c})^2$ and 1 GeV, centered at 3.5 $(\mathrm{GeV/c})^2$ and 7 GeV, respectively. Useful results should be obtained for π^+ (actually, positively charged hadrons), π^0, and ρ°, while K^0_S is marginal. The results for π° are particularly promising, since the statistical accuracy is very good and complete particle identification is possible.

The distribution of resolution in z for the same four particle types is shown in Fig. 4. For each species, all particles with z >0.5 were binned. The sample was taken for unit bins in Q^2 and ν centered at 4 $(\mathrm{GeV/c})^2$ and 7 GeV, respectively. For each Lund-model event, the resolution $\sigma(z)/z$ was calculated using the resolutions

for the appropriate components in the simple detector model. The distribution of these values is what is plotted in Fig. 4. In all cases the resolution is less than 15%, which is adequate for the proposed studies.

The triggering requirements for the hadronization measurements are fairly simple. It should suffice to trigger on events that deposit more than a few GeV in the end cap calorimeters. Determination of the vertex position off line should also be straightforward, since the average charged-hadron multiplicity is typically 3 to 4, and there is a high probability of finding one or more charged tracks that penetrate the entire drift chamber. However, this has not yet been modeled.

The above discussion has concentrated on measurements of the leading hadrons. However, a complete understanding of the hadronization process in a nucleus, including possible effects of the nuclear environment on the hadronization mechanism, requires observation of the entire hadron spectrum as a function of z (or x_F). A depletion of the leading hadrons from a nuclear target is expected to be compensated by an enhancement at lower values of z. Such an enhancement accommodates particles scattered down from the high-z region as well as effects of intranuclear cascading. An analysis of the z dependence of the SLAC data (Osb78) has recently been made by Gyulassy and Plümer (Gyu90). They have come to the interesting and provocative conclusion that final-state cascading cannot account for the observed z-dependence, and that the hadronization process itself is seriously modified by the nuclear environment. They have strongly argued for new measurements to check the correctness of the earlier data and to provide more detailed tests of their hadronization model. The low-z region will be readily accessible in the measurements planned for PEGASYS/Mark II, since the hadrons in this region are typically emitted at larger angles than for the leading hadrons.

We conclude this section with an example that underlines the need to update the earlier measurements and shows the importance of making attenuation measurements on a variety of nuclear targets. We employ here a model (Bialas and Chmaj, Bia83) that describes the nuclear absorption in terms of two parameters, a "quark-nucleon" cross section σ_{qN} describing the attenuation before hadrons are formed, and a formation length τ. The cross section for attenuation of the hadrons after they are formed is assumed known (approximately 20 mb). The measured transmission for a given target does not determine the two parameters separately, but does yield a relationship between them. If measurements are made on several targets and the model is correct, the curves relating σ_{qN} and τ for each target should intersect at a point that determines the two parameters separately.

Figure 5 shows an application of this analysis to the data of (Osb78). Values of the measured transmission in Be, C, Cu, and Sn for positive hadrons and for $Q^2 > 1$ (GeV/c)^2 were taken from the data reproduced in Fig. 1; data in the bins near $z_{cm} = 0.5$ and 0.8 were averaged. Curves of constant transmission for the four targets in the $\tau - \sigma_{qN}$ plane are shown in the upper portion of Fig. 5. In the lower portion of the figure, the curves are replaced by uncertainty bands reflecting the uncertainties in the measured transmissions. It is noteworthy that there is little overlap of the bands for the various targets. Whether this indicates a failure of the model or is simply a consequence of systematic errors and coarse binning in the experiment is one of the interesting open questions that will be addressed by the proposed measurements with PEGASYS/Mark II.

References

(Bia83) A. Bialas and T. Chmaj, Phys. Lett. 133B, 241 (1983).

(Gyu90) M. Gyulassy and M. Plümer, to be published in Nucl. Phys. B.

(Osb78) L. S. Osborne et al., Phys. Rev. Lett. 40, 1624 (1978).

(Wom86) "A Study of Forward Hadron Production in Deep Inelastic Muon-Nucleus Scattering," W. J. Womersley, Thesis, Oxford (1986).

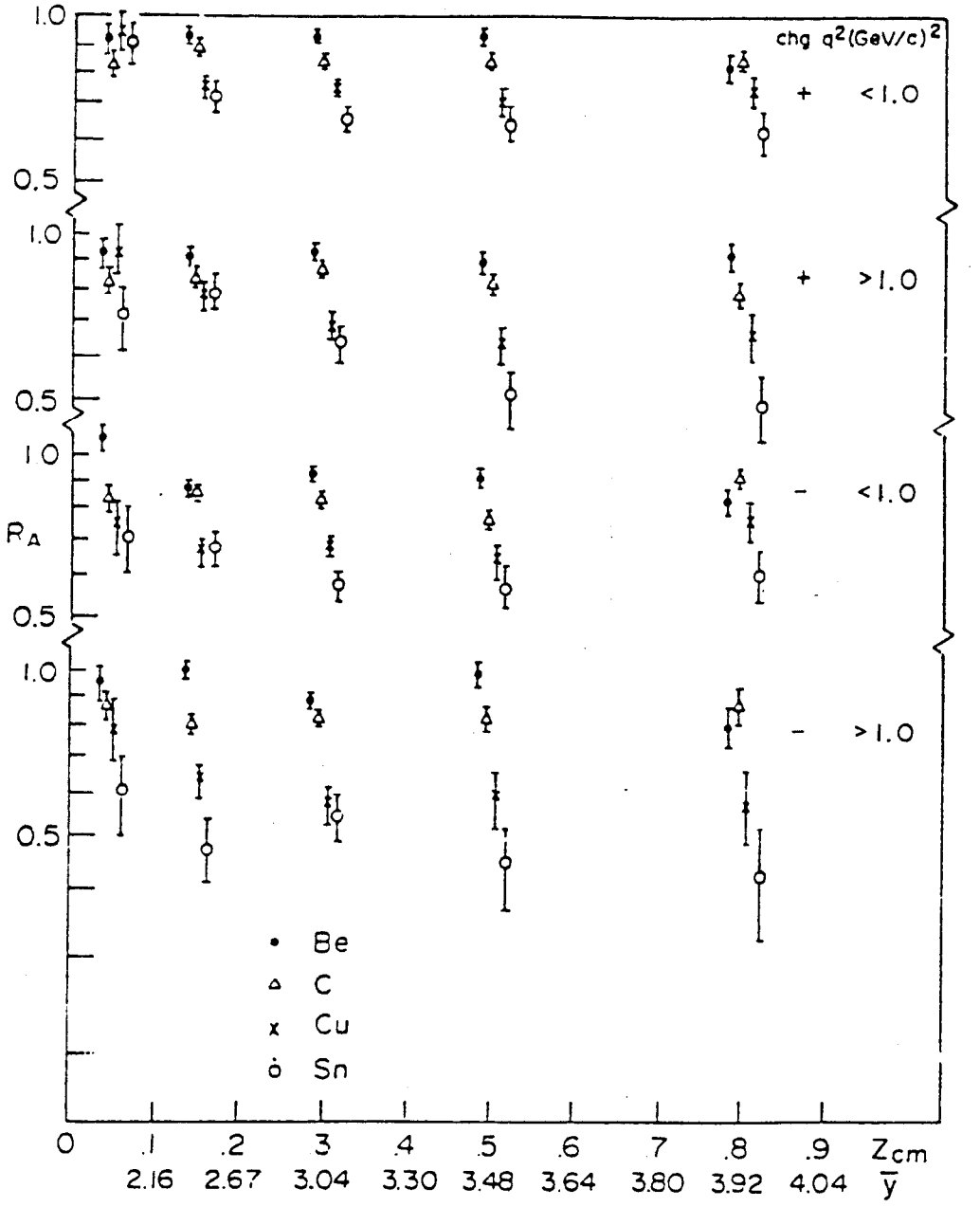

Figure 1. Nuclear transmission factor R_A for forward hadrons produced on targets of Be, C, Cu and Sn compared to deuterium as a function of z from the SLAC experiment by Osborne *et al.* (Osb78). This data covered the kinematic range $0.35 < Q^2 < 5$ (GeV/c)^2; data for Q^2 above and below 1 (GeV/c)^2 are shown separately. The data are integrated over ν spread between 3 and 17 GeV, with an average of 10 GeV. R_A would be is unity if there is no increased absorption of hadrons in heavy nuclei compared to deuterium.

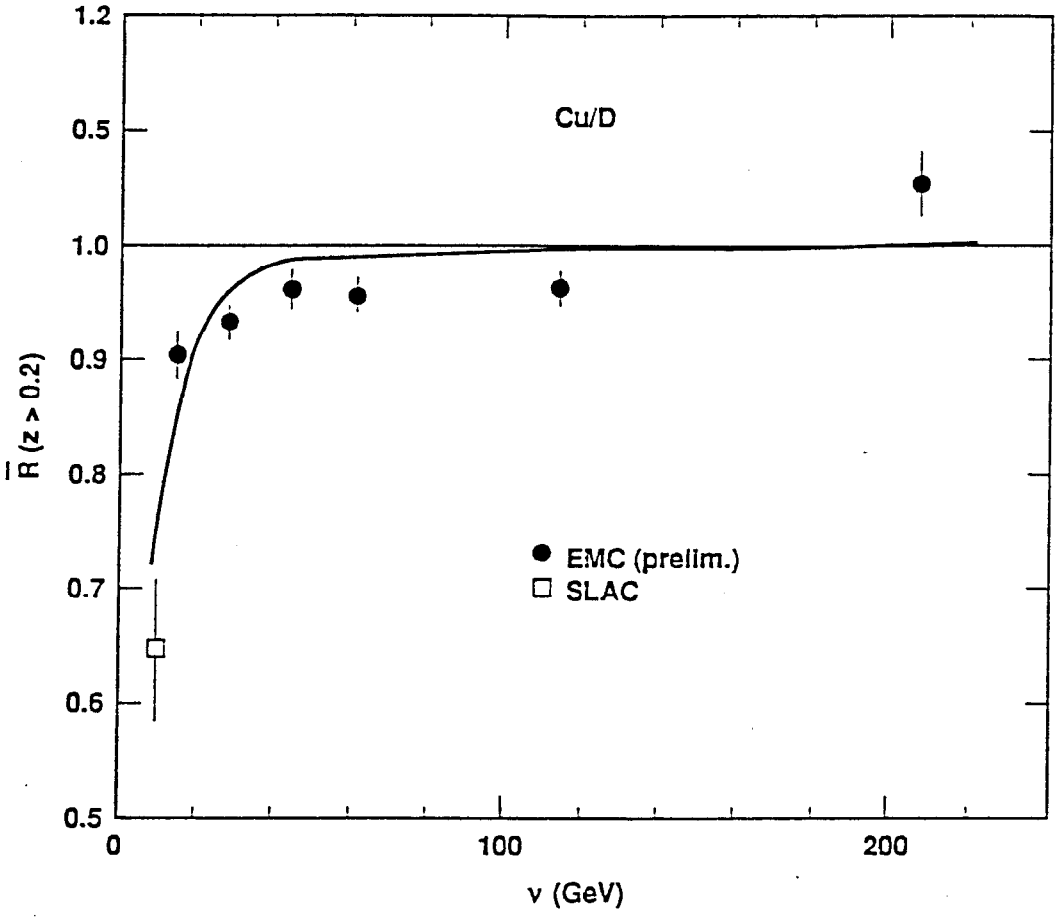

Figure 2 The nuclear transmission factor R for copper compared to deuterium as a function of the energy transfer ν as measured in the SLAC (Osb78) and EMC experiments (Wom86,Ren88). The curve is the prediction of the Lund string model assuming the constituent length determines the onset of hadronic cross section for the recoiling quarks.

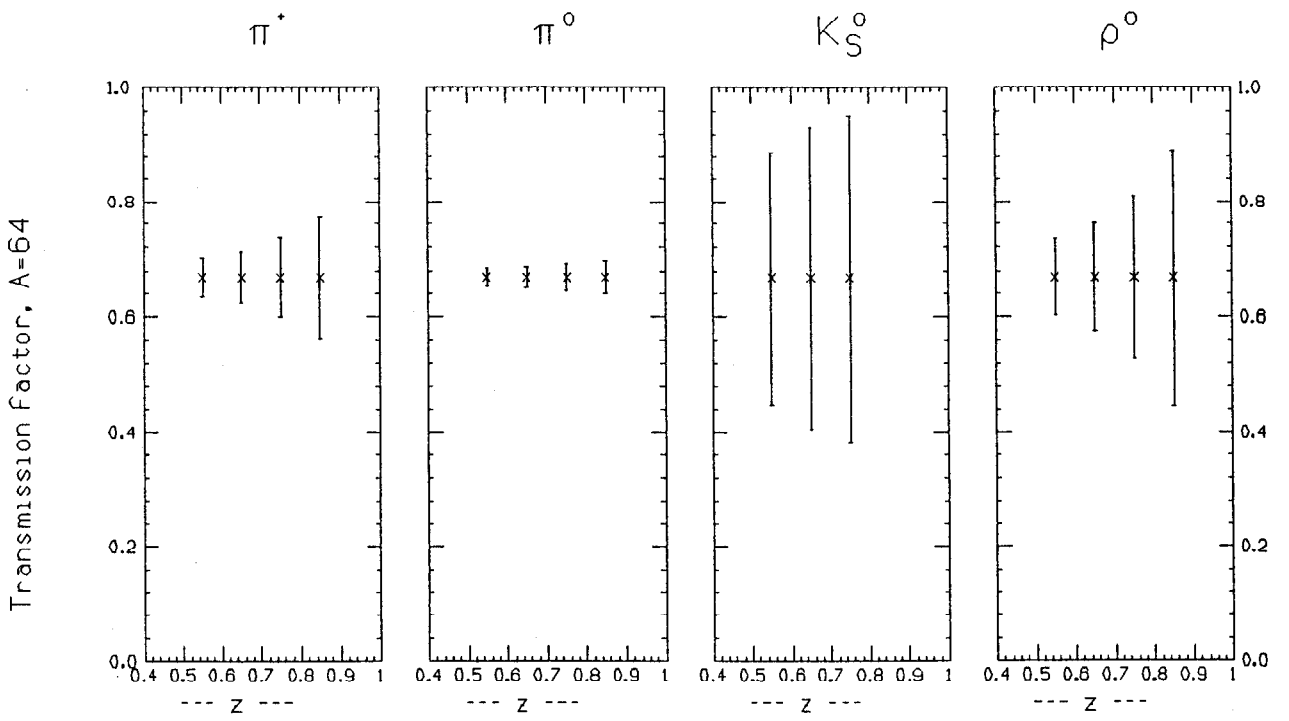

Figure 3 Estimated statistical uncertainty in measuring the nuclear transmission for four particle types for a 90-day run on a medium weight nucleus (A=64). Bin sizes are Δz=0.1, ΔQ^2=2 (GeV/c)^2 centered on Q^2 = 3.5 (GeV/c)^2, and $\Delta\nu$ = 1 GeV centered on ν= 7 GeV. Data will be taken simultaneously in many such bins.

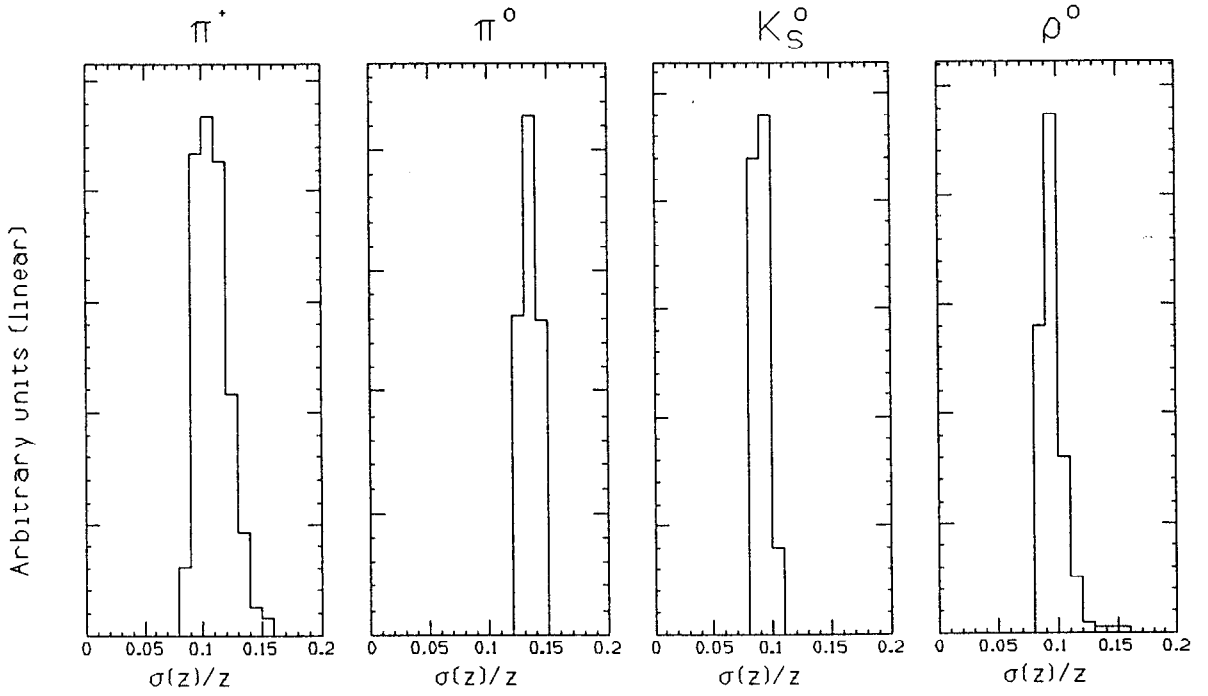

Figure 4 Histograms of the resolution for four particle types in unit bins centered on Q^2 = 4 (GeV/c)^2 and ν= 7 GeV, for hadrons with z >0.5.

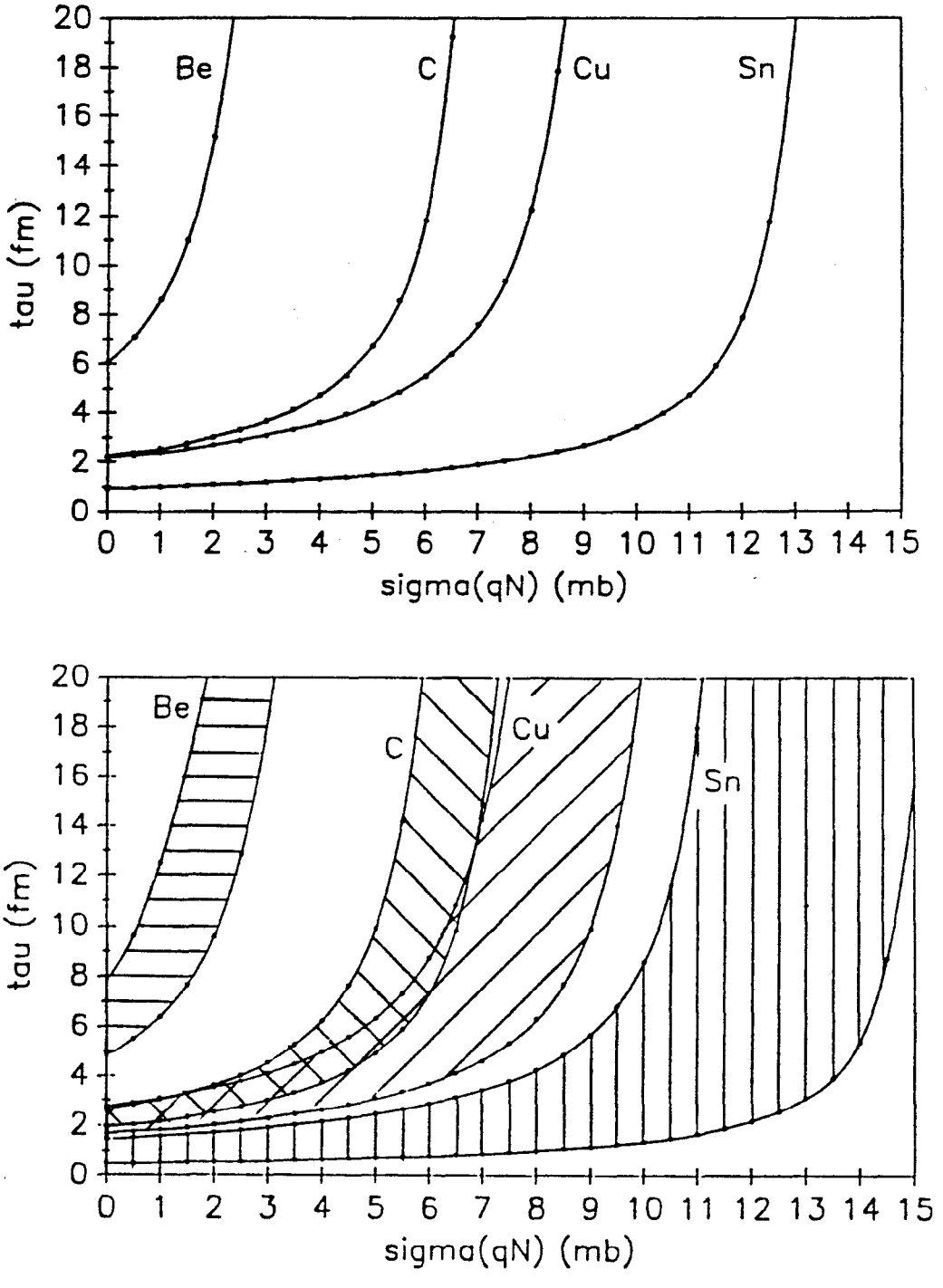

Figure 5 Upper portion: Curves of constant transmission for Be, C, Cu, and Sn, using the model of (Bia83) and the values of transmission measured by (Osb78). Lower portion: same, showing uncertainty bands deduced from the uncertainties in the transmission measurements.

III.B Nuclear Transparency in Exclusive Electroproduction Reactions

Introduction

For some years there have been indications, both experimental and theoretical, that the nucleus may have unexpected transparency to the passage of energetic hadrons. In other words, under some conditions the attenuation of fast hadrons within the nucleus may be appreciably less than that predicted on the basis of the free hadron-nucleon cross section and the nuclear density (Glauber theory). In particular, it has been argued by Mueller and Brodsky that a phenomenon called "color transparency" occurs for sufficiently large values of the momentum transfer.

To obtain an appreciable amplitude for a high momentum transfer exclusive reaction (e.g. elastic scattering), the valence colored constituents should be transversely close together, and there should be no additional sea quarks or gluons at the time of scattering. If the constituents are close together, their soft interactions with the nuclear medium are suppressed. If the escape time of the high energy outgoing particle is sufficiently short it can remain small throughout its travel in the nucleus and therefore escape the medium without further interaction. The feature that the particle suffers no distortion, *i.e.* that the nucleus is 'transparent', leads to the name 'color transparency' and it is a testable prediction of QCD. Moreover if the concept holds, the nucleus can be used to filter out the soft contributions to various large angle exclusive processes.

Some tantalizing hints of color transparency have been seen at BNL by means of quasielastic proton scattering on nuclear targets at high momentum transfers. A complementary way to test color transparency is to study the attenuation of the outgoing hadrons produced in exclusive meson electroproduction and in high momentum transfer quasielastic electron scattering from nuclei.

Exclusive ρ Meson Production

Since the time of the December, 1988, Draft Proposal, Ralston and Pire (Ral89) have enunciated a generalization of the color transparency hypothesis, which they term 'nuclear filtering'. Succinctly, what is claimed is that the nuclear medium should filter away amplitudes where quarks in hadrons are not in a transversely small minimal Fock state, and therefore any hard QCD process should appear purer when performed with a nuclear target (A>>1) than with a bare nucleon target.

In this spirit, we wish to demonstrate here the possibility of studying color transparency in exclusive ρ electroproduction, independently for longitudinally and transversely polarized ρ^0's, as was suggested but not developed further in our original proposal. It is argued that at large Q^2, exclusive ρ electroproduction

$p(e, e'\rho^0)p$ in perturbative QCD should only produce longitudinally polarized ρ^0's, via the diagram of Figure 1. How nature produces transversely polarized ρ^0's, which persist even up to $Q^2 = 10$ (GeV/c)^2, is not understood. Could it be that the longitudinally polarized ρ^0 will be produced in a spatially small Fock state, and thus exhibit color transparency, while the transversely polarized ρ^0 is produced non-perturbatively, *i.e.* 'born big', and will be filtered out by the nuclear medium?

Our method will use the self-analyzing property of the ρ^0. We may write the ρ^0 decay angular distribution as

$$W(\cos(\theta)) = [A_L W_L(\cos(\theta)) + A_T W_T(\cos(\theta))],$$

with $W_L = \frac{3}{2}\cos^2(\theta)$, $W_T = \frac{3}{4}(1 - \cos^2(\theta))$, and where the A_L is the quantity $r^{04}{}_{00}$ of (Aub85) and the Draft Proposal.

Having determined the helicity decomposition from an isoscalar combination of nucleons (*i.e.* deuterium) as a function of Q^2 (Aub85), we then imbed the process in a nuclear target, where we measure a *modified* angular distribution

$$W^A(\cos(\theta)) = [A_L{}' W_L(\cos(\theta)) + A_T{}' W_T(\cos(\theta))].$$

If the cross sections for the longitudinally and transversely polarized ρ^0 are equal (*i.e.* neither or both color transparent), the shape of the nuclear angular distribution will be the *same.* The integrated cross section will then reflect the degree of color transparency of the ρ^0 in the usual way. If the longitudinal ρ^0 evidences color transparency, but the transverse ρ^0 does not, the angular distribution will become *sharper.* On the other hand, if the transversely polarized ρ^0 were to be color transparent, and the longitudinal ρ^0 not, the angular distribution would become *flatter.*

We demonstrate the sensitivity of this technique by Monte Carlo within the context of simple models for color transparency. As in the Draft Proposal, the details of the 'small' cross section and its evolution to asymptotic size are from Farrar (Far88). The asymptotic $\rho^0 N$ cross section was taken to be 27.1 mb. We first generated the angular distribution in $\cos(\theta)$ for a deuterium target, with the statistics reflecting the ρ^0-electroproduction cross section dependence, the target luminosity, and the detector acceptance for the four-body final state in $A(e, e'p\rho^0)(A-1)^*$, $\rho^0 \rightarrow \pi^+\pi^-$. The range of kinematics chosen was a small bin in Q^2 and W ($Q^2 = 3 - 4$ (GeV/c)^2, $W = 3 - 4$ GeV). The values $A_L = 0.6$ and $A_T = 0.4$ are roughly what is expected over the PEGASYS kinematical range (Aub85). This

distribution is plotted in Figure 2(a), along with the curve representing the best fit to the synthetic data. We then calculated the *attenuated* $A_{L,T}$ for ^{40}Ar, where we may make *independent assumptions* about the behavior of the longitudinal and transverse ρ^0. The remaining panels in Figure 2 represent the cases where we assume (b) the L,T ρ^0 *both* start small and expand according to the pQCD prescription of (Far88); (c) the L ρ^0 evolve according to pQCD, but the T ρ^0 are born with their asymptotic cross section (Glauber assumption); and (d) L (Glauber) and T (pQCD). It can readily be seen by eye that the distributions differ significantly. Results of numerical fits are presented in Table I, where it can be seen that the errors are small enough to distinguish among the various physical assumptions. These measurements would be simultaneously made in many bins of Q^2 and W.

		Input			Fitted		
Tgt	Cts	A_L	A_T	Cts	A_L	A_T	$\chi^2/D.F.$
D	9300	0.6	0.4	9133	0.5989	0.4011	0.754
					± 0.0088	± 0.0079	
Ar	885	0.4085	0.2723	892	0.4052	0.2756	1.110
		(pQCD)	(pQCD)		± 0.0303	± 0.0237	
Ar	771	0.4085	0.1843	774	0.3987	0.1941	1.178
		(pQCD)	(Glauber)		± 0.0319	± 0.0223	
Ar	713	0.2764	0.2723	738	0.2728	0.2759	1.303
		(Glauber)	(pQCD)		± 0.0197	± 0.0230	

Table I Input and fitted initial $(A_{L,T})^D$ and attenuated $(A'_{L,T})^{Ar}$, for different assumptions concerning the evolution of the longitudinally and transversely polarized ρ^0. $Q^2 = 3-4$ (GeV/c)^2, $W = 3-4$ GeV.

While the count rates appear large enough to look for color transparency in exclusive ρ^0 electroproduction, and even to look for differences between transversely and longitudinally polarized ρ^0's, the poor electron resolution will make it difficult to isolate exclusive production from the case where the residual nucleus is excited sufficiently to emit additional pions or nucleons. Studies are under way to determine the best way to use hermiticity, missing momentum, and other cuts to determine the relative strength of the exclusive cross section leaving the residual nucleus with a small excitation energy. Studies are also in progress to investigate

the usefulness of measuring other self-analyzing particles (such as the Λ) for tests of nuclear filtering.

Exclusive A(e,e' p) Reaction

While one may view the determination of color transparency in quasielastic scattering as more fundamental than in exclusive meson electroproduction, it is experimentally more difficult with PEGASYS/Mark II because the relevant Q^2 will almost surely be higher than for meson electroproduction, and count rates are low at high Q^2. However, we show below that meaningful measurements can be made up to 10 (GeV/c)^2, well above the $Q^2 \approx 5$ region where color transparency effects are expected to become important.

Table II shows the expected rates for a luminosity of 1.7×10^{32} for hydrogen and 1.7×10^{30} for Argon, with a target length of approximately 240 cm. Scattered electrons or positrons are required to be detected in the ECC, and the protons are required to pass through at least four superlayers in the drift chamber.

Q^2	Hydrogen		Argon	
	rate per hr	total events	rate per hr	total events
all (Q^2 >4GeV/c)	5.3	15 k	1	2.5 k
$Q^2 > 5$ GeV/c	3.5	10 k	0.7	2 k
$Q^2 > 7$ GeV/c	1.2	3 k	0.2	0.7 k
$Q^2 > 10$ GeV/c	0.3	800	0.05	150

TABLE II. Expected rates and yields in a 90 day run.

One model for nuclear transparency (Far88) gives a value of about 0.3 for no color transparency and from 0.6 to 0.9 for Q^2=9 (GeV/c)^2 with color transparency included. The statistics in the above Table should be adequate to distinguish between these models. The main difficulty lies in the resolution, which is about 0.4 (GeV/c)^2 in Q^2, 0.6 GeV in ν, and 0.6 GeV in W, roughly independent of Q^2. The poor resolution in W means that the residual nucleus could have an excitation energy greater than 30 or 40 MeV, where the color transparency concept is likely to break down. Theoretical estimates for the excitation energy spectrum of the residual nucleus can be made, from which estimates of the spectrum of knocked-out energetic protons and pions can be made. Since the Mark II has a solid angle of about 80% of 4π for detected protons with $P_\perp > 0.15$ GeV/c or pions with $P_\perp > 0.05$ GeV/c, the theoretical excitation spectrum can be indirectly tested

experimentally. Studies are under to way to determine how reliably this can be done.

In summary, we have found that if the resolution problems can be overcome, the rates should be high enough to test color transparency in ep quasielastic scattering. Other exclusive reactions that are under study and seem to have reasonable counting rates include A(e,e'Δ) and A(e,e'N*). The S_{11} resonance is particularly interesting due its large strength at high Q^2 and its clean identification through the 50% branching ratio to $N\eta$. Color transparency in exclusive π and K production are also being studied.

References

(Aub85) J.J. Aubert, *et al*, Phys. Lett. **161B** (1985) 203

(Far88) G.R. Farrar, H. Liu, L.L. Frankfurt, M.I. Strikman, Phys. Rev. Lett. **61** (1988) 686

(Ral89) Bernard Pine and John P. Ralston, in Proceedings of the NPAS Topical Conference on Electronuclear Physics with Internal Targets p. 229 (SLAC, January 1989), ed. R.G. Arnold (World Scientific, Singapore, 1990); and to be published in the Proceedings of the 24^{th} Recontre de Moriond (Les Arcs, France 1989), edited by J. Tran Thanh Van (Editions Frontiers, Gif-sur-Yvette, France, in press); and John Ralston, private communication.

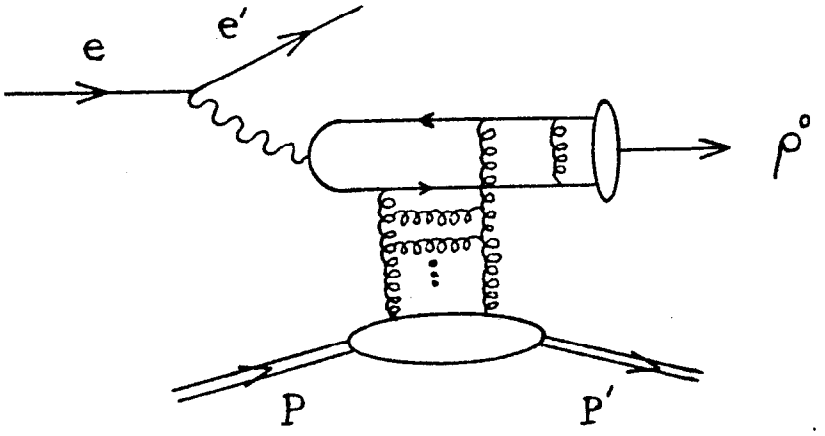

Figure 1. Lowest order diagram describing ρ^0 electroproduction at large Q^2. The resulting ρ^0 is longitudinally polarized.

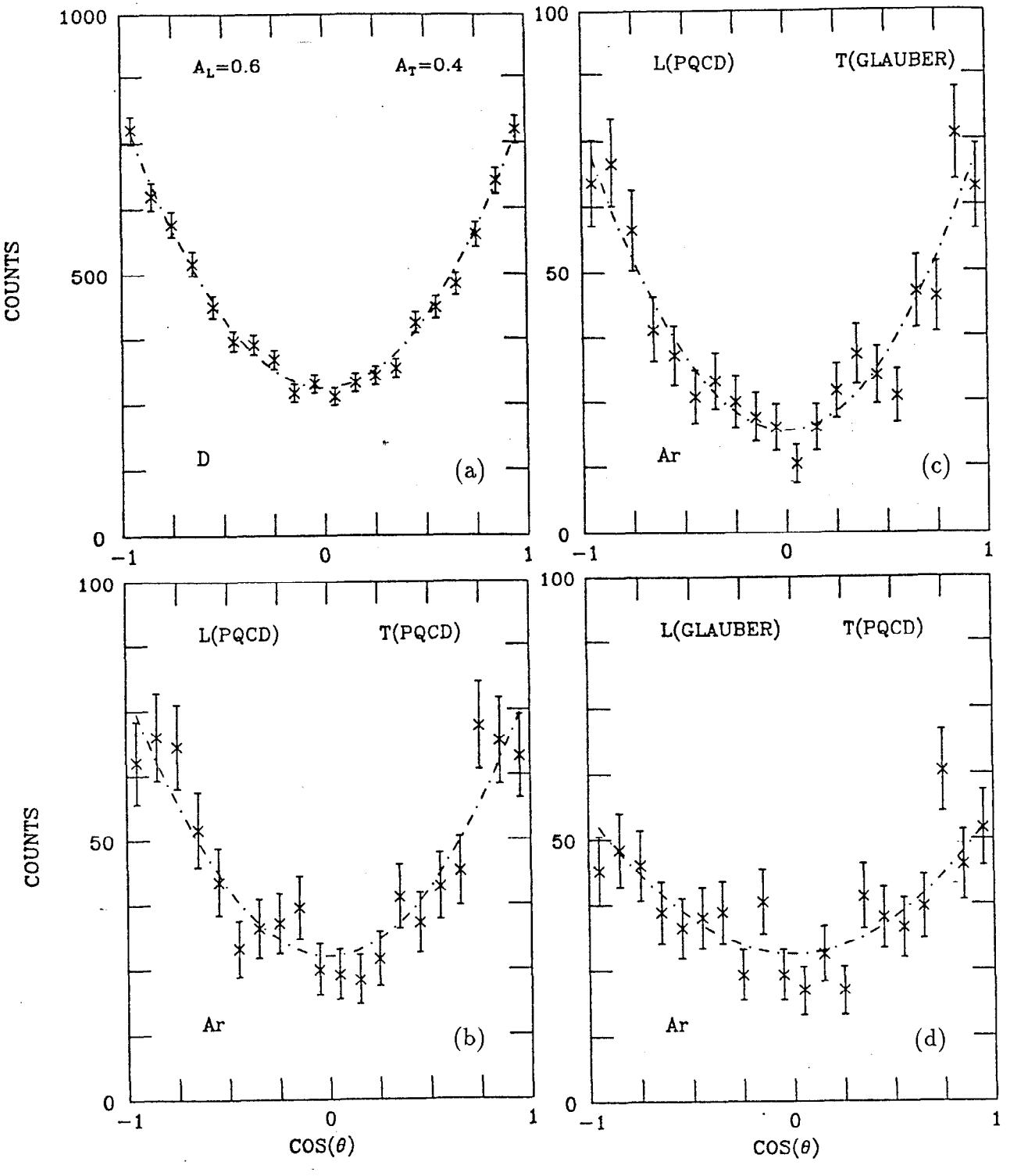

Figure 2. Synthetic data for the ρ decay angular distribution, $\rho \rightarrow \pi^+\pi^-$, and least-squares fits to them. (a) For D; for ^{40}Ar: (b) L(pQCD), T(pQCD); (c) L(pQCD), T(Glauber); (d) L(Glauber), T(pQCD). See text for explanation.

III.C. Azimuthal Distributions of Leading Hadrons from the Nucleon

The analysis of the data on hadronization will rely heavily on the validity of the quark-parton model, in which the virtual photon is absorbed on a single quark. In the simplest versions of this model the hadron spectra can be characterized in terms of the single variable $z = E_h/\nu$, and thus retain no memory of the parameters characterizing the initial reaction, such as Q^2. Moreover, the reactions are assumed to take place only through the absorption of transverse virtual photons. Corrections to the quark-parton model involve longitudinal photon absorption and amplitudes that vary as powers of $1/\sqrt{Q^2}$; these are so-called "higher twist" effects. Such terms are to be expected since measurements (Das88) of the ratio of longitudinal to transverse virtual absorption in inclusive deep-inelastic scattering show a clear $1/Q^2$ behavior that is inconsistent with the naive quark-parton model.

PEGASYS/Mark II will address this issue through measurements of the azimuthal angular distributions of the produced hadrons. This will involve identifying the ϕ-dependent terms in the expression for the differential cross section for production of a hadron with unpolarized beam and target:

$$\frac{d^6\sigma}{d\Omega dE' dz dp_T d\phi} \propto \sigma_T + \epsilon\sigma_L + \epsilon\sigma_{TT}\cos(2\phi) + \sqrt{2\epsilon(\epsilon+1)}\sigma_{TL}\cos(\phi).$$

In this expression, the first three terms refer to cross sections for transverse unpolarized, longitudinal, and transverse plane-polarized virtual photons; the last term is the contribution from transverse-longitudinal interference. The angle ϕ is between the plane containing the virtual photon and the scattered electron and the plane containing the virtual photon and the detected hadron; ϵ is the photon polarization parameter determined by the electron-scattering observables.

To date there have been few measurements of the azimuthal dependence of hadron production in the region of the onset of Bjorken scaling. An example is shown in Fig. 1, from a SLAC experiment at 19.6 GeV electron energy (Dak74). The statistical precision is insufficient to characterize the angle-dependent terms convincingly. Moreover, there was no binning in Q^2 in this experiment, and the lower cut on $Q^2 \approx 0.5$ (GeV/c)^2 weights the data in a region in which the validity of Bjorken scaling is questionable.

We note two higher-twist effects that may contribute to the ϕ-dependent terms. One of these is a simple kinematic effect arising from the initial (primordial) transverse momentum of the struck quark (Cah78). This effect, which implies negative values of $<\cos(\phi)>$ for hadrons in the region $x_F > 0$, has been observed by EMC

(Arn87, Aub86). The second effect, more interesting but controversial, is a prediction (Ber80) based on perturbative QCD of a longitudinal absorption mechanism for pion production that becomes increasingly important with increasing z. This second mechanism, for which $<\cos(\phi)>$ should be positive, appears to have been observed in Drell-Yan experiments (Ale86), but is not seen at the predicted level in a search conducted by EMC (Aub86). Further details on these mechanisms may be found in the December, 1988, PEGASYS Draft Proposal.

The goal of PEGASYS/Mark II is to characterize the ϕ-dependent terms in the kinematic region near the onset of scaling as a function of Q^2, z, and p_T, and if they are present at a significant level, to understand whether they are consistent with the expectations of models such as those indicated above. Measurements can be made in the first phase of PEGASYS/Mark II running, using the drift chamber and end-cap calorimeters as the important detector elements. The available kinematic region and the resolution in z are as indicated in Section III.a on hadronization; approximately, these are $Q^2 > 3$ (GeV/c)^2, ν in the range 5 to 9 GeV, and resolution in $\nu, \sigma(\nu)/\nu$, of 10 to 15%. These should be adequate for the proposed studies.

Figure 2 illustrates the possibilities and potential difficulties of measuring the ϕ-dependent terms. The results shown were generated by calculating π^+ and π^0 spectra with the Lund model and then passing these spectra through the same detector model employed in the section on hadronization. The Lund calculations do not contain the higher twist effects, and consequently the ϕ distributions that are input to the detector model are uniform in ϕ. The strong ϕ dependence in the detected particle distributions is entirely due to the forward-angle hole in the detector acceptance. The counts are normalized to a 90-day run on a deuterium target with luminosity corresponding to a 12-hour beam lifetime. All detected π^+ and π^0 with $z > 0.5$, ν from 4.5 to 9.5 GeV, and any Q^2 are binned. In practice, most of the detected particles have $Q^2 > 2$. If the average value $<\cos(\phi)>$ is 0.05, which is consistent with the sketchy data presently available, the ratio of counts at 180 degrees to that at 90 degrees would be altered by twice this value, or 10%. The figure shows that for both π^+ and π^- there will be sufficient counts to make statistically significant measurements of $<\cos(\phi)>$ at this level, even after subdividing the data into much smaller bins in the relevant variables, such as Q^2, z, and p_T. However, the detector acceptance itself has very large $\cos(\phi)$ components, as indicated in the figure. Consequently, it will be necessary to understand the detector acceptance very well if the proposed measurements are to be reliable. This is a subject for further study with a more detailed detector model.

References

(Ale86) J. P. Alexander *et al.*, Phys. Rev. D34, 315 (1986).

(Arn87) M. Arneodo *et al.*, Z. Phys. C34, 277 (1987).

(Aub86) J. J. Aubert *et al.*, Z. Phys. C30, 23 (1986).

(Ber80) E. L. Berger, Z. Phys. C4, 289 (1980).

(Cah78) R. N. Cahn, Phys. Lett. 78B, 269 (1978).

(Dak74) J. T. Dakin *et al.*, Phys. Rev. D10, 1401 (1974).

(Das88) S. Dasu *et al.*, Phys. Rev. D15, 2425 (1977).

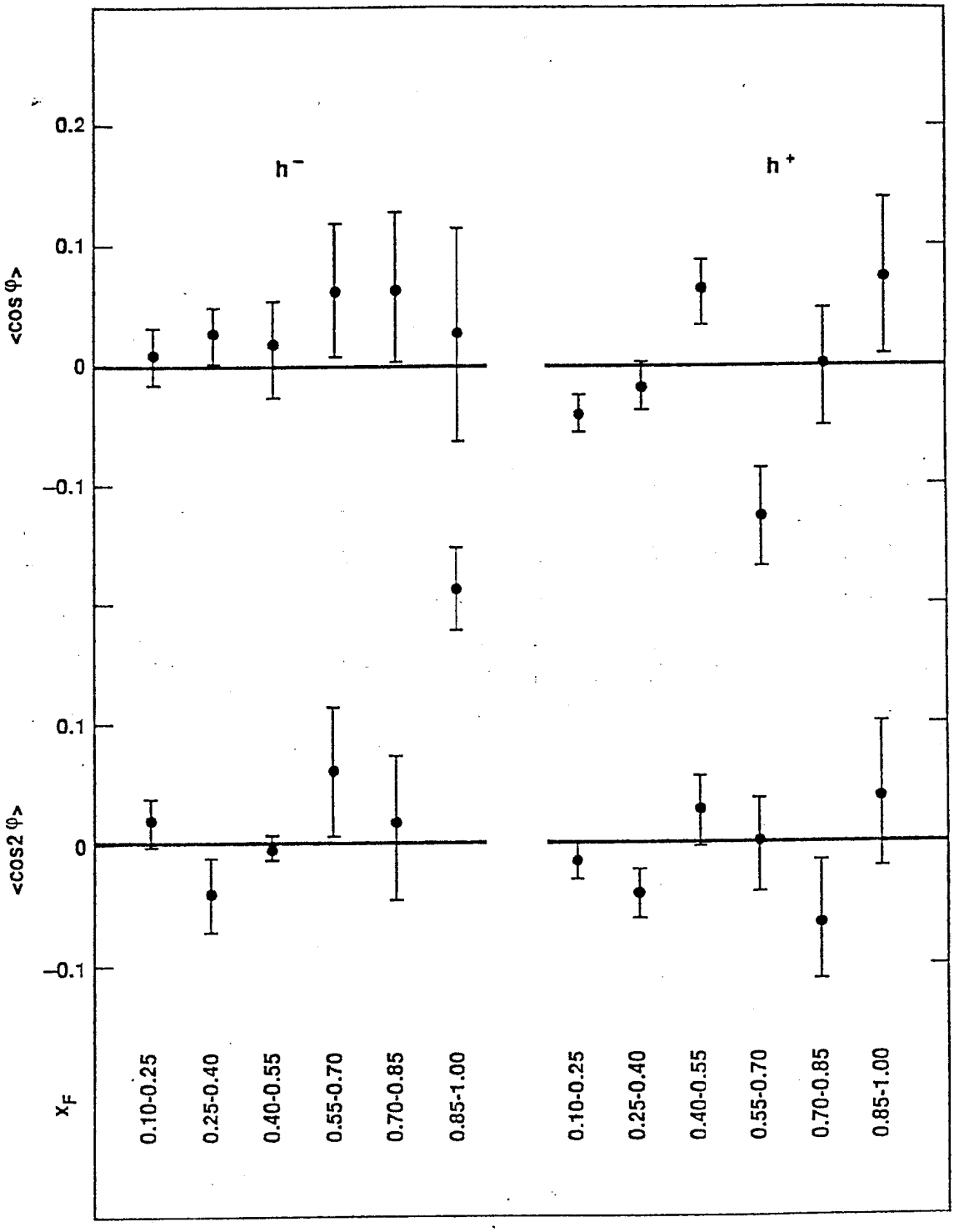

Figure 1. $\langle \cos \phi \rangle$ and $\langle \cos 2\phi \rangle$ for positive and negative hadrons versus x_F (approximately equivalent to z) for 19.6 GeV interactions in hydrogen by Dakin *et al* (Dak74).

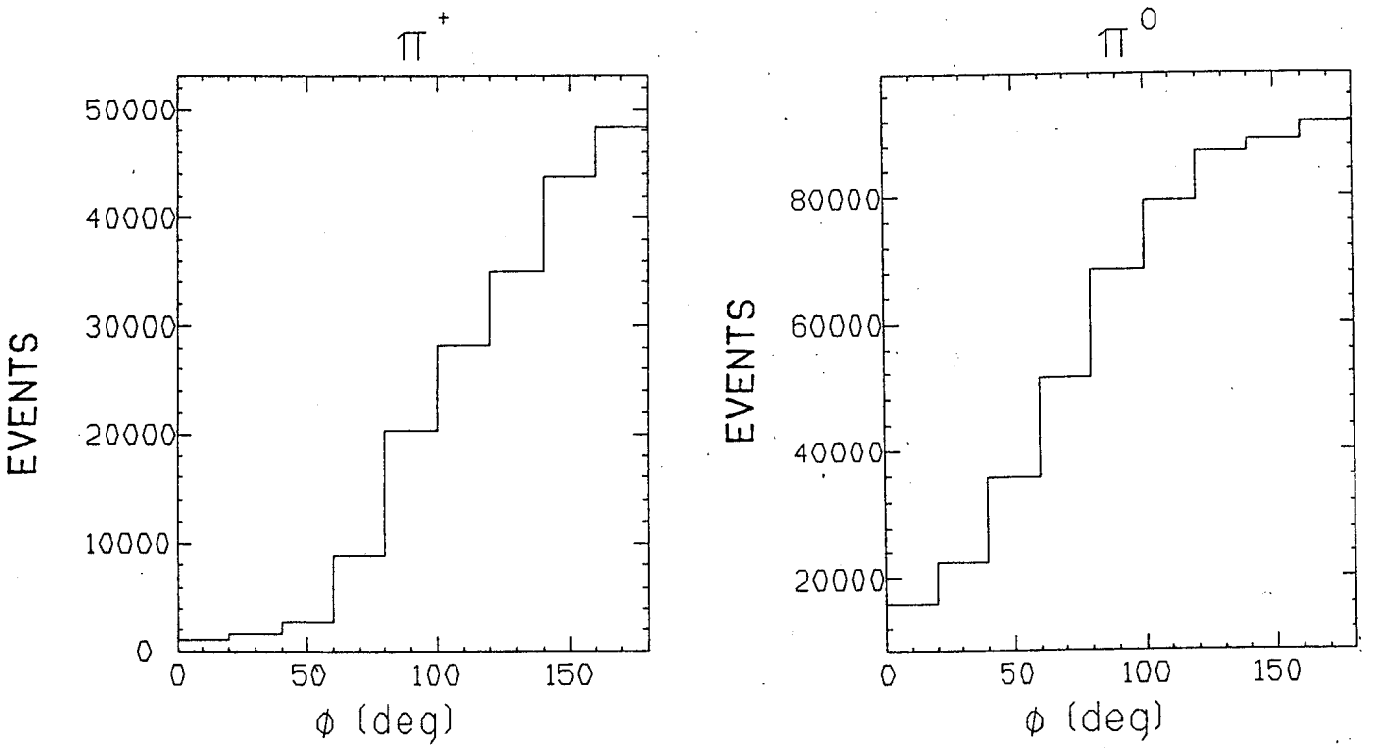

Figure 2. Estimated detector response to Lund-model events, showing the azimuthal angular distribution of detected hadrons corresponding to an initial distribution that is uniform in ϕ. See text for significance of the vertical scale.

III.D. Cumulative Production; Tagged Structure Functions

For over a decade the observation of backward-going nucleons in reactions induced on nuclear targets by a variety of high energy probes, including protons, pions, and photons, has attracted strong interest. This interest is due to the fact that such backward nucleons are kinematically forbidden for reactions on a stationary nucleon target. Observation of backward nucleons thus provides a laboratory for studying potentially interesting correlation effects inside the nucleus, such as scattering from multinucleon clusters or six-quark bags. Such backward emission of hadrons is often referred to as "cumulative production" (see, e.g., Bal74, Bal75). Many studies have shown a striking uniformity in the momentum distributions of backward nucleons emitted above the Fermi momentum. For sufficiently high projectile energies, these distributions are independent of the type and energy of the projectile; see (Gav89) for a recent review of this "nuclear scaling" phenomenon. Some first results on backward production in electron-nucleus scattering have already been obtained by looking at 5-GeV electrons interacting with the background gas in another "4π" detector, the ARGUS detector at DESY (Deg90). Apart from this and a few results from neutrino scattering in bubble chambers (noted below), there is little information on backward-particle production from lepton scattering on nuclei.

By measuring backward-going hadrons in coincidence with deep-inelastically scattered electrons in PEGASYS/Mark II, we can expect to obtain new information on the properties and origin of these hadrons, since the well-understood electromagnetic probe permits a better understanding of the initial conditions in the nucleus leading to hadron emission than hadronic projectiles. Moreover, the sample of events will be much larger than those obtained in neutrino reactions. The data we will acquire may be viewed in several different ways. In one approach, the properties of the cumulatively produced hadrons can be characterized as a function of Q^2 and ν, and the results compared with those using hadronic probes. These properties include the momentum and angular dependence of the backward-going particles, as well as their dependence on target mass. In another interpretation, the Q^2 and ν dependence of the reaction rates will be measured as a function of the backward-hadron properties; i.e., deep-inelastic structure functions tagged on the hadrons will be measured. Frankfurt and Strikman (Fra81) have shown how shifts in the tagged structure functions, compared with those measured in inclusive reactions, can be used to obtain information on nuclear correlations. While both approaches will be used in understanding the data, for purposes of illustrating the capabilities of PEGASYS/Mark II we show below a single example, that of backward proton production from deuterium using the Frankfurt and Strikman model.

The model of Frankfurt and Strikman (Fra81) as applied to the deuteron assumes that lepton scattering occurs from a quark in a nucleon which is far off-shell, but which has equal and opposite Fermi momentum k to its partner which is nearly on-shell. The DIS process causes the struck nucleon to hadronize into fully on-shell products. In the process, the spectator is liberated with momentum k. The momentum of the spectator accurately reflects the momentum-space wave function of the deuteron. Frankfurt and Strikman argue that if one observes these spectators at backward laboratory angles, contributions of fast nucleons from direct processes (i.e. nucleons that are products of the struck nucleon and its subsequent hadronization) are negligible.

Because one of the two nucleons in the deuteron is a spectator in this model, the coincidence cross section is factorizable into a product of the nucleon momentum distribution in 3-space and a rescaled DIS cross section for the scattered lepton. The momentum distribution is simply the Fourier transform of the deuteron wavefunction, and the DIS cross section is rescaled by the transformation $x \Rightarrow x/(2-\alpha)$, which takes into account the intrinsic motion of the struck nucleon before it was hit. The light-cone fraction of the deuteron momentum carried by the struck nucleon is given by $\alpha = (\sqrt{m^2+p^2} - \mathbf{p}\cdot\hat{\mathbf{q}})/m$ in which m is the nucleon mass, $\mathbf{p}$ is the spectator momentum, and $\mathbf{q}$ is the 3-momentum transfer. The cross section takes the form

$$\frac{d\sigma}{dxdyd^3k} = \frac{2\pi\alpha_F^2}{mEx^2y^2}(2-\alpha)^2\left\{(1-y)F_2(\frac{x}{2-\alpha},Q^2) + \frac{xy^2}{2-\alpha}F_1(\frac{x}{2-\alpha},Q^2)\right\}\rho(k)$$

in which $\rho(k)$ is the deuteron wave function in momentum space, $x = Q^2/2m\nu$, $y = \nu/E$, E is the beam energy, and α_F is the fine structure constant. The light-cone variable α approaches the limit $\alpha = 2$ at backward angles. If the spectator model is correct, it can be verified experimentally by observing scaling of the structure functions. In this case, the data provide an accurate measure of the high momentum components of the nuclear wavefunction. Deviations from this simple model (probably at $\alpha > 1.5$ (Str90)) may indicate where the nucleon picture of the deuteron breaks down.

In order to estimate rates for Mark II, we have assumed the Frankfurt and Strikman model for the deuteron and have taken the deuteron wave function from a calculation using the Paris potential. The results are presented in Table 1. Here we have assumed a beam energy of 14.5 GeV and an average luminosity of $1.7 \times 10^{32}/\mathrm{cm}^2/\mathrm{sec}$ during a 90-day run. This implies an integrated luminosity of $2.6 \times 10^6/\mathrm{nb}$. Each bin in Q^2 and ν is taken to be 1 GeV^2 and 1 GeV wide, respectively, and W^2 is kept above 4 GeV^2. The data in Table 1 are presented

in terms of the central values of Bjorken $y = \nu/E_{\rm beam}$ and $x' = x_{\rm Bj}/(2-\alpha)$ corresponding to the bins in Q^2 and ν. The data are limited to $y > 0.3$ because of detector inefficiencies. Low values of y correspond to small electron-scattering angles which are detected in Mark II only for interactions at the down-stream end of the gas target. These events, however, are too far back for the drift chamber to detect protons emitted at lab angles as large as 160°. For $y > 0.3$ the drift chamber can detect protons out to 160° which turns out to be sufficient to make the experiment possible. The estimates of Table 1 assume an integrated proton yield for angles between 90° and 160° at fixed values of α ranging from unity to 1.8. The largest contribution comes from the most backward angles. The count-rates include an efficiency factor for electron detection but assume a 100% efficiency for proton detection in the drift chamber within the specified angular range. The dE/dx resolution of the drift chamber is sufficient to identify protons up to 1 GeV/c momentum. The energy loss in the walls of the target container and the inner wall of the drift chamber is not a problem for momenta above 200 MeV/c. Therefore, Mark II is nicely suited for such tagged structure function studies.

Table 1 lists the number of counts expected for bins in x', y, and α. The widths of the α-bins is ± 0.1. These estimates indicate that the spectator model can be tested over a large range of y and x' for α between 1 and 1.6. Measurements at $\alpha = 1.8$ are only possible for low x', but even this single point at large α is crucial for a sensitive test of the Frankfurt and Strikman model.

The spectator model should also apply in heavy nuclear targets, and observation of the dependence of the structure-function shift on the kinematics of the backward nucleon in principle yields information on pair-like correlations within the nucleus. Neutrino-induced events in bubble chambers filled with liquids in the A=20 range (Ber78, Efr80, Mat89) indeed show evidence for such shifts. Since it was found in these experiments that backward nucleons are observed in 5-10% of the deep inelastic events, there will be an adequate sample of events for making measurements on nuclear targets. However, the results with BEBC (Mat89) indicate the presence of a sizeable component of backward nucleons from multiple scattering, and thus considerable care must be taken in interpreting the data. The BEBC group was able to identify the shift effect on a neon target by cutting on events in which only a single backward nucleon was produced. Additional modeling will be required to understand whether backward protons from nuclear targets will yield interesting information with the Mark II detector when interpreted with the spectator model.

In a similar vein, it may be possible to determine the $\Delta\Delta$ admixture in the deuteron by measuring $ed \rightarrow e'\Delta X$ in deep inelastic kinematics, with the Δ detected at backwards angles, for which $\alpha_\Delta > 1$ (Fra90). It is estimated that

spectator Δ's should overwhelmingly dominate Δ's that rescattered. In addition, there are experimental observables which can further distinguish and enhance the spectator Δ mechanism, such as the Δ^{++}/Δ^0 ratio, and tagging the events with forward-angle pions. The first experiment testing these ideas, the BEBC neutrino scattering experiment (All86), was very encouraging. Their search for Δ^{++} in the kinematics corresponding to $\alpha_\Delta > 1$ established that the background was small, and they were able to set a limit $P_{\Delta\Delta} < 0.004$ at the 90% confidence level, limited only by the low statistics of the experiment.

References

(All86) D. Allosia *et al.*, Phys. Lett. **B174**, 450 (1986).

(Bal74) A. M. Baldin *et al.*, Sov. J. Nucl. Phys. **18**, 41 (1974)

(Bal75) A. M. Baldin *et al.*, Sov. J. Nucl. Phys. **20**, 629 (1975)

(Ber78) J. P. Berge *et al.*, Phys. Rev. **D18**, 1367 (1978)

(Deg90) P. V. Degtyarenko *et al.*, Z. Phys. **A335**, 231 (1990).

(Efr80) V. I. Efremenko *et al.*, Phys. Rev. **D22**, 2581 (1980)

(Fra81) L. L. Frankfurt and M. I. Strikman, Phys. Rep. **76**, 215 (1981), and references within.

(Fra90) L. L. Frankfurt and M. I. Strikman, Proc. of Les Houches School, 1990 (in press).

(Gav89) V. B. Gavrilov and G. A. Leksin, ITEP (Moscow) preprint ITEP 89-128.

(Mat89) E. Matsinos *et al.*, Z. Physik **C44**, 79 (1989).

(Str90) M. Strikman, private communication.

Table 1

y	x'	$N_{\alpha=1.0}$	$N_{\alpha=1.2}$	$N_{\alpha=1.4}$	$N_{\alpha=1.6}$	$N_{\alpha=1.8}$
0.17	0.32	2000000	1600	84.6	27.0	6.5
0.17	0.53	430000	330	18.2	5.9	1.4
0.24	0.23	2700000	2070	110.1	3.9	8.5
0.24	0.38	690000	530	28.5	9.4	2.2
0.24	0.53	200000	160	8.5	2.8	0.6
0.24	0.69	55000	42	2.3	0.7	0.2
0.31	0.18	2500000	2999	100.1	35.4	8.2
0.31	0.30	750000	580	31.2	10.2	2.4
0.31	0.41	270000	210	11.9	3.7	0.9
0.31	0.53	100000	80	4.2	1.4	0.3
0.31	0.65	34000	26	1.4	0.5	0.1
0.31	0.77	9900	7	0.4	0.1	0.0
0.38	0.15	2300000	1700	96.3	31.1	7.4
0.38	0.24	700000	550	30.5	9.8	2.3
0.38	0.34	290000	220	12.2	4.0	0.9
0.38	0.44	120000	98	5.3	1.7	0.4
0.38	0.53	54000	42	2.3	0.7	0.2
0.38	0.63	22000	17	0.9	0.3	0.1
0.45	0.12	2000000	1561	84.1	27.2	6.4
0.45	0.21	650000	500	27.0	9.0	2.1
0.45	0.29	280000	220	11.5	3.9	0.9
0.45	0.37	130000	100	5.7	1.9	0.4
0.45	0.45	66000	51	2.8	0.9	0.2
0.45	0.53	32000	24	1.3	0.4	0.1
0.52	0.11	1700000	1361	73.3	24.1	5.6
0.52	0.18	590000	450	24.2	8.1	1.9
0.52	0.25	260000	200	11.9	3.7	0.9
0.52	0.32	130000	100	5.7	1.9	0.4
0.52	0.39	72000	55	3.0	1.0	0.2
0.52	0.46	38000	29	1.6	0.5	0.1
0.59	0.09	1400000	1100	62.1	20.3	4.7
0.59	0.16	500000	390	21.6	6.9	1.6
0.59	0.22	230000	180	9.9	3.2	0.8
0.59	0.28	120000	96	5.2	1.7	0.4
0.59	0.34	70000	54	2.9	1.0	0.2
0.59	0.41	30000	30	1.7	0.5	0.1
0.66	0.08	1200000	960	52.4	17.1	4.0
0.66	0.14	430000	330	18.4	5.9	1.4
0.66	0.20	200000	160	8.7	2.8	0.7
0.66	0.25	110000	87	4.7	1.5	0.4
0.66	0.31	65000	50	2.7	0.9	0.2
0.66	0.36	39000	30	1.6	0.5	0.1

III.E. Study of Inelastic and Quasi-Elastic Scattering at Large x_{Bj}

In the original PEGASYS proposal of December 1988 we proposed several experiments to study coincident inelastic scattering off deuterium and other light nuclei in the range of x_{Bj} around 1. One proposal was to disentangle the quasi-elastic and inelastic part of the cross section by measuring the inclusive cross section with at least one additional pion in the final state (Section III.E. of the original proposal). We also proposed to study high-momentum components in the deuteron wave function via the reaction d(e,e'p) (Section III.K). Clearly, both experiments are not feasible in their original form with the Mark II detector in its present configuration, since the moderate resolution of the outgoing electron momentum leads to large error bars in the crucial quantity x_{Bj}. However, there are at least two avenues for resurrecting at least part of the physics program that these experiments addressed. One possibility would be a substantial upgrade of the energy resolution for forward going electron tracks in the Mark II, which could be achieved by either an improvement of the existing electromagnetic calorimeters (ECC, SAM) or by a dedicated forward spectrometer ("Mini-toroid"). Both options are presently under study by the PEGASYS collaboration (see Section IV.G. of this proposal), and at least one of them will likely be implemented for the second round of running at PEP. In that case both proposals would become feasible again, and actually would be dramatically improved by the vastly increased acceptance of Mark II for large angle protons and pions. Even in the present configuration, some of the original physics goals as well as additional issues can be addressed by looking for fully reconstructed events with only charged particles (and neutral pions) in the final state. For instance, by studying the exclusive reaction $d(e, e'pp\pi^-)$, one can:

a Reconstruct the momenta of all final state particles even if the electron energy is not well known, and determine either by missing mass resolution (compare Section III.M.), missing momentum cuts, or by hermicity arguments that all particles have actually been detected.

b Determine which proton was the spectator, using the fact that its momentum is in general lower and uncorrelated to the 3-momentum transfer **q**. The momentum distribution of these protons alone is a direct measurement (in the PWIA picture) of their initial momentum distribution in the deuteron.

c Reconstruct the invariant $p\pi^-$ mass and thus study excitation of the Δ resonance on a neutron, which is by itself an interesting topic and also is an important contribution to the non-quasielastic inclusive cross section.

We will continue to investigate these possibilities in more detail.

III.F. Nuclear Response to Deep Inelastic Scattering

Up to the present time there is very little information on the behavior of the nucleus when a momentary separation of color is created by deep inelastic scattering. In addition to the intrinsic interest in the dynamics of nuclear excitation following such a separation of color, this issue is of great relevance to the current search for a quark-gluon plasma in relativistic heavy ion collisions. The question of whether a quark-gluon plasma can really be formed in such collisions is critically dependent on how much of the energy of a struck quark is thermalized in the nuclear medium. Without this information heavy-ion theorists are faced with the problem of calculating complex reactions without a clear view of the underlying processes.

The amount of energy deposited in a nucleus via deep inelastic scattering and its modes of deexcitation are diagnosed by observing the types of particles emitted from the decaying nuclear system and their energy spectra. Ideally, it would be desirable to measure the spectra of neutrons, protons, and complex fragments at kinetic energies from a few MeV per nucleon to several hundred MeV per nucleon. Very recently, a group of PEGASYS collaborators have gotten a start on this problem by measuring the spectra of 1 to 10 MeV neutrons emitted from carbon, calcium, and lead targets in the Fermilab Muon Tevatron Experiment (E-665). Preliminary analysis shows that the measurements were successful, and should eventually yield information on the mean nuclear energy deposition in deep inelastic scattering.

The Fermilab measurements were undertaken partly as a test of the techniques planned for time-of-flight neutron detection in the PEGASYS spectrometer as originally conceived. While these measurements will not be possible with PEGASYS/Mark II, measurements of protons in the drift chamber from reactions with nuclear targets should yield complementary and potentially very interesting information. In particular, it should be possible to characterize the fraction of events in which the energy deposition is very large (typically 100 MeV or more) by looking for events with several protons energetic enough to penetrate into the drift chamber. The range of proton momenta that will be useful for these measurements is approximately 200 to 1000 MeV/c; particle identification should be possible in this range from time of flight and drift-chamber dE/dx. In contrast, events in which the residual nucleus is left fairly cold (excitation energies up to a few tens of MeV) will decay predominantly by neutron emission.

It should be possible to look for multi-proton events in the first round of running with PEGASYS/Mark II. Having a large acceptance for multiprong events with approximately isotropic emission of the nuclear decay products requires cutting

on events that occur well within the detector volume. Consequently, it will be necessary to use the small-angle monitors (SAM's) to detect the scattered electrons and identify the events as deep inelastic. Although the energy resolution in the SAM's is poor, even a crude determination of the Q^2 and ν should suffice to determine whether a significant fraction of deep inelastic events leads to a highly excited residual nucleus.

Count rates will be sufficiently high that a first look at the multiplicity of protons emitted from the target will be obtained easily in the first round of experiments with PEGASYS/Mark II. As an example, consider a xenon target, and deep-inelastic events in a bin 1 $(\mathrm{GeV/c})^2$ wide in Q^2 centered about $Q^2 = 2$ $(\mathrm{GeV/c})^2$ and 1 GeV wide in ν centered about ν=7 GeV. At a luminosity corresponding to a 12 hour beam lifetime, the event rate is approximately 200 per hour. The scattered electron angle is 7.8 degrees, and thus electrons from events at the center of the detector will hit the SAM toward its outside edge. If it is necessary to prescale the SAM by a factor of 20, the rate of recorded events will be 10 per hour, which is adequate to obtain a sample of 1000 events in this bin in about 4 days. Such a sample will be adequate to determine whether a significant fraction of the events (let us say 10%) show unusual properties, such as a high proton multiplicity. The resolutions in Q^2 and ν, which are less than 20% for the bin considered here, are adequate for an initial study.

We summarize this section by reiterating that the physics territory to be explored here is uncharted, and that the Mark II detector, because of its excellent coverage for wide-angle hadrons, is ideally suited to determine whether the physics is interesting with even a very short run. As a specific example of the potential interest of these measurements, we note the recent model of Gyulassy and Plümer (Gyu90) for hadronization following deep inelastic scattering in a nuclear environment (a very similar model has been proposed by Kopeliovich (Kop90)). This model predicts that the hadronization process is strongly modified by the nuclear medium, and that several low-mass (<2 GeV) strings will be produced inside the nucleus due to color exchange between the fast-moving quark and the nucleons in its path. The deexcitation of these strings may lead to a large energy deposition within the nucleus that could be detected by observing a large multiplicity of nuclear decay products.

References

(Gyu90) M. Gyulassy and M. Plümer, Nucl. Phys., to be published.

(Kop90) B. Z. Kopeliovich, Phys. Lett. B243, 141 (1990).

III.G. Inclusive Virtual Compton Scattering

Photon scattering is a fundamental second–order electromagnetic process. The $(e, e'\gamma)$ reaction provides new physics in the form of the longitudinal polarization and the mass (Q^2) of the virtual photon and the interference between the Bethe-Heitler (bremsstrahlung) and Compton amplitudes as shown in Fig. 1. By inclusive Compton scattering we refer to the $(e, e'\gamma)$ reaction on the proton or on nuclear targets in the deep inelastic regime: the net four-momentum transfer to the target $(q - k)$ and the final state hadronic mass are both large. The next section will discuss the prospects for virtual Compton scattering to exclusive nucleon final states.

In general, each electron-photon vertex in Fig. 1 contributes a factor of the electron charge to the associated amplitude. Therefore, the Compton amplitude changes sign when electrons are interchanged with positrons, whereas the Bethe-Heitler amplitude does not. Thus the Compton – Bethe-Heitler interference is directly measured by the difference

$$d\sigma(e^+, e^+\gamma) - d\sigma(e^-, e^-\gamma). \tag{1}$$

The Mark-II detector is nearly ideal for this experiment, with symmetric electromagnetic (EM) calorimeters and simultaneous electron and positron beams. The hadronic background (*e.g.* $\pi^0 \to \gamma\gamma$) is symmetric in $e^\pm$, and cancels in the difference (Eq. (1)). For deep inelastic Compton scattering, it is argued (Bro72) that the Compton amplitude involves a single (asymptotically) free quark. Thus the Compton amplitude depends upon the square of the quark charge and the Bethe-Heitler amplitude only linearly upon the quark charge. The interference term (hence the asymmetry) depends upon the cube of the quark charge, which can be written as a weighted sum of the quark charge and the baryon number. Thus (Bro72) predicts a scaling law for deep inelastic $(e, e'\gamma)$ and a sum rule which measures the quark charges.

A preliminary $p(e^\pm, e^\pm\gamma)X$ asymmetry measurement (at 13.5 GeV) is reported in (Fan77). With 3×10^{15} $e^\pm$ incident on a 12.5 cm liquid hydrogen target for $Q^2 > 1.5$ (GeV/c)^2, they measured 2366 $e^+p \to e^+\gamma X$ and 2161 $e^-p \to e^-\gamma X$ events: a $9\% \pm 3\%$ asymmetry. This large $(e^\pm, e^\pm\gamma)$ asymmetry is in contrast with the $0.3\% \pm 0.4\%$ asymmetry measured simultaneously in the single arm $e^\pm \to e^\pm X$ experiment, for which no asymmetry is expected.

At a luminosity of 10^{32} cm^{-2} sec^{-1}, PEGASYS will achieve the same integrated luminosity as in (Fan77) in approximately 4 months. The small angle monitor (SAM) is a near perfect match to the kinematic coverage of the previous experiment for both electrons and photons. However, the 2π azimuthal coverage in the SAM yields a Mark-II acceptance 25 times greater than that of (Fan77). Thus we can repeat the previous experiment in just 100 hours, and improve the statistical precision by a factor of 5 in a 90 day run. In addition to these improved statistics at the same kinematics, the 2π azimuth covers a wider kinematic domain.

Due to the high singles rate and poor resolution in the SAM, it may be impractical to use the SAM for this experiment in the first year of PEGASYS running. For $Q^2 > 4.0$ GeV^2, the Mark-II $(e, e'\gamma)$ acceptance is dominated by the End Cap Calorimeter (ECC). Monte Carlo calculations based on the $(e, e'\gamma)$ formalism of (Bro72) indicate the counting rate will be a factor of 10 lower in the ECC than the SAM. Thus in a 90 day run using only the ECC, we can achieve a factor of two improved statistics, but at a much higher Q^2 than the previous experiment. In addition, the ECC will cover a wider range of $(e, e'\gamma)$ kinematics, thus providing greater leverage for testing the scaling law predictions for this experiment. The systematic errors on our results will depend on how accurately we can model any asymmetries in the Mark II acceptance, and the dilution of the measured asymmetry from photons from π^0 decays. Studies are under way to estimate these errors.

References

(Bro72) S.J. Brodsky, J.F. Gunion, and R.L. Jaffe, Phys. Rev. **D6**, 2487 (1972).

(Fan77) D.L. Fancher *et al.*, Phys. Rev. Lett. **38**, 800 (1977).

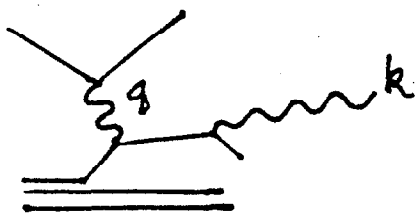

Figure 1a: Compton diagram: The virtual photon is absorbed on a target constituent which propagates before radiating the detected photon.

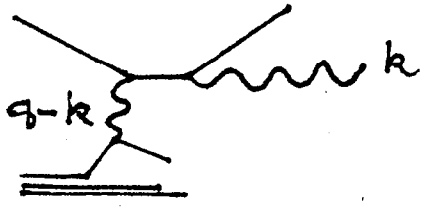

Figure 1b: Bethe-Heitler diagram: This is the radiative tail of deep inelastic electron scattering.

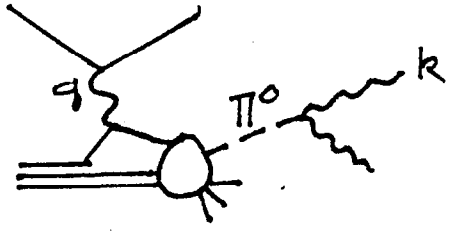

Figure 1c: Decay background: A π^0 (for example) is produced which decays into two photons, one of which is detected. Although kinematically identical, the hadron decay does not interfere quantum mechanically with a) and b) because the final states are in principle distinguishable.

III.H. Exclusive Virtual Compton Scattering

The exclusive virtual Compton reaction $p(e, e'\gamma p)$ at large Q^2 probes the nucleon wave-function in a complementary way to elastic scattering $p(e, e')p$. In addition, the Compton/Bethe-Heitler interference is sensitive to the phase of the Compton amplitude. A perturbative QCD (pQCD) calculation of virtual Compton scattering was recently published in (Far90). We will not argue the *a priori* validity of pQCD at the kinematics accessible to PEGASYS. Instead, we use these pQCD calculations as a guide to count rate estimates, and to our sensitivity to the underlying amplitudes. We note that additional theoretical work is in progress in this area, notably on a di-quark model in (Kro90).

The unpolarized exclusive Compton cross section depends upon five independent variables, including the incident electron energy. Thus the cross section is differential in four variables, not including the trivial dependence on the electron azimuth. A convenient set of variables is $Q^2 = -q_\mu^2$, $S = (q + P)^2$ or ν, $\cos\theta_{kq}^{CM}$ or $t = (q - k)^2$, and ϕ_{kq}. Here S is the invariant mass squared of the photon plus nucleon, θ_{kq}^{CM} is the photon scattering angle in the photon plus nucleon center of mass frame, t is the invariant momentum transfer to the nucleon, and ϕ_{kq} is the azimuth of the scattered photon around the virtual photon direction. The variable ϕ_{kq} is independent of boosts along the **q** direction.

The primary prediction of pQCD is a scaling law (Bro73) for the virtual photon absorption cross section:

$$S^6 \frac{d\sigma_\Lambda(\gamma, \gamma')}{dt} = \text{function of } Q^2/S,\ t/S \text{ only.} \tag{1}$$

The subscript Λ refers to the polarization state of the two virtual photons in the squared amplitude: L, T, LT, TT for longitudinal, transverse, and interference terms, respectively. The explicit dependence of the electron scattering cross section on the other variables (S, ϕ_{kq}) is then contained in a virtual flux factor (times S^{-6}) which can be evaluated in closed form from the equations of (Far90).

In Fig. 1 we plot the $p(e, e'\gamma p)$ cross section integrated over ϕ_{kq}, ϕ_e and the virtual photon flux for $S > 5$ GeV^2. The resulting cross section is differential only in the scaling variables Q^2/S and t/S (or $\cos\theta_{kq}^{CM}$). This cross section has the form

$$\frac{d\sigma(e, e'\gamma p)}{d(Q^2/S)d(\cos\theta_{kq}^{CM})} = \sum_\Lambda \frac{d\Gamma_\Lambda}{d(Q^2/S)} \left[S^6 \frac{d\sigma(\gamma, \gamma')_\Lambda}{dt} \right]_{Q^2/S, \cos\theta_{kq}^{CM}}, \tag{2}$$

where $d\Gamma$ is the virtual photon flux, differential only in Q^2/S. The curves in Fig. 1 are for $Q^2/S = 0.25$, 0.5, 0.75, and 1. The error bars in the figure are the

expected statistical error bars in bins of $[\Delta(Q^2/S), \Delta\cos\theta_{kq}^{CM}] = [0.25, 0.1]$ for a 90 day PEGASYS run at a luminosity of $1.6 \times 10^{32}\text{cm}^{-2}\text{sec}^{-1}$. We note that at $Q^2 = 0$, the pQCD calculations are a factor of ten lower than existing data. Thus our estimates in Fig. 1 are conservative.

At $Q^2/S = 0.25$, the pQCD calculation is dominated by the longitudinal term. This results from the sharp dip in the transverse amplitudes near $Q^2/S = 0.25$, as displayed in (Far90). This emphasizes that the virtual Compton reaction is not a simple extrapolation of the real Compton reaction, but contains new physics. The LT interference term, its sign, and expected error bars in extracting this term from the experimental azimuthal distributions are shown in Fig. 2. The change in sign at small angles results from the dramatic variation in phase in the underlying amplitudes. These figures indicate that the dramatic helicity dependent behavior seen in the pQCD calculations (Far90) will be manifest in the unpolarized $p(e, e'\gamma p)$ cross section.

Complete reconstruction of the Compton final state is critical to event triggering and background suppression for this experiment. The photons will be detected in the End Cap Calorimeter (ECC) with acceptance that is everywhere greater than 50%. The recoil protons will be tracked in the central drift chamber with comparable acceptance. At modest S (which dominates the counting rate) the electrons will be detected in the small angle monitor (SAM). Due to the high singles rate in the SAM, a very specific trigger must identify $(e, e'\gamma p)$ events. This can be formed by coincidence of a high energy electron in the SAM, a photon above an appropriate threshold ($\approx$ 2 GeV) in the ECC, and one additional charged track in the central drift chamber. The exact cut on photon energy required for triggering will restrict the kinematic acceptance at large photon angles. For $k > 2$ GeV and $S = 5$ GeV^2, $\cos\theta_{kq}^{CM} > 0.34$ at $Q^2/S = 0.25$, but $\cos\theta_{kq}^{CM} > 0.10$ at $Q^2/S = 0.50$. For $S = 7$ GeV^2 and $Q^2/S = 0.25$, $k > 2$ GeV requires $\cos\theta_{kq}^{CM} > -0.13$. Thus a wide kinematic zone can be explored, even with the cuts necessary for triggering.

In the original PEGASYS proposal, the primary source of background was expected to be from exclusive π^0 production, $p(e, e'p\pi^0)$ with only one of the γ's from the π^0 decay detected. The missing mass resolution from the detected electron and proton would have been good enough to ensure that more than one pion was not produced. From real Compton data (Shu79) it is known that the $p(e, e'\gamma p)$ to $p(e, e'\pi^0 p)$ cross section ratio is in the range of 1-5%. However, the γ's from unreconstructed π^0's form a broad distribution under the sharp peak due to exclusive Compton γ's in both the θ and ϕ distributions, so angular cuts would have produced an estimated signal-to-background of 3:1.

Simulations such as these have yet to be performed for the Mark II detector. Because the missing mass resolution will be worse than in the original PEGASYS, it will not always be possible to distinguish one-pion from multi-pion production, leading to more background from unreconstructed π^0's. On the other hand, the relatively good hermiticity of the detector should permit a very large percentage of π^0's to be vetoed because both photons would be detected. This percentage depends sensitively on the minimum photon energy that can be reliably detected in the various calorimeters, which in turn depends on background conditions with a gas target in the detector. This is one experiment that would benefit considerably from better energy resolution in an upgraded SAM.

Exclusive delta production $p(e, e'\gamma\Delta^+)$ and $n(e, e'\gamma\Delta^0)$ have similar cross sections to $p(e, e'\gamma p)$ (they are somewhat smaller according to (Far90)). The large acceptance of the Mark-II suggests that Compton Δ-production experiments on hydrogen and deuterium might also be feasible. These reactions would be detected as $p(e, e'\gamma\Delta^+ \rightarrow p\pi^0)$ and $d(e, e'\gamma p\Delta^0 \rightarrow p\pi^-)$.

Further study and practical experience with the Mark II will determine the feasibility of studying exclusive virtual Compton scattering from the proton, a reaction with a rich potential for helping to unravel the complex valence structure of the nucleon.

References

(Bro73) S.J. Brodsky and G.R. Farrar, Phys. Rev. Lett. **18** 1153 (1973).

(Far90) G.R. Farrar and H. Zhang, Phys. Rev. **D41** (1990) 3348; G.R. Farrar and H. Zhang, Phys. Rev. Lett. **D65** (1990) 1721.

(Kro90) P. Kroll and M. Schürmann, University of Wuppertal preprint WU B 90-15, July 1990.

(Shu79) M. Shupe *et al.*, Phys. Rev. **D19** 1921 (1979).

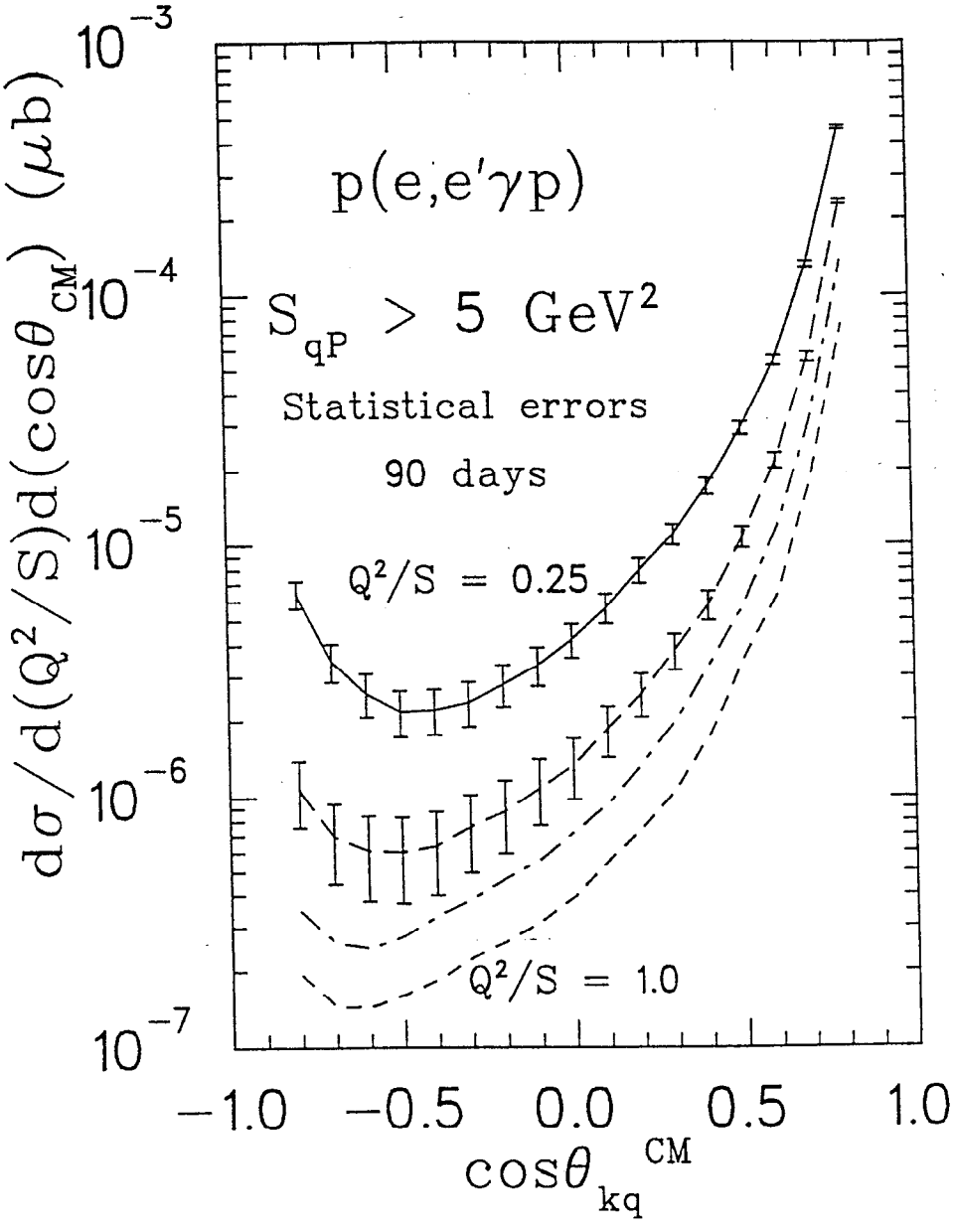

Figure 1. Differential cross sections (based on a pCQD model) and statistical error bars for a 90-day run for exclusive Compton scattering on the proton for Q^2/S = 0.25, 0.5, 0.75, and 1.0.

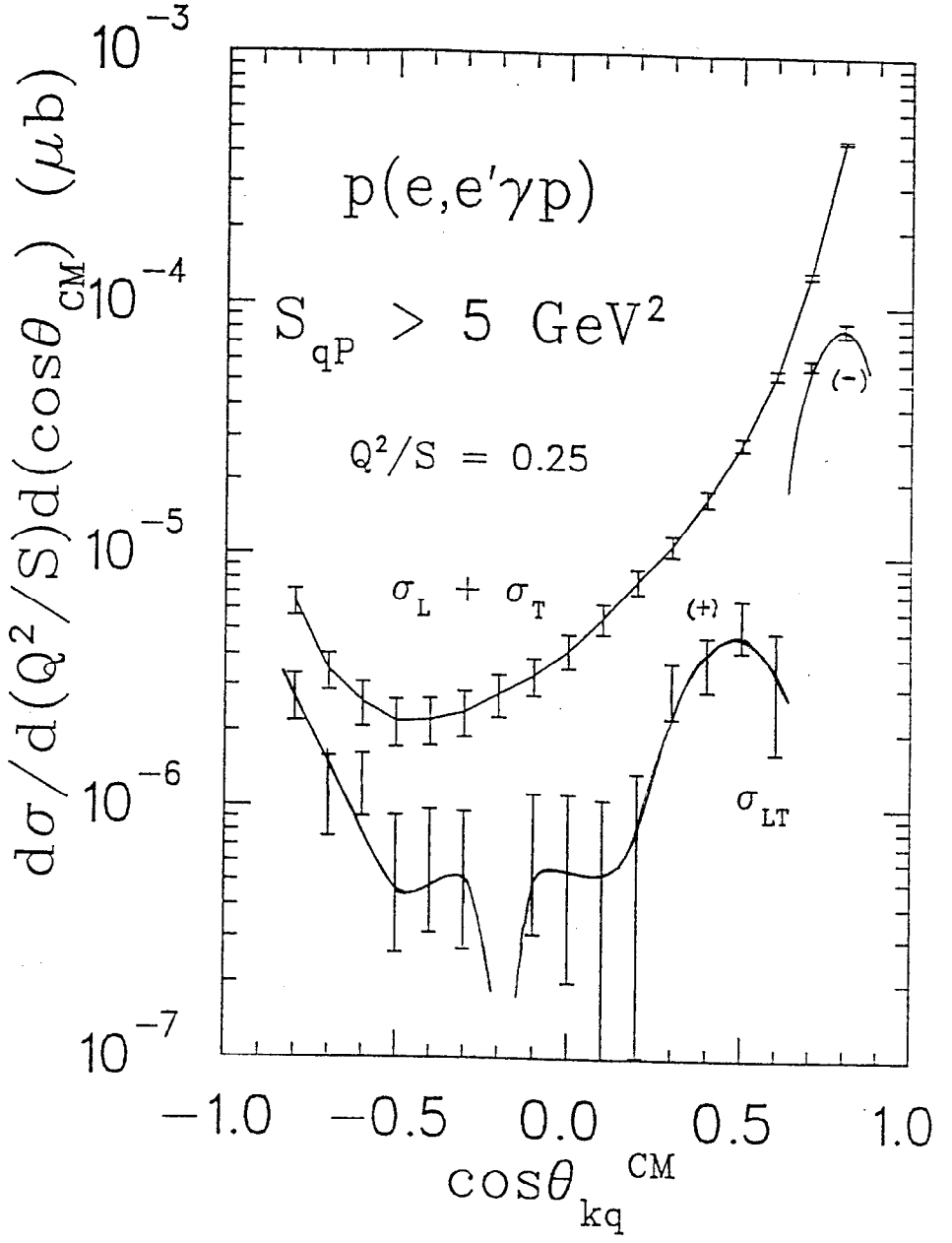

Figure 2. Same as Fig. 1, but showing the $(\sigma_L + \sigma_T)$ and σ_{LT} contributions separately for $Q^2/\mathrm{S} = 0.25$.

III.J. Precision Measurement of Internal Bremsstrahlung

All charged lepton scattering experiments must apply radiative corrections to obtain the final cross section. The magnitude of these corrections for electron scattering at SLAC energies are up to and sometimes larger than 30%. In principle they could be evaluated exactly if enough high-order Feynmann diagrams were evaluated. In practice (Bar82, Tsa71) the calculations stop at second order and approximations (e.g., exponentiation) are used to approximate higher order terms. With the advent of experiments (Das88) with statistical and systematic accuracies better than 1%, it has become important to make experimental tests of the radiative correction calculations.

The radiative corrections consists of both "external" and "internal" parts. The "external" is due to energy loss from bremsstrahlung and ionization by the electron in the target material both before and after the hard scattering on a particular nucleon. It is zero in the limit of very thin targets. The "internal" is due to real bremsstrahlung from the incoming and outgoing electron lines (as well as the hadron lines), virtual photon emission and absorption, and virtual pair production in the same diagram as the hard scatter. The "external" radiative corrections have been experimentally tested in SLAC Experiments E139 (Arn84) and E140 (Das88) to the 1% level by measuring cross sections from different target thicknesses at the same kinematics. The accuracy is limited by measurements of target thickness and can be improved in experiments in End Station A at SLAC. The "internal" corrections are more difficult to test, especially the effects of the virtual particles. The real photons from both "internal" and "external" bremsstrahlung have been measured by the EMC collaboration (Aub84, Aub81) using muons with energies of several hundred GeV. Their results agree with calculations based on the method of Tsai (Tsa71) in both energy and angular dependence within the errors of up to 30%. Clearly a more accurate measurement is needed for the more precise SLAC experiments.

PEGASYS/MarkII is suited for measuring the "internal" photon flux radiated by the scattered electron. The target is very thin so "external" corrections will be negligible. Most of the photon flux is peaked either along the incoming beam direction (s-peak) or along the scattered electron direction (p-peak). In PEGASYS the scattered electron is bent by the magnetic field sufficiently to spatially separate the p-peak photons from the scattered electron in the end-cap calorimeter. Unfortunately we will be unable to measure the s-peak because the photons go down the beam pipe with the beam. The measurement will consist of both a consistency check on radiative corrections and a direct comparison with theoretical calculation. The consistency check will compare the cross sections obtained by 1) using the entire measured energy of the p-peak (photons + electron) in the calorimeter

radiatively corrected for the very wide angle photons, with 2) the cross sections obtained using the electron energy measured in the Central Drift Chamber and the conventional radiative corrections. A direct detailed comparison of the measured and predicted photon angular and momentum spectrum can be done by examination of the spatial and energy distribution in the calorimeter. In addition we can measure the photon flux as a function of the atomic number of the target.

The counting rates are high and the measurement can be made over a large kinematic range. Electrons and photons go into the ECC with typical separations of between 2 and 4 cm depending on the momentum and angle. The ECC has a transverse granularity of 1.5 cm and a position resolution of 0.27 cm. Thus there will be some overlap between the scattered electron and the radiated photons. The end-cap calorimeter has an angular resolution of < 2 mr, which will enable us to measure the angular shape of the p-peak which is about $\sqrt{m_e/E'} \sim 10$ mr wide (Mo69). The background flux of photons from π^o decay are more uniformly distributed and will form a small background under the p-peak. The ECC is sensitive to photons with energies as low as 0.4 GeV.

Figure III-J-1 shows the fraction of the inclusive electron cross section as a function of the photon energy emitted in the p-peak region. The scattered electron has a detected energy of 6 GeV, but before internal bremsstrahlung may have had energies up to 11 GeV. Most of the cross section is at low photon energy due to the $1/E_\gamma$ shape of the bremsstrahlung spectrum. The effect of the resonances and elastic peak can be seen at high photon energies. The difference between the dashed and solid curves is the effect of soft photon radiation.

Table III.J.1 illustrates, for some selected kinematics, the number of events which include a bremsstrahlung energy greater than 0.5 GeV. The running conditions are: a luminosity of $1.7 \times 10^{32}\text{cm}^{-2}\text{sec}^{-1}$ for a 30 day run with a hydrogen target with an incident energy of 14.5 GeV. The events at each kinematics are for a scattered electron in an acceptance of ± 1.0 GeV and ± 2.5 degrees in scattering angle. The total electromagnetic energy in the p-peak must be greater than the trigger energy of 4.5 GeV, but the electron alone could have significantly less than this (e.g. a 2 GeV electron with 3 GeV of bremsstrahlung energy). Column 5 shows the total number of scattered electrons. Column 6 shows the calculated number of events which also include a "hard" photon of energy greater than 0.5 GeV. Between 1 and 7% of electrons have such a photon. The next column shows the number of events with total photon energy ("hard" + "soft") greater than 0.5 GeV. This includes the effect of multiple "soft" photons emission in addition to the "hard" photon. The calculation involves an infinite number of higher order diagrams, the effects of which can only be approximated by an exponential. The next column shows that the effect of these "soft" photons is estimated to be about

10% in the counting rate. The high statistics of this experiment enables us to measure the effects of these soft photons to an accuracy of better than 1% in most of our bins. In addition, the " soft" photons will be emitted along the direction of the scattered electron while many of the hard photons will be at larger angles.

As improvements are made on the Mark II detector much more data will be accumulated. In particular, upgrading of the forward angle detector will enable us to make measurements at smaller x, which is where radiative corrections have the greatest model dependence.

In conclusion, PEGASYS provides us with an opportunity to measure the bremsstrahlung spectrum from "internal" radiation and thus make an accurate test of a critical part of the radiative corrections procedure.

References

(Arn84) A. Arnold *et al.*, Phys. Rev. Lett **52**, 727 (1984).

(Aub81) J. J. Aubert *et al.*, Z. Phys. **C10**, 101 (1981).

(Aub84) J. J. Aubert *et al.*, Z. Phys. **C22**, 341 (1984).

(Bar81) D. Y. Bardin *et al.*, Nucl. Phys. **B197**, 1 (1982).

(Das88) S. Dasu, Ph. D. Thesis, University of Rochester (1988).

(Mo 69) L. W. Mo and Y. S. Tsai, Rev. of Mod. Phys. **41**, 205 (1969).

(Tsa71) Y. S. Tsai, SLAC-PUB-848 (1971).

Table III.J.1–BREMSSTRAHLUNG PHOTONS at E_o=14.5 GeV.
Electrons into acceptance $\Delta E' = 2GeV$ and $\Delta\theta = 5^o$
Luminosity= 1.7×10^{32} and 30 day run. $E_\gamma \geq 0.5$ GeV.

E'_e	θ	Q^2	x	$\times 10^3$ electron	hard Photon	hard+soft Photon	ratio	% error
2.00	10.00	0.88	0.04	2646	72731	69173	1.05	0.37
4.00	10.00	1.76	0.09	2059	147144	131943	1.12	0.26
6.00	10.00	2.64	0.17	1970	136643	119733	1.14	0.27
8.00	10.00	3.52	0.29	1927	96116	82199	1.17	0.32
10.00	10.00	4.41	0.52	1270	23638	19557	1.21	0.65
2.00	15.00	1.98	0.08	940	13604	12873	1.06	0.86
4.00	15.00	3.95	0.20	624	31650	27884	1.14	0.56
6.00	15.00	5.93	0.37	413	13810	11892	1.16	0.85
8.00	15.00	7.90	0.65	123	1261	1051	1.20	2.82
2.00	20.00	3.50	0.15	415	2478	2347	1.06	2.01
4.00	20.00	7.00	0.36	196	5265	4618	1.14	1.38
6.00	20.00	10.49	0.66	39	311	264	1.18	5.67
2.00	25.00	5.43	0.23	200	309	293	1.05	5.69
4.00	25.00	10.87	0.55	43	441	385	1.14	4.76

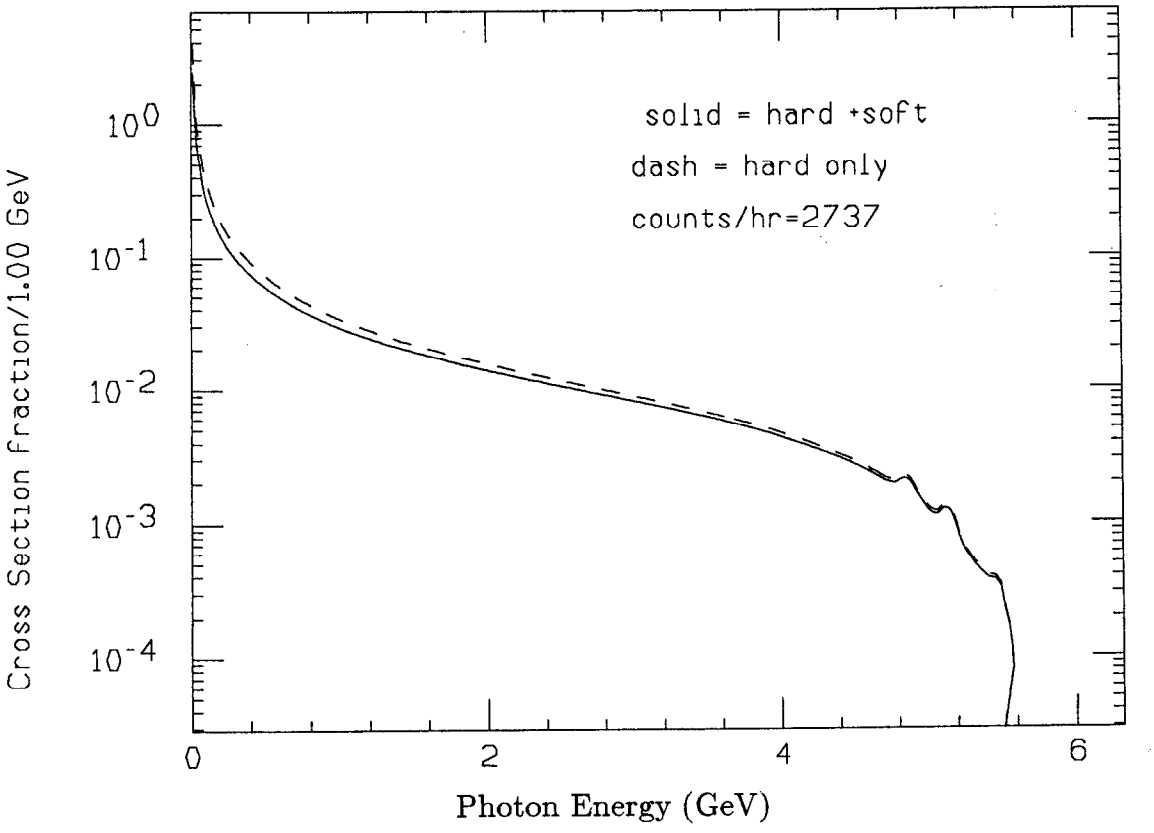

Figure III-J-1. The energy distribution of emitted photons. The vertical axis is the fraction of the cross section per 1.0 GeV which includes photons of total energy specified on the horizontal axis. The solid line is the "hard" photon calculation, while the dashed curve includes "soft" photons. The kinematics are for $E = 14.5$ GeV, $E' = 6$ GeV, $\theta = 10°$, $Q^2 = 2.64$ (GeV/c)^2, and $x = 0.17$.

III.K J/ψ production

The electroproduction of heavy quarks is an important test of perturbative QCD calculations and can serve as a probe of the quark-gluon structure of nuclei. As compared to light meson electroproduction, J/ψ electroproduction is unique because of the large mass of the charmed quark and the relatively simple quark structure of the J/ψ. Data from EMC, shown in Figure 1, demonstrate that the z distribution of J/ψ mesons, where $z = E_{J/\psi}/\nu$, is remarkably different from that of light mesons (Slo88). The cross section peaks at $z = 1$ and as z decreases the cross section falls; for light mesons the cross section peaks at $z = 0$ and decreases with increasing z. String hadronization models cannot describe this behavior of the J/ψ, presumably because the charmed quark is so massive. Since the energy threshold for photoproduction on the nucleon is 8.2 GeV, an experiment using PEP would cover the near threshold region of the electroproduction process. Near threshold, the total photoproduction cross section is believed to vary rapidly with energy, while high energy experiments ($\nu > 100$ GeV) have demonstrated a saturation of the photoproduction cross section with respect to photon energy. Figure 2 shows a compilation of total photoproduction cross sections as a function of photon energy.

The photon-gluon-fusion (PGF) model has had success in describing the high energy ($\nu > 100$ GeV) J/ψ electroproduction data from CERN and Fermilab, particularly in regions of low z and high p_T where perturbative QCD is expected to apply. PGF, diagrammed in Figure 3, is the lowest order QCD diagram for J/ψ electroproduction and is sensitive to the gluon structure of the nucleon. Berger and Jones (Ber81) have argued that the PGF model should be valid for $z < .9$ and $t > 1$ GeV^2, where t is the square of the four-momentum transfer to the residual hadronic system, $t = (p_{J/\psi} - q)^2$. To ensure a color singlet J/ψ, a minimum of two gluons must be exchanged in the PGF model, and the kinematic conditions ensure that the exchange gluons in the process are hard.

At PEP energies the PGF model may not be valid. Assuming a single hard gluon exchange in the PGF model, it can be argued that J/ψ photoproduction is sensitive to the gluon momentum distribution at a momentum fraction given by

$$\eta \approx \frac{\mathrm{t}}{2\mathrm{M}(\nu - \mathrm{E}_{\mathrm{J}/\psi})}.$$

For typical kinematics with PEGASYS, $\eta \approx 1$; for the CERN and Fermilab experiments η was less than 0.1. Figure 4 shows the gluon momentum distribution for the nucleon measured with J/ψ photoproduction, and the approximate momentum range that the experiments probed. At high values of η the gluon distribution is

vanishingly small and the PGF model should be near the limit of its reliability. Furthermore, at low photon energies it is known that coherent (elastic) production dominates. Coherent production is a higher order, possibly non-perturbative, QCD process.

At low photon energies it has been suggested that intrinsic charm should be the dominant mechanism for charm production (Hoy90). Arguments based on the uncertainty principle indicate that there should be a significant c-$\bar{c}$ component in the nucleon wavefunction at large x_B and large p_T, which is precisely the kinematic range that PEGASYS/Mark II covers most naturally. Furthermore, the intrinsic charm effect should be enhanced in multiquark clusters (*i.e.* nuclei) because of the overlap of light quarks. An important prediction of the intrinsic charm model, that can be easily tested with the Mark II, is that the J/ψ is a spectator in the production process and should be produced nearly at rest in the laboratory frame. This is in contrast to the PGF model where most of the photon energy is transferred to the J/ψ, which moves in the direction of **q**.

Assuming vector meson dominance, the incoherent J/ψ photoproduction cross section on a nucleus can be used to infer the J/ψ absorption cross section on a nucleon, σ(J/ψN). The technique is to measure the production cross section as a function of mass number, and then extract the absorption cross section from the mass number dependence. Recent data from Fermilab (Ald90) show a mass number dependence that goes as $A^{0.94}$, where A is the mass number, and absorption in the target nucleus with σ(J/ψN) in the range of 1-2 mb (Sok86). Brodsky and Mueller (Bro88) have pointed out that this analysis might be flawed because it neglects the possible effects of color transparency, i.e. the physical J/ψ state is actually produced outside of the nucleus. Farrar *et al.* (Far90) find a J/ψ formation length much shorter, and conclude that color transparency is of little importance at these energies. Clearly, this question merits further experimental work.

Trigger, acceptance and resolution

Detection of $\mu^+\mu^-$ or e^+e^- pairs from J/ψ decay, combined with its narrow width, gives the J/ψ a unique experimental signature. Acceptances for J/ψ detection were calculated using an event generator modeled on the z and p_T distributions measured by the EMC. To calculate the acceptance for $\gamma N \rightarrow J/\psi X$ events, where $J/\psi \rightarrow e^+e^-$ or $\mu^+\mu^-$, a Monte Carlo was written to simulate the size and resolution of the Mark II detector. For triggering on $J/\psi \rightarrow e^+e^-$ events, both tracks were required to deposit a minimum of 3 GeV of energy in the end-cap-calorimeter (ECC) or liquid argon shower counter. Monte Carlo studies have shown that the J/ψ acceptance is very sensitive to the low energy cutoff in the calorimeters; the lower the threshold the higher the acceptance. For example, it is much better to

require 3 GeV in both tracks than 5 GeV in a single track. From considerations of e/π separation, it is believed that 5 GeV is the lowest possible threshold for triggering on a single track. It is probable that requiring 3 GeV in two tracks will regain much of the background rejection lost in going to 3 GeV, although detailed background calculations must still be performed to prove this. For triggering on $J/\psi \rightarrow \mu^+\mu^-$ events, both muons were required to cross at least four super-layers in the central drift chamber (CDC), and to hit a muon chamber. The target interaction region was within ± 1 meter of the center of the detector.

The acceptance for $J/\psi \rightarrow e^+e^-$ rises from approximately 20% at $\nu = 9$ GeV to 30% at $\nu = 14$ GeV; variation of the acceptance with Q^2 is weak. The acceptance, while averaging around 25%, increases at higher photon energies because electrons from J/ψ decay become more energetic and more of them pass the energy cut in the calorimeter. The predicted FWHM of the J/ψ mass distribution is approximately 500 MeV, nearly independent of Q^2 and ν.

The Monte Carlo shows that most of the muon tracks are emitted at an angle of less than 45°. This result is nearly independent of Q^2 and ν. Since the muon counters on the Mark II only extend down to an angle of approximately 45°, acceptance for $J/\psi \rightarrow \mu^+\mu^-$ events is small and can be neglected when making count rate estimates. A future upgrade of the Mark II that adds muon chambers in the forward direction would greatly improve the acceptance for this decay mode.

Another possibility to increase the acceptance for J/ψ is to detect some of its hadronic decay modes, such as

$$J/\psi \rightarrow 2(\pi^+\pi^-)\pi^0$$

which has a branching ratio of 3.4%. This will be much more difficult than leptonic decay because of the numbers of particles involved. In the example above it will be necessary to detect four pions and two gamma rays. Nevertheless, we plan to seriously evaluate the prospects for observing the hadronic decays since they can only serve to increase our acceptance for J/ψ.

Untagged J/ψ rate

The J/ψ singles rate was estimated using the virtual photon flux, and detection of $J/\psi \rightarrow e^+e^-$ events. For a beam energy of 15 GeV the virtual photon flux for photon energies of 8 GeV to 14 GeV drops from 3×10^{-3} photons/GeV to 1.4×10^{-3} photons/GeV, so the average virtual photon flux over this interval was taken to equal 2.2×10^{-3} photons/GeV. In the threshold region the total cross section varies quite rapidly with photon energy. For a conservative rate estimate it was

assumed that the total photoproduction cross section is 1 nb/nucleon, independent of photon energy. Assuming a luminosity of $1.7 \times 10^{32}\mathrm{cm}^{-2}\mathrm{s}^{-1}$, a running time of 90 days on deuterium, and the use of both e^+ and e^- beams gives 5,700 J/ψ events. This is assuming 100% acceptance for detection of $J/\psi \rightarrow e^+e^-$ events.

It is expected that the average detector acceptance equals approximately 25%, giving approximately 1400 detected J/ψ per 90 day run, which is more than sufficient. An important measurement will be to study the mass number dependence of the coherent and incoherent cross sections averaged over photon energies from threshold to 15 GeV. Coherent and incoherent scattering can be isolated by placing cuts on p_T, and by the detection of additional hadronic tracks in the CDC. For coherent scattering, which is expected to dominate at PEP energies, it might be possible to reconstruct the photon energy by detection of the recoil proton.

Tagged J/ψ rates

To get a coincidence rate for $(e, e'J/\psi X)$ it is necessary to integrate the electroproduction cross section over the phase space covered by the Mark II, weighted by the acceptance for detecting $J/\psi \rightarrow e^+e^-$ events. EMC has parameterized the Q^2 and ν dependence of the $\gamma N \rightarrow J/\psi X$ reaction, and their parameterization was used to make cross section estimates. The electroproduction cross section is given by,

$$\frac{d^2\sigma}{dQ^2 d\nu} = \Gamma(\sigma_T + \epsilon\sigma_L)$$

where Γ is the virtual photon flux,

$$\Gamma = \frac{\alpha}{2\pi} \frac{2(1-y) + y^2 + Q^2/2E^2}{Q^2(Q^2+\nu^2)^{1/2}}$$

and $y = \nu/E$. σ_T and σ_L are the total J/ψ electroproduction cross sections for transverse and longitudinal photons. EMC fit the transverse cross section to a dipole form,

$$\sigma_T = \frac{\sigma(\gamma N \rightarrow J/\psi X)}{(1 + Q^2/M_d^2)^2}$$

where M_d is approximately equal to 4 GeV, and $\sigma(\gamma N \rightarrow J/\psi X)$ is the total photoproduction cross section. For these estimates it was assumed that σ_L is negligible. For a 90 day run on deuterium at a luminosity of $1.7 \times 10^{32}\mathrm{cm}^{-2}\mathrm{s}^{-1}$, and using both e^+ and e^- beams, the total number of coincident $(e, e'J/\psi X)$ events

were estimated as 230. The statistics for tagged production will be sufficient to examine rates as a function of ν and x_B, which can be used to test J/ψ production mechanisms.

Summary

We propose to investigate the threshold production of J/ψ mesons. At PEP energies the production mechanism is expected to be much different than that of the high energy experiments at CERN or Fermilab; the influence of intrinsic charm in the nucleon may be strong at low energies. Studies of the A-dependance will tell us about J/ψ propagation in nuclei. An experimental program of J/ψ production could start right away without any modifications to the Mark II. For triggering it will be necessary to lower the minimum energy in the calorimeters as far as possible, and it might be optimal to require two calorimeter hits of approximately 3 GeV. A conservative estimate for the nominal 90 day run on deuterium, gives approximately 1400 untagged J/ψ events, and approximately 230 tagged J/ψ events, with a mass resolution of approximately 500 MeV. Coherent (non-perturbative) production can be separated from incoherent (perturbative) production by placing cuts on p_T and by looking for additional hadronic tracks in the CDC. The rates for tagged production will be sufficient to bin the data as a function of ν and x_B, giving an important test of production models.

References

(Ald90) D. M. Alde *et al.*, to be published.

(Ber81) E. L. Berger, and D. Jones, Phys. Rev. D **23**, 1521 (1981).

(Bro88) S. J. Brodsky and A. Mueller, Phys. Lett B **206**, 685 (1988).

(Far90) G. R. Farrar, L. L. Frankfurt, M. I. Strikman, and H. Liu, Phys. Rev. Lett., **64**, 2996 (1990).

(Hoy90) Private communication, P. Hoyer and S. J. Brodsky.

(Slo88) T. Sloan, G. Smadja, and R. Voss, Phys. Rep. **162**, 45 (1988).

(Sok86) M. D. Sokoloff, *et al.*, Phys. Rev. Lett. **57**, 3003 (1986).

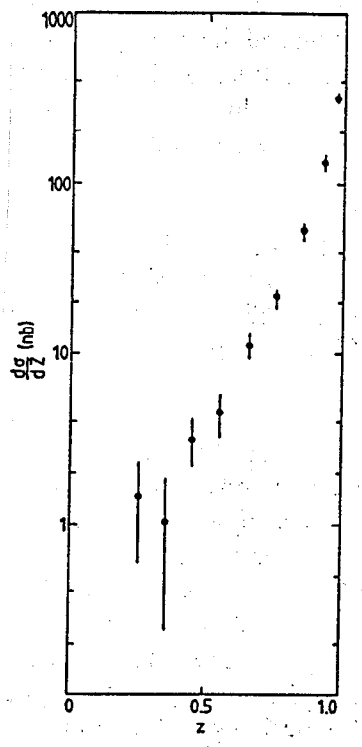

Figure 1. The measured z distribution for J/ψ production in deep inelastic muon scattering.

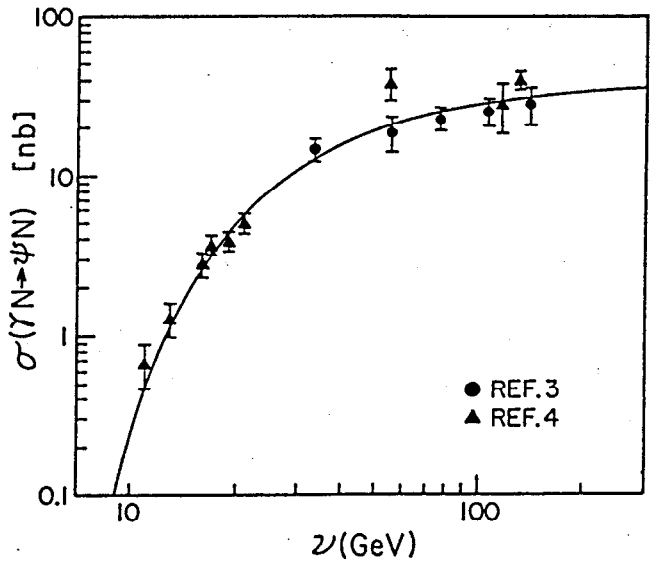

Figure 2. Total photoproduction cross sections for J/ψ. The curve is a photon-gluon fusion model fit to the data.

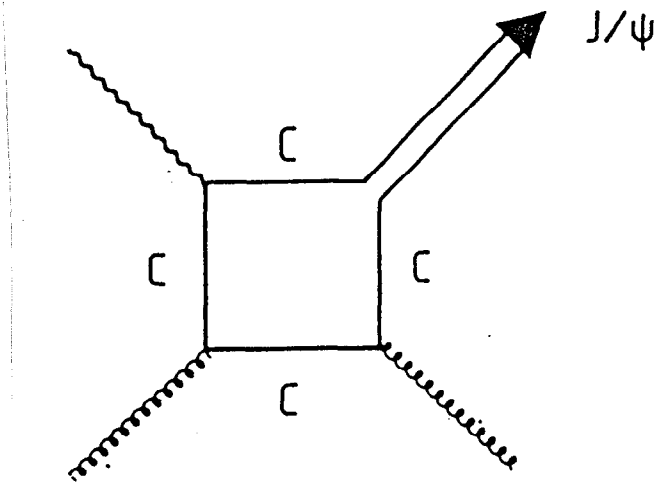

Figure 3. The photon-gluon fusion model for J/ψ production.

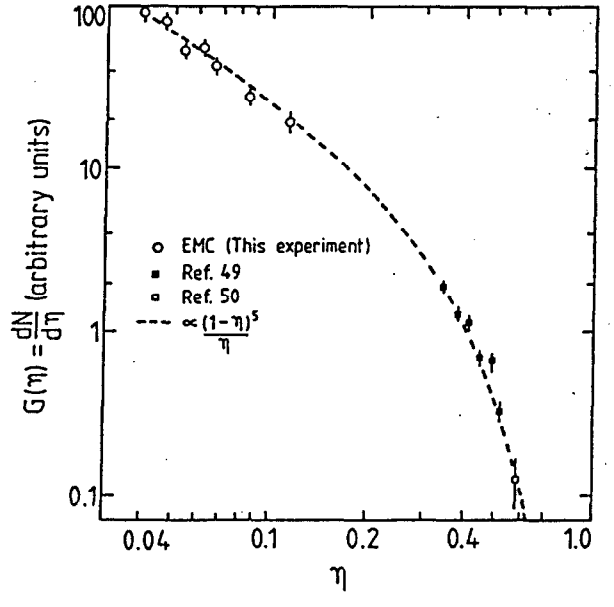

Figure 4. Gluon momentum distribution derived using the first-order photon-gluon fusion model. The curve shows the distribution $G(\eta) = 3(1-\eta)^5/\eta$ where the normalization is arbitrary.

III.L. Open Charm Production

Measurements of open charm production are interesting because they can be used to investigate the production mechanism of heavy quarks and the propagation of charmed particles through nuclei. Charmed baryons are difficult to produce from e^+ e^- experiments, because three quarks in association must be produced. In hadron collisions, charmed baryons are hard to study because of the many spectator quarks. Thus, photo- or leptoproduction appear the cleanest and most effective ways to study charmed baryons.

Part of the open charm produced is associated with the emission of a charmed hyperon. The cross section for associated charm production is expected to be larger than the J/ψ production cross section because the phase space available for the charmed quarks is larger in the case of associated charm. Indeed, in the case of the J/ψ production, the two charmed quarks need to be strongly correlated.

This effect has been observed by the EMC experiment (Aub83), in which 250-GeV muons were scattered from an iron target. Dimuon and trimuon events were detected and were shown to originate predominantly from charm production. The total cross sections for real photoproduction of open charm were obtained by extrapolating data to $Q^2 = 0$. Between 50 and 200 GeV, the open charm photoproduction was observed to be 20 times the J/ψ photoproduction cross section.

A parallel can be drawn between the comparison of associated charm and J/ψ production and the comparison of associated strangeness and ϕ production. The associated strangeness cross section is also 10 times bigger than the ϕ photoproduction cross section. The open associated charm production has been predicted by H. Fritzsch (Fri78) in a simple model of photon-gluon fusion. S. Brodsky (Bro90) assumes an important contribution to the cross section due to intrinsic charm must be added at threshold.

Lepto-photoproduction of Open Charm

In Table 1 the main channels for associated charm production and their threshold are listed.

Table 1

Reaction	Center of mass energy at threshold in GeV	Photon energy in Laboratory at threshold in GeV
(1) $\gamma\, p \rightarrow \Sigma_C^{++}\, D^-$	4.321	9.483
(2) $\gamma\, p \rightarrow \Sigma_C^{+}\, \bar{D}^0$	4.317	9.464
(3) $\gamma\, p \rightarrow \Lambda_C^{+}\, \bar{D}^0$	4.1495	8.706

The decay reactions of the charmed meson and the charmed hyperon can be classified in three categories:

A - The decay cascade of the particle to be studied involves only charged particles.

B - In the decays, only charged particles *and* photons are produced (and both types are detected).

C - Neutrinos, K_L^0 and neutrons are produced and will never be detected.

Among the known cascades of charmed mesons and hyperons, Table 2 gives the relative importance of the three categories.

Table 2

decaying particle	Rate of type A decay (%)	Rate of type B decay (%)	Rate of type C decay (%)
Σ_C^{++}	7.3	6.6	10
Λ_C^{+}	7.3	6.6	10
Σ_C^{+}	0	14	10
$D_C^{\pm}$	21	24	18
$\bar{D}_C^0$	16	47	14

These values are lower limits based on the known decays as listed in (PDG90): the actual rates will be higher when decay channels that have not yet been established are included. The Mark II detector, because of its large acceptance, allows the detection of all the charged particles and the photons with reasonable probability for many of the decay channels.

Count Rates

In this section we calculate the total rate for photoproduction of charmed baryons. We used the following parametrization of the associated charm production cross section:

$$\sigma(K) \;=\; \sigma(\infty)\,(\frac{K^*}{q^*})$$

where K is the meson momentum in the laboratory frame; q^* and K^* are respectively the photon and the meson momentum in the center of mass frame. It means that the matrix element does not depend on the photon energy, except through the phase space factor $(\frac{K^*}{q^*})$.

We considered associated charm production to originate dominantly from quasi-real photons. Their flux was conservatively evaluated using a 2% equivalent radiator. The number N^c of associated charm events per second was then given by:

$$N^c \;=\; .02 \times \int_{E_{th}}^{E_{max}} (\frac{dK}{K})\cdot\sigma(\infty)(\frac{K^*}{q^*})\cdot Lu$$

where Lu is the luminosity of the electron beam, E_{th} is the threshold for associated charm, and E_{max} is the threshold for the production of a $D\bar{D}$ pair (around 11.5 GeV). We used a luminosity of 10^{32} nucleons/cm^2/s.

The ratio of $\Sigma^+/\Lambda^+/\Sigma^{++}$ is 1/1/1 following simple quark permutation considerations. We use two values for $\sigma(\infty)$; one estimation (1.6 μb) by Fritzsch and the value measured by EMC (0.4 μb). Our results will be given for these two values of $\sigma(\infty)$. We obtain, depending on the hypothesis:

$\sigma(\infty)$	1.6 μb	0.4 μb
$\Sigma^{++} + \Sigma^+ + \Lambda^+$	1.3 counts/s	0.3 counts/s

Simulation

We next evaluated the percentage of the charmed baryons and mesons that would have all the decay products detected. We simulated the Mark II acceptance assuming a 15 GeV electron beam with the following hypothesis:

1 - We assume a 2-meter long uniform hydrogen target centered at the intersection point.

2 - For the category A and B events, all the charged particles were required to pass through at least 4 superlayers of the drift chamber. For the category B events, the photons were required to have a minimum energy of 200 MeV and hit either the ECC or the liquid Argon calorimeter.

3 - For each decay, the angular distribution depends only on phase space.

4 - The angular distribution in the center of mass of the initial reaction was taken to be:

$$\frac{d\sigma}{d\Omega} = (\frac{1}{2} + \frac{7}{18}\cos\theta)$$

by analogy to the process $\gamma + p \rightarrow K + \Lambda$.

As a first sample, we considered the following decays of charmed particles:

$$\Sigma_C^{++} \rightarrow \Lambda_C^+ \pi^+$$

$$\Lambda_C^+ \rightarrow (p\ K^-\ \pi^+)\ \ or\ \ (\Sigma^+\ \pi^+\ \pi^-)\ \ or\ \ (p\ \bar{K}^0)$$

$$\Sigma^+ \rightarrow p\ \ \pi^0$$

$$D^- \rightarrow (K^+\ \pi^-\ \pi^-)\ \ or\ \ (K^0\ \pi^-)$$

$$\bar{D}^0 \rightarrow (K^+\ \pi^-)\ \ or\ \ (K^0\ \pi^-\ \pi^+)\ \ or\ \ (K^+\ \pi^-\ \pi^0)$$

$$K_S^0 \rightarrow (\pi^+\ \pi^-)\ \ or\ \ (\pi^0\ \pi^0)$$

In Table 3 we list the global detection efficiency for these decays for the case when all decay particles are detected. It can be seen that these values are on the order of a few percent.

Table 3

decaying particle	Type A	Type B	Target conditions
Σ, Λ	2 %	0.4 %	target at $z = 0$ and
$D^0, \bar{D}^0$	5 %	1.5 %	Length=2 m

We estimate in Table 4 lower limits on the number of each particle type that would be produced and have all its decay products detected for a 90 day run at a luminosity of 10^{32} assuming $\sigma(\infty) = 1.6\mu b$.

Table 4

	Type A	Type B
Σ_c^{++}	> 5400	> 950
Λ_c^+	> 5400	> 950
Σ_c^+	> 0	> 1900
D^-	35000	12000
D^0	54000	47000

It can be seen that a substantial number of each particle type would be detected, allowing measurements of the decay angular distributions. Based on the results for lighter particles presented in section IV.E, it is expected that the mass resolution for these particles will typically be 1 to 10 MeV, small enough to clearly distinguish them from combinatorial backgrounds. It can also be seen that significant numbers of charmed particles would be produced even with 20 times less luminosity, thus allowing measurements of the overall A-dependence of open charm photoproduction.

Triggering

Two types of triggers are useful for identifying associated charm photoproduction. The first is in the case when the D meson decays weakly, producing an electron (18% for $D^{\pm}$, 7% for D^0). Studies are under way to determine the efficiency and cleanness of requiring an electron above some threshold in coincidence with a minimum of 3 or 4 other particles. A second trigger relies on the observation that most charmed particles produce many decay products. Thus a trigger that simply requires a minimum of 6 or 7 particles above some threshold should be reasonably efficient in keeping associated charm events, but have a small probability of triggering on most photoproduction events (which produce 1 or 2 particles) as well as most electroproduction events (in a sample of 1000 Lund events in which the electron is detected in the SAM or the ECC, only 10 had a detected multiplicity of 6 or more charged particles). Work is in progress to evaluate the efficiency and feasibility of these triggers. Although the production rates for electroproduction will be down significantly from the photoproduction rates, the triggering through the electron triggers designed for the bulk of the experiments in this proposal will be very efficient for high Q^2 events in which the electron scatters into the ECC, while the efficiency for low Q^2 events with the electron hitting the SAM will depend on the prescaling factor.

Summary

Although detailed studies are still being pursued, it appears likely that PEGASYS can contribute in a very clean way to several new areas of charm physics. Among these are:

1- The study of the charmed hyperons: their decay modes and polarization through the angular distributions of the decay products.

2- The determination of the charm production mechanism. For instance, intrinsic charm and photon-gluon fusion model predict different angular distributions for the charmed hyperons. Polarization observables could also be used to disentangle the models. If the photon-gluon fusion model is adequate, then it may be possible to extract information on the gluon distribution in the nucleon.

3- Electroproduction rates have yet to be evaluated, but crude estimates indicate that something like 10 to 1000 associated charm events may be observed in a 90 day run. If the rates are high enough, several interesting studies could be done: for example the Q^2-dependence of the ratio of the production rates of the Λ_C^+ and the Σ_C^+ could be compared to the Q^2-dependence of the Λ^0 and the Σ^0.

4- The study of photoproduction in nuclei, particularly its A-dependence. This should be very useful to check if the intrinsic charm is significantly related to short-range correlations, as claimed by S. Brodsky (Bro90).

5- Charmed particles can also be used to search for exotic states (see section III.M for a discussion of using strange particles for such studies).

6- We may be able to observe production of $D\bar{D}$ pairs and see the influence of opening this new channel on associated photoproduction.

While studies are still under way to evaluate the feasibility of open charm experiments with PEGASYS/MARK II, the first results indicate that associated photoproduction from light nuclei appears tractable, and many of the other topics listed above may also prove feasible.

References

(Aub83) J.J. Aubert et al, Nuclear Physics **B213** (1983) 31.

(Bro90) S. Brodsky, private communication.

(Fri78) H. Fritzsch and K.-H. Streng, Physics Letters **72B** (1978) 385.

(PDG90) Particle Data Group, Phys. Lett. B **239** (1990) 1.

III.M. Exclusive Kaon Production from the Proton and Deuteron

Introduction

Exclusive kaon production from the proton and deuteron using Mark II at PEP is interesting from several points of view. As will be seen below, we have the opportunity to increase the statistical accuracy of previous data by several orders of magnitude. This will allow the separation of the four cross section components, which is important for studies of the strange content of the nucleon and the kaon form factor. Measurement of K^0 final states will be possible for the first time (previous experiments only measured K^+). It will also be possible for the first time to tag the reactions with the final state Λ or Σ particles, which are detected with good probability in the Mark II. Since the Λ is polarization self-analyzing, good precision polarization measurements will accompany all cross section measurements. Measurements of kaon production from the neutron (which up to now are very limited) will be possible using the deuteron as a target. This target also offers the exiting possibility of observing possible narrow strangeness-1 dibaryon resonances for the first time.

The Elementary $p(e,e'K^+\Lambda)$, $p(e,e'K^0\Sigma^+)$, and $p(e,e'K^+\Sigma^0)$ Cross Sections

Motivation

Our present knowledge of the elementary exclusive kaon electroproduction cross sections from the nucleon can be described as scanty at best. We propose to greatly increase that statistical accuracy of present data and extend the kinematic range in Q^2, W^2, and θ^* (or t). This information is not only needed for studies of kaon production from nuclei (formation of hypernuclei), but is fundamentally interesting in its own right (Cot86) for 1) measuring the strange content of the nucleon, 2) an improved understanding of pseudo-scalar meson production, 3) improved knowledge of the kaon form factor and the $KN\Lambda$ and $KN\Sigma$ coupling constants, 4) determining if kaon PCAC (which is severely violated since $M_K \simeq 3M_\pi$) is a worthwhile concept, 5) further constraints on scaling and various SU(N) predictions, such as the ratio of Σ^0 to Λ production and 6) the transition from the VMD picture which dominates at low t to QCD descriptions of hard scattering at high t ($\theta^* \sim 90°$). Furthermore, tests of crossing calculations (Wil90) can be made by comparisons to radiative capture experiments, which have been improving in quality in recent years.

The cross section for exclusive kaon electroproduction can be written as

$$\frac{d\sigma}{dE'd\Omega d\Omega^*} = \Gamma[\frac{d\sigma_T}{d\Omega^*} + \epsilon\frac{d\sigma_L}{d\Omega^*} + \cos 2\phi\frac{d\sigma_{TT}}{d\Omega^*} + \cos\phi\sqrt{2\epsilon(\epsilon+1)}\frac{d\sigma_{LT}}{d\Omega^*}]$$

where ϵ is the photon polarization, Γ is the virtual photon flux, and θ^* and ϕ are defined with respect to the virtual photon direction. Separations of the four cross section components (which can be done by taking data with two different beam energies) is of particular interest, as an enhancement of σ_L at small θ^* (corresponding to small t, where t is the squared four-momentum transfer to the residual baryon) would likely indicate the influence of quasi-free scattering from the kaon, as has been seen in pion electroproduction. As in the case of the pion, the Q^2 dependance can then be used to determine the kaon form factor, while the x dependance at small Q^2 can be used to determine the strangeness content of the nucleon. The latter is of particular interest, as both the spin EMC effect (the low value for the Ellis-Jaffe sum rule found in the proton deep-inelastic spin structure function) and the large experimental value of pion-nucleon sigma term $\Sigma_{\pi N}(0) \sim 55$ MeV compared to the theoretical expectation of about 25 MeV indicate that the strangeness content of the nucleon may be much larger than expected (see extensive discussion in Ber89).

A large portion of all existing data for $p(e,e'K^+\Lambda)$ and $p(e,e'K^+\Sigma^0)$ are shown in Fig. 1 (from Bra79). It can be seen that the statistical accuracy was relatively poor, and the Q^2 range limited to 1.5 $(\mathrm{GeV/c})^2$ with W fixed at 2.21 GeV. This experiment found σ_{TT} and σ_{LT} to be small compared to σ_T, but the limited statistics did not permit meaningful separations. Since Rosenbluth separations were not done, photoproduction data and the Q^2 dependence at fixed t were used to determine that σ_L/σ_T is relatively small. However, the one experiment (Beb77) that made a Rosenbluth separation (varied ϵ) found results that are consistent with a significant σ_L contribution for $p(e,e'K^+\Lambda)$, although the errors are very large. Clearly much better measurements are required to establish if in fact σ_L is measurably large and can be used in constraining the strangeness content of the nucleon and determining the kaon form factor at low Q^2. At $Q^2 > 3$ $(\mathrm{GeV/c})^2$ the diagrams involving nucleon form factors are expected to decrease in importance, so Rosenbluth separations should not be needed to determine the Q^2 dependence of the kaon form factor at large Q^2.

Another topic of interest is the test of the quark-parton prediction for the ratio $p(e,e'K^+\Sigma^0)/p(e,e'K^+\Lambda)$ as a function of Q^2. The prediction is that the ratio should go to zero at high Q^2, with the rate of decrease being sensitive to the strange sea content. The upper and lower limits from (Nac74) are shown with existing data in Fig. 2. The predictions can be much more extensively tested by

a) extending the ratios to higher Q^2 and b) seeing if the rate of falloff depends on W^2. The Mark II offers a great advantage in this regard since the final state Λ's and Σ's can be detected and used to tag the reactions, whereas all previous experiments have determined the final state from the missing mass distributions, in which the Σ peak is difficult to disentangle from the tail of the much larger Λ peak.

Finally, detailed measurements of the separated cross sections σ_T, σ_L, σ_{TT}, and σ_{LT} as a function of Q^2, W^2, and θ^* will be of enormous value in constraining detailed models of kaon electroproduction, such as those of Cotanch and Hsiao (Cot86, Wil90), Cohen (Coh87), and Adelseck and Saghai (Ade90). A large body of data will constrain the assumptions about the underlying dynamics and determine the unknown parameters. Next to the kaon form factor, one of the greatest uncertainties is in the coupling to various resonances. By measuring the polarization of the Λ due to its self-analyzing polarization property, we will be able to determine the relative importance of resonance versus Born diagrams. The only polarization data in existence is from photoproduction, and is shown in Figure 3. It can be seen that the error bars are large, and several models which give good fits to the cross section data give quite large differences in polarization. We will be able to measure polarizations with statistical errors of from 0.03 to 0.2 as a function of Q^2, W^2, and θ^*, providing very strong constraints to the models.

A good knowledge of the elementary kaon production process will be necessary before experimental studies of hypernuclear bound states planned at CEBAF and elsewhere can be interpreted. It has been pointed out (Sag90) that different models of the elementary process can produce orders of magnitude difference in hypernuclear cross sections to bound states.

Kinematic Range and Rates

We have studied the kinematic range over which measurements of kaon electroproduction could be made with the Mark II in Phase I. Only the reaction $p(e,e'K^+\Lambda)$ was studied, although similar results will be obtained for the $p(e,e'K^0\Sigma^+)$ and $p(e,e'K^+\Sigma^0)$ reactions (although with count rates between 1 and 10 times smaller, depending on Q^2). To estimate the virtual photon cross sections, we used the fit of Bebek *et al.* (Beb77) to forward angle data ($\theta^* < 15°$) at $< W >= 2.15$ GeV

$$\frac{d\sigma}{d\Omega^*} = \frac{500\text{nb/sr}}{(1+Q^2/2.67)^2}$$

and made the approximation that the cross section is independent of θ^* and scales with W^2 as $p^*/W(W^2-M^2)$. At large Q^2, the actual cross sections near $\theta^* = 90°$ will be smaller than in this simple model. For a beam energy fixed at 15 GeV

and given values of E', $\theta_{e'}$ and θ^* , Monte Carlo selection of the production point (between 0 and 100 cm from the IP), the kaon polar angle ϕ^* and the c.m. decay angle for the decay of the Λ into a proton and a pion were made. The electron was considered to be detected if it impinged on the SAM or the endcap calorimeter within their fiducial volumes, and the resolution was determined using the calorimeter resolutions. The other three particles were considered to be detected if they passed through at least 3 superlayers in the drift chamber. Their momentum resolution was determined by the drift chamber and the multiple scattering by the beam pipe. The number of counts expected for a given bin in E', $\theta_{e'}$ and θ^* was determined using the probability of detecting all four particles, the 64% Λ decay probability into $p\pi^-$, a 1 GeV bin in E', a 0.5° bin in $\theta_{e'}$, a 30° bin size in θ^*, a luminosity of 2×10^{32}, and a running time of 90 days. The resulting count rates are shown for two representative values of $\theta_{e'}$ and three representative values of E' in Tables I and II. It can be seen that when the detection efficiency is reasonably high, the number of counts in a given bin is quite high; enough to further subdivide the data into many bins in ϕ^* and accurately separate $d\sigma_{TT}/d\Omega^*$ and $d\sigma_{LT}/d\Omega^*$. It can be seen that the kinematic region where the detection efficiency is small corresponds to large W^2 (where θ_q is small) and either small values of θ^* (where the kaon angle is too small to go through the drift chamber) or large values of θ^* (where the proton or pion from the Λ decay are emitted at too-small angles). This situation would be much improved in Phase II with the addition of a forward-angle hadron identification capability. Even in Phase I it can be seen that a large kinematic range (Q^2 up to 6 $(\mathrm{GeV/c})^2$, W^2 from threshold to 20 $(\mathrm{GeV})^2$, range in θ^* depending on W^2) can be covered with at least 1000 counts per bin. This represents a vast improvement over existing data, which generally only covered the region near $W = 2$ GeV and Q^2 up to 1.5 $(\mathrm{GeV/c})^2$, and had insufficient statistics to meaningfully separate the four cross section components.

It is important to tag the reactions as exclusive. If the Λ were not detected, the missing mass resolution would not be adequate to isolate the Λ from the Σ final state. However, by tagging all final state particles, the missing mass resolution (shown under $\sigma(W)$ in Tables I and II) is generally less than the pion mass, so the production of an additional pion could be excluded. Also shown in these Tables is the Λ invariant resolution, which is generally on the order of a few MeV, small enough to distinguish Λ's from random $\pi^-\pi^+$ pairs, which is of importance because protons and pions cannot be reliably separated above a few GeV momentum. Once a Λ has been identified, the kaon can be separated from a pion by conservation of strangeness if the momentum is too large for other techniques to work.

A further experimental advantage of the $p(e,e'K^+\Lambda)$ reaction is that the Λ typically decays 5 to 15 cm from the primary vertex. The tracking from the drift chamber is good enough to use this feature in identifying Λ's. As mentioned above, the most exciting feature of detecting the Λ (which was not done in any of the previous experiments) is that it is polarization self-analyzing, given by $N(\theta) = [1 + (0.62 \pm 0.07)P_\Lambda \cos(\theta)]/4\pi$, where θ is the c.m. angle between the direction of the Λ polarization and the proton momentum (Cro63). For a given number of Λ's in a given kinematic bin N, this gives a statistical error on $P_\Lambda \sim 2/\sqrt{N}$, or typically 0.01 to 0.2. Systematic errors depend on a good knowledge of the acceptance function, and may be less than 0.03. This is smaller than the photoproduction errors, and can be used to isolate the resonant components (which produce large Λ polarizations) from the Born terms (which leave the Λ unpolarized) as a function of Q^2, W^2, and θ^*.

While the Mark II offers a great opportunity to separate $\sigma_T + \epsilon\sigma_L$, σ_{TT}, and σ_{LT} with Λ polarization over a large range of Q^2, W^2, and θ^* in Phase I, one of the most interesting tasks, the separation of σ_L and σ_T at small θ^* is somewhat compromised. Table III illustrates the number of counts expected in 90 day runs at 7 and 15 GeV as a function of Q^2 for $W^2 \sim 4$ (GeV)^2. It can be seen that the typical error on $R = \sigma_L/\sigma_T$ is 0.15 to 0.3, which is considerably smaller than the errors of typically 0.8 of (Beb77), and small compared to the values seen in pion electroproduction. However, the errors are largest at small Q^2. These errors could be greatly reduced by making measurements at larger W^2, where the difference in ϵ is larger. This requires detection of kaons at smaller angles than presently allowed by the drift chamber, and so the efficiency vanishes. If we have the ability to identify kaons at small angles in Phase II, we would be able to reduce the error on R to less than 0.1 even at small Q^2. Another handle on the longitudinal contributions will come from measurements of σ_{LT}, which measures the interference between transverse and longitudinally polarized photons, and does not require a Rosenbluth separation to measure. The tradeoffs between these two methods have not yet been evaluated.

Detailed Monte Carlo studies have not been done for the $p(e,e'K^+\Sigma^0)$ and $p(e,e'K^0\Sigma^+)$ reactions, but Σ^+ should be detected with good efficiency from the 52% decay probability into $p\pi^0$, while the Σ^0 decays to $\Lambda\gamma$. This will permit the first measurements ever of the ratio of K^+/K^0 production tagged on a final state Σ. The cross sections are typically an order of magnitude smaller than for Λ production, but the rates will still be quite reasonable integrated over a 90-day run.

Exclusive Kaon Production from the Deuteron

Kaon Production from the Neutron

There are two principal topics of interest in kaon electroproduction from the deuteron. The first topic is the comparison of cross sections from the proton and neutron, using the deuteron as a source of quasi-free neutrons. Previous measurements (Beb77, Qui79 which is photoproduction only) are even more scanty and imprecise than measurements from the proton. As shown by (Cot86), measurements from the deuteron not only provide additional constraints on the kaon form factor and effective coupling constants, but are also sensitive to relativistic effects and final state KN and ΛN interactions. Kaon electroproduction has an advantage over pion electroproduction in such studies because the relatively weaker KN interaction makes the calculations more tractable. The rates for this production from a neutron should be very comparable with the rates from the proton discussed in the previous sections, which are reasonably good. However, we have found that the missing mass resolution in Phase I if the spectator proton is not detected is several hundred MeV, insufficient to clearly determine if an extra pion was produced. This problem can be overcome in two ways: 1) assuming that the spectator protons are emitted approximately isotropically with a momentum distribution given by the deuteron wave function, about 15% of them will be detected (the losses are mainly due to energy loss in the beryllium pipes) and 2) making a scaled subtraction of events in which a pion is detected (the subtraction should not be large due to the good efficiency for detecting pions). We therefore conclude that meaningful comparisons of separated cross sections from the proton and neutron will be possible over a large kinematic range. It will be especially interesting to compare Σ and Λ cross sections. For example, the ratio of photoproduction data from the deuteron compared to the proton

$$R = \frac{(\gamma d \rightarrow K^+\Sigma^0 n) + (\gamma d \rightarrow K^+\Sigma^- p)}{(\gamma p \rightarrow K^+\Sigma^0)}$$

is expected to be 3.0 (Cot 88) in the impulse approximation if there is no isospin 3/2 strange boson contribution (there are none known). A 6% contribution of an exotic $I = 3/2$ was found to be necessary to reproduce the experimental value of $2.37 \pm .11$. Electroproduction studies will determine if this interesting anomaly persists at finite Q^2.

Search for Dibaryon Resonances

The second topic of interest in kaon production from the deuteron is a search for possible narrow strangeness-1 dibaryon states. Space does not permit a review of the considerable literature on dibaryons. While it is generally accepted that six-quark configurations other than the deuteron should occur with finite probability, experimental evidence to date suggests that the non-strange states are relatively weak and no narrow resonances have been unambiguously observed, although many candidates have come (and most have gone). For a review, see *e.g.* (Loc87). The best chance to observe narrow dibaryon resonances may be in the strange sector. There are two types possible. The H dibaryons are the analog of the deuteron and belong to the color representation $(Q^6)_1$. In the MIT Bag model of Jaffe (Jaf77) the two lightest members of the octet are the H_1^0 and H_1^+ with masses of 2.220 to 2.230 GeV. These are above $\Lambda N\pi$ threshold and couple strongly to BB states (where B is a baryon), and so are expected to be quite wide (Aer85). However, dibaryon states can also be formed with $(Q^4)_3-(Q^2)_3$ color configurations. The two lightest are the D_s and D_t, with masses calculated to be 2.11 and 2.16 GeV respectively (Mul80), just above the ΛN threshold of 2.05 GeV. Since they are below pion threshold and do not couple easily to a BB final state, they are expected to be very narrow, on the order of 1 MeV (Aer85). While the absolute value of the D_s and D_t masses is somewhat uncertain, the mass difference of about 50 MeV is much less model dependent. The advantage of using photons beams to search for these states is that both can be excited, while with a kaon beam (used in all searches to date) only the D_t can be produced at forward angles. A peak has in fact been seen (Pig85) in the $d(K^+,\pi^-)$ reaction, but its mass (2129 MeV) is almost coincident with the Σ^+n threshold, and so cannot be distinguished from a cusp effect.

The best way to search for these possible resonances at PEP would be with the $D(e,e'K^0\Lambda p)$ reaction, in which all final state particles can be detected since the Λ decays most of the time to a $p\pi^-$ pair and the K^0 has a good decay probability into $\pi^+\pi^-$. The $D(e,e'K\Lambda n)$ reaction can also be studied, but the poor efficiency for detecting neutrons means that they would have to be identified by the missing mass, and the relatively poor electron resolution generates a neutron missing mass resolution of typically several hundred MeV, making it difficult to tell if an additional pion was produced. For this reason, we have chosen the $D(e,e'K^0\Lambda p)$ reaction for detailed Monte Carlo studies of resolutions and efficiencies.

Detection Efficiencies and Resolutions for Dibaryon Search

In order to study the detection efficiencies and resolutions, a simple Monte Carlo program was written that for a specific beam energy of 15 GeV and selected values of Q^2 and W^2 generates a neutral kaon and a dibaryon final state of mass M_{Ds} isotropically in the c.m. system. For simplicity, only the results for M_{Ds}

of 2.11 GeV are shown, but the conclusions are similar for higher masses. The dibaryonic state then decays isotropically in the c.m. to a nucleon and a Λ. The Λ decays into a proton and a π^-. The neutral kaon is assumed to decay into a charged pion pair, although the dibaryon mass resolution would not be affected much if the decay were into three neutral pions, and the detection probability and kaon identification would still remain good. Multiple scattering effects and drift chamber resolutions are then applied to each charged particle. For the electron, the calorimeter information is used to define the momentum. In order to be considered as detected, a charged particle must pass through at least 3 superlayers of the drift chamber. The production point was chosen at random from 0 to 100 cm from the center of the detector.

Some results of the study of the $D(e, e'K^0\Lambda p)$ reaction are shown in Table IV. Electron kinematics were chosen that span the available missing mass W_d (defined using a deuteron target) region for moderate Q^2 values. It can be seen that the detection probability of the two protons and the pion needed to define the dibaryon invariant mass is quite high and relatively insensitive to the electron kinematics. Adding the requirement that the kaon be detected to identify the reaction as strangeness-producing only reduces the efficiency slightly, to about 0.33. As was seen in the studies of Lund-generated events, the mass resolution for K_0 and Λ is only a few MeV, and combined with the vertex offset of typically 10 to 20 cm can be used to clearly identify these final states, even though the pions and protons from their decay cannot be individually identified above about 1.5 GeV/c. The D_s resolution increases slowly with W^2 and Q^2, but remains below 5 MeV, comparable to the predictions. Thus the resolution is very well matched to a search for possible narrow states.

Also given in the table are the average production angles and momenta for each particle. The production angles are generally in the forward direction, as expected, and become smaller as Q^2 increases. Increasing Q^2 also increases the average particle momenta. The proton from the D_s decay becomes difficult to distinguish from a pion at high W^2, but conservation of baryon number and charge can be used to help. Note that the average proton momenta for D_s production are much higher than if the proton was a spectator to quasi-free electroproduction form the neutron. Even if no resonance is found, events with large proton momenta will allow the study of final state interactions and help in our understanding of the relatively poorly known ΛN interaction.

Conclusion

The counting rates, resolutions, and particle identification for exclusive kaon electroproduction from the proton and deuteron are sufficient to greatly increase our knowledge of this relatively poorly-understood process over a wide range of kinematics. The ability to measure the polarization of the produced hyperons will be of particular value in constraining models and testing SU(3) constraints. The experiments are very feasible for the Mark II in Phase I, although as for all electroproduction experiments would benefit from improved forward-angle particle measurements and a higher-rate data taking ability.

References

(Aer85) A. T. M. Aerts and C. Dover, Nucl Phys. B253, 116 (1985).

(Ade90) R. Adelsek and B. Saghai, Phys. Rev. C42, 108 (1990).

(Beb77) C. J. Bebek *et al.*, Phys. Rev. D15, 594 (1977) and Phys. Rev. D15 3082 (1977).

(Ber89) R. Bertine, Nucl. Phys. A497, 307c (1989).

(Bra79) P. Brauel *et al.*, Z. Physik C3, 101 (1979).

(Coh86) J. Cohen, in Report of the 1986 Summer Study Group, Research Program at CEBAF (II) p305-374 and references therein, such as Phys. Rev. C32, 543 (1985) and Phys. Lett. 153B, 367 (1985).

(Cot86) S. Cotanch and S. Hsiao, Nucl. Phys. A450, 419 (1986); Czech J. Phys B36, 426 (1986); Phys. Lett. 163B, 300 (1985).

(Cot88) S. Cotanch, Int. Conf. on Medium and High Energy Nuclear Phys., Taipei, Taiwan (1988). Proceedings (1989 W.-Y. P. Hwang, K. F. Liu, Y. Tzeng, ed.) p. 666-678.

(Cro63) J. Cronin and O. Overseth, Phys. Rev. 129, 1795 (1963).

(Loc87) M. P. Locher, M. E. Sainio, A. Svarc, Advances in Nuclear Physics, Vol 17, 47 (1987).

(Mul80) P. Mulders, A. Aerts, J. de Swart, Phys. Rev. D21, 2653 (1980).

(Nac74) O. Nachmann, Nucl. Phys. B74, 422 (1974).

(Pig85) C. Pigot *et al.*, Nucl. Phys. B249, 172 (1985).

(Qui79) D. J. Quinn *et al.*, Phys. Rev. D20, 1553 (1979).

(Sag90) B. Saghai, private communication.

(Wil90) R. Williams, C.-R. Ji, S. Cotanch, Phys. Rev. D41, 1449 (1990).

$\theta_{e'} = 5.0$, $E' = 5.0$ GeV, $Q^2 = 0.57(\text{GeV/c})^2$, $W^2 = 19.5$ $(\text{GeV})^2$, $\epsilon = 0.59$										
θ^*	Det. Eff.	Counts	$\sigma(W)$	$\sigma(M_\Lambda)$	$<\theta_K>$	$<\theta_p>$	$<\theta_\pi>$	$<P_K>$	$<P_p>$	$<P_\pi>$
(deg)		90 days	(GeV)	(GeV)	(deg)	(deg)	(deg)	(GeV/c)	(GeV/c)	(GeV/c)
15	0.00	0	0.000	0.000	0.0	0.0	0.0	0.0	0.0	0.0
45	0.03	432	0.128	0.002	13.9	32.7	38.1	7.8	2.5	0.4
75	0.59	10513	0.141	0.002	19.1	24.9	26.2	6.1	4.0	0.7
105	0.36	6379	0.117	0.003	27.4	18.0	19.3	4.2	5.5	1.1
135	0.01	130	0.091	0.003	38.7	13.5	15.0	2.6	6.6	1.7
165	0.00	0	0.000	0.000	0.0	0.0	0.0	0.0	0.0	0.0
$\theta_{e'} = 5.0$, $E' = 8.0$ GeV, $Q^2 = 0.91(\text{GeV/c})^2$, $W^2 = 13.1$ $(\text{GeV})^2$, $\epsilon = 0.83$										
θ^*	Det. Eff.	Counts	$\sigma(W)$	$\sigma(M_\Lambda)$	$<\theta_K>$	$<\theta_p>$	$<\theta_\pi>$	$<P_K>$	$<P_p>$	$<P_\pi>$
(deg)		90 days	(GeV)	(GeV)	(deg)	(deg)	(deg)	(GeV/c)	(GeV/c)	(GeV/c)
15.	0.00	0.	0.000	0.000	0.0	0.0	0.0	0.0	0.0	0.0
45.	0.17	4121.	0.125	0.002	16.0	35.9	37.6	5.7	1.6	0.3
75.	0.76	25668.	0.124	0.002	21.7	27.5	29.6	4.3	2.9	0.5
105.	0.51	17224.	0.099	0.002	30.8	21.0	23.7	2.9	4.1	0.8
135.	0.10	2390.	0.092	0.002	46.8	15.8	18.3	1.6	5.2	1.0
165.	0.00	0.	0.000	0.000	0.0	0.0	0.0	0.0	0.0	0.0
$\theta_{e'} = 5.0$, $E' = 11.0$ GeV, $Q^2 = 1.26(\text{GeV/c})^2$, $W^2 = 7.1$ $(\text{GeV})^2$, $\epsilon = 0.95$										
θ^*	Det. Eff.	Counts	$\sigma(W)$	$\sigma(M_\Lambda)$	$<\theta_K>$	$<\theta_p>$	$<\theta_\pi>$	$<P_K>$	$<P_p>$	$<P_\pi>$
(deg)		90 days	(GeV)	(GeV)	(deg)	(deg)	(deg)	(GeV/c)	(GeV/c)	(GeV/c)
15.	0.09	2350.	0.091	0.001	15.6	30.3	53.1	3.6	0.6	0.1
45.	0.35	24735.	0.105	0.002	20.9	31.5	42.5	3.2	1.0	0.2
75.	0.73	71475.	0.083	0.002	25.9	29.8	34.0	2.5	1.8	0.3
105.	0.57	55880.	0.081	0.002	36.1	25.5	28.7	1.6	2.6	0.5
135.	0.32	22832.	0.091	0.002	58.2	19.7	23.6	0.8	3.2	0.6
165.	0.05	1219.	0.096	0.003	81.1	15.1	18.1	0.3	3.5	0.7

Table I. Kinematics, detection efficiencies, and counting rates for the $p(e, e'K^+\Lambda)$ reaction at $\theta_{e'}$=5° and three values of E'. The detection efficiency is to detect all four final state particles (electron, kaon, and proton and pion from the Λ decay). The number of counts is for a simple cross section model and requires all four final particles to be detected, for a luminosity of 2×10^{32} and a 90 day run. Bin sizes of 1 GeV in E', 0.5° in $\theta_{e'}$, 30° in θ^*, and 2π in ϕ^* were used. The resolution for the four-particle missing mass is listed under $\sigma(W)$ and is always less than the pion mass. The Λ invariant mass resolution $\sigma(M_\Lambda)$ is also given, along with the average production angles and momenta for the kaons, protons, and pions.

$\theta_{e'} = 10.0$, $E' = 5.0$ GeV, $Q^2 = 2.28(\text{GeV/c})^2$, $W^2 = 17.4$ $(\text{GeV})^2$, $\epsilon = 0.59$										
θ^*	Det. Eff.	Counts	$\sigma(W)$	$\sigma(M_\Lambda)$	$<\theta_K>$	$<\theta_p>$	$<\theta_\pi>$	$<P_K>$	$<P_p>$	$<P_\pi>$
(deg)		90 days	(GeV)	(GeV)	(deg)	(deg)	(deg)	(GeV/c)	(GeV/c)	(GeV/c)
15	0.00	0	0.000	0.000	0.0	0.0	0.0	0.0	0.0	0.0
45	0.05	122	0.101	0.001	14.7	30.8	29.3	8.1	2.2	0.5
75	0.38	1357	0.099	0.002	18.5	23.6	24.7	6.3	3.8	0.7
105	0.23	833	0.083	0.002	25.7	18.2	19.5	4.1	5.6	1.1
135	0.02	52	0.125	0.003	36.1	14.7	15.5	2.4	7.1	1.4
165	0.00	0	0.000	0.000	0.0	0.0	0.0	0.0	0.0	0.0
$\theta_{e'} = 10.0$, $E' = 8.0$ GeV, $Q^2 = 3.65(\text{GeV/c})^2$, $W^2 = 10.4$ $(\text{GeV})^2$, $\epsilon = 0.82$										
θ^*	Det. Eff.	Counts	$\sigma(W)$	$\sigma(M_\Lambda)$	$<\theta_K>$	$<\theta_p>$	$<\theta_\pi>$	$<P_K>$	$<P_p>$	$<P_\pi>$
(deg)		90 days	(GeV)	(GeV)	(deg)	(deg)	(deg)	(GeV/c)	(GeV/c)	(GeV/c)
15.	0.02	31.	0.108	0.002	13.7	21.4	40.3	6.6	0.7	0.2
45.	0.20	734.	0.097	0.002	16.9	27.4	34.1	5.8	1.5	0.3
75.	0.33	1627.	0.102	0.002	21.0	23.6	25.8	4.2	3.0	0.5
105.	0.29	1414.	0.076	0.002	27.3	21.0	22.1	2.6	4.3	0.8
135.	0.16	590.	0.121	0.002	45.0	16.7	18.6	1.2	5.5	1.0
165.	0.00	4.	0.000	0.000	74.2	12.8	17.6	0.4	5.9	1.3
$\theta_{e'} = 10.0$, $E' = 11.0$ GeV, $Q^2 = 5.01(\text{GeV/c})^2$, $W^2 = 3.4$ $(\text{GeV})^2$, $\epsilon = 0.94$										
θ^*	Det. Eff.	Counts	$\sigma(W)$	$\sigma(M_\Lambda)$	$<\theta_K>$	$<\theta_p>$	$<\theta_\pi>$	$<P_K>$	$<P_p>$	$<P_\pi>$
(deg)		90 days	(GeV)	(GeV)	(deg)	(deg)	(deg)	(GeV/c)	(GeV/c)	(GeV/c)
15.	0.39	1045.	0.056	0.002	21.1	28.5	35.3	2.6	1.7	0.3
45.	0.38	2759.	0.054	0.002	22.6	27.2	31.0	2.4	1.9	0.3
75.	0.35	3502.	0.056	0.002	26.6	24.3	28.7	2.0	2.2	0.4
105.	0.33	3268.	0.064	0.002	28.5	24.1	27.4	1.4	2.8	0.5
135.	0.40	2954.	0.071	0.002	34.8	22.2	24.7	1.0	3.1	0.6
165.	0.45	1215.	0.067	0.002	37.2	22.4	24.4	0.7	3.3	0.6

Table II. Same as Table I except for $\theta_{e'}$=10°.

	$E = 7$ GeV		$E = 15$ GeV		
Q^2	ϵ	counts	ϵ	counts	$\delta\frac{\sigma_L}{\sigma_T}$
0.5	0.94	5051.	0.99	87389.	0.32
1.0	0.92	10125.	0.99	55220.	0.17
1.5	0.89	6011.	0.98	26172.	0.16
2.0	0.86	3675.	0.97	13992.	0.16
2.5	0.83	2259.	0.97	4605.	0.18
3.0	0.79	1239.	0.96	2192.	0.20
3.5	0.75	560.	0.96	697.	0.27
4.0	0.70	374.	0.95	1248.	0.24

Table III. Number of counts expected for 90 day runs at 7 and 15 GeV for the $p(e, e'K^+\Lambda)$ reaction with $\theta^* < 30°$ as a function of Q^2. The count rate assumptions are the same as in Table I. The final column shows the approximate resulting error on σ_L/σ_T.

	$W_d^2 = 10$ (GeV)^2			$W_d^2 = 25$ (GeV)^2			$W_d^2 = 40$ (GeV)^2		
Q^2 (Gev/c)^2	1.0	2.0	4.0	1.0	2.0	4.0	1.0	2.0	4.0
E' (Gev/c)	13.0	13.1	12.5	9.4	9.2	9.0	4.3	4.8	4.3
$\theta_{E'}$ (deg)	4.1	5.9	8.5	4.9	7.1	10.3	6.6	9.6	14.5
Detection Efficiencies									
$K_0 \rightarrow \pi^-\pi^+$	0.84	0.82	0.85	0.82	0.81	0.80	0.73	0.76	0.74
$\Lambda \rightarrow p\pi^-$	0.71	0.77	0.78	0.70	0.68	0.65	0.67	0.64	0.61
$D_s \rightarrow \Lambda p$	0.61	0.68	0.71	0.65	0.62	0.59	0.63	0.60	0.57
D_s and K_0	0.49	0.53	0.57	0.51	0.46	0.41	0.38	0.39	0.34
Invariant Mass Resolutions (Mev)									
$K_0 \rightarrow \pi^-\pi^+$	1.0	1.0	1.0	1.0	1.1	1.1	1.2	1.2	1.3
$\Lambda \rightarrow p\pi^-$	1.5	1.5	1.8	2.1	2.7	2.8	3.4	4.0	4.0
$D_s \rightarrow \Lambda p$	2.1	2.0	2.0	2.8	3.1	3.1	3.9	4.4	4.7
Average Momenta (GeV/c)									
π^+ (from K_0)	0.50	0.53	0.58	1.77	1.70	1.79	2.69	2.87	2.93
π^- (from K_0)	0.50	0.54	0.58	1.75	1.74	1.83	3.00	2.87	2.99
p (from Λ)	0.84	0.98	1.24	1.70	1.90	2.06	2.65	2.78	2.92
π^- (from Λ)	0.19	0.21	0.25	0.34	0.37	0.39	0.52	0.50	0.56
p (from D_s)	0.86	0.98	1.25	1.73	1.89	2.08	2.61	2.73	2.90
Average Angles (deg)									
π^+ (from K_0)	60.5	56.4	56.1	37.1	38.8	36.8	30.3	30.2	29.6
π^- (from K_0)	58.0	56.8	57.2	37.0	38.6	37.2	30.5	30.0	29.3
p (from Λ)	37.8	37.8	35.5	33.5	31.5	30.6	29.4	28.5	27.1
π^- (from Λ)	49.0	49.4	44.2	39.5	36.6	35.1	31.1	31.4	29.5
p (from D_s)	38.7	37.1	35.6	33.5	31.7	30.1	29.5	28.7	27.0

Table IV. Kinematics, resolutions, and efficiencies for the reaction $D(e, e'K^0\Lambda p)$ with the Λp system assumed to have a fixed mass of 2.11 GeV, corresponding to a possible narrow D_s dibaryon resonance. A beam energy of 15 GeV was used.

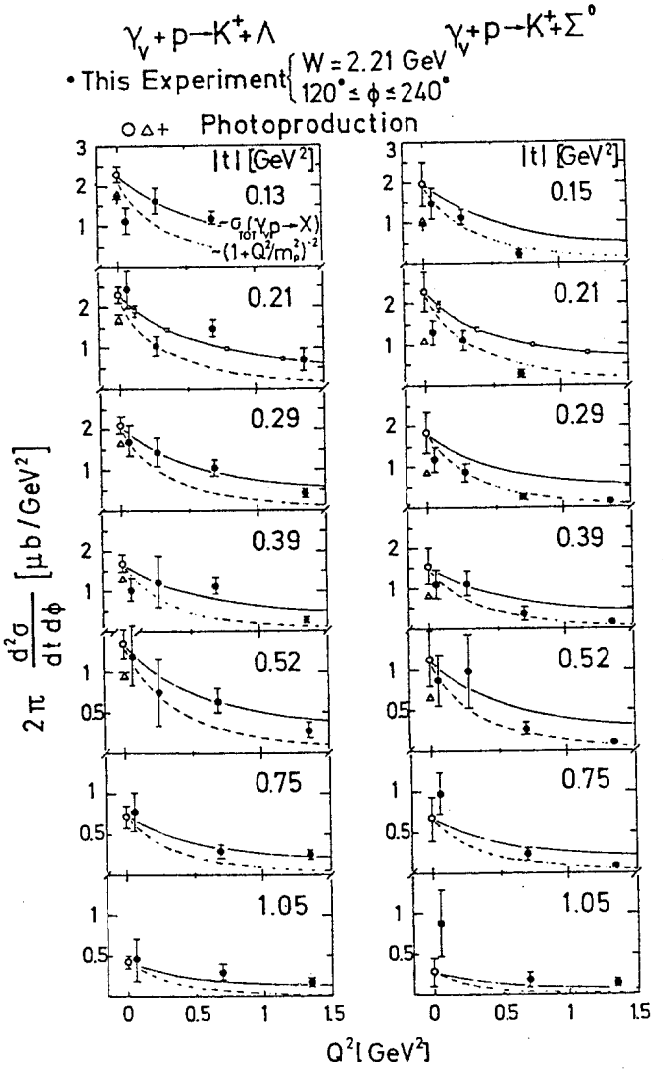

Fig. 1. A summary of much of the existing data for kaon electroproduction from the proton from (Bra79). The solid line is proportional to $\sigma_{tot}(\gamma_v p)$ and the dashed line to $(1 + Q^2/M_\rho^2)^{-2}$.

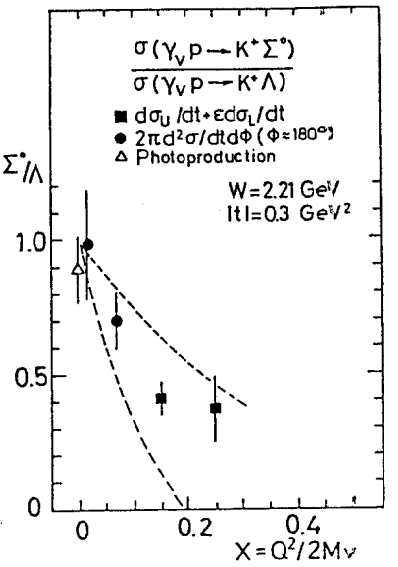

Fig. 2. The ratio of $K^+\Sigma^0$ to $K^+\Lambda$ electroproduction as a function of $x = Q^2/2M\nu$ from (Bra79). The curves show the limits given by a quark-parton model (Nac74).

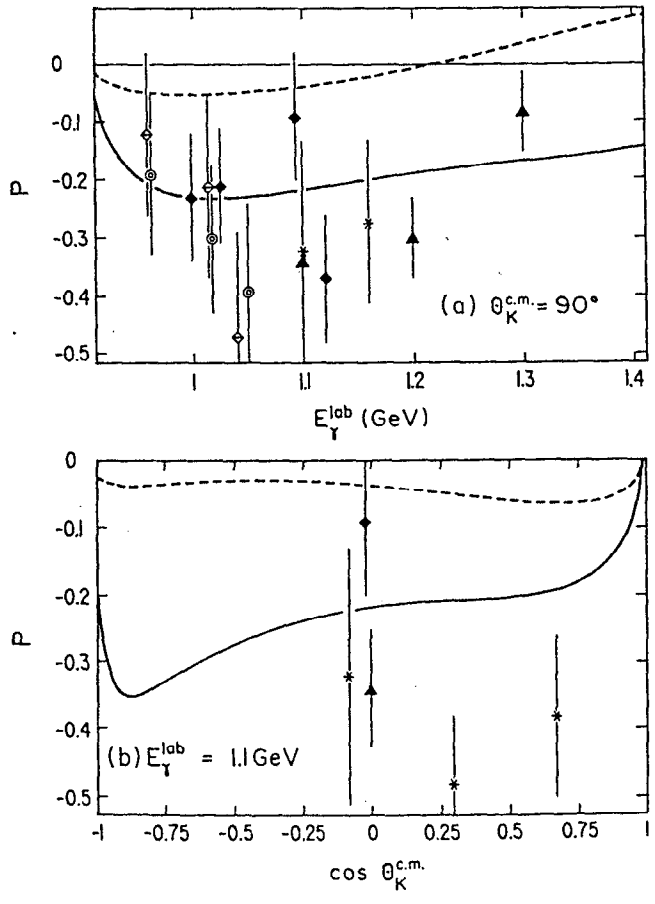

Fig. 3. Λ polarization asymmetry in $\gamma p \rightarrow K^+\Lambda$ (a) as a function of photon energy at $\theta^* = 90°$, and (b) as a function of kaon angle at 1.1 GeV. The two curves represent two models that are in agreement with photoproduction cross section data from (Ade90). See this reference for references to data points.

III.N. Search for New Particles Coupling Only to Leptons

Introduction

As was described in the 1988 PEGASYS Draft Proposal, we have two general goals and one specific goal in studying electroproduction of lepton pairs. The first general goal is to experimentally test the predictions from QED. The second is to see if data in which both leptons are measured can be used to explain the observed rates of single positrons and muons, which in some cases were found to be much larger than was expected. Our specific goal is to search a proposed new particle (the λ) which would couple only to charged leptons (PEG88, Haw89). We report here a study to determine the exclusion limits which would be set on the λ when the Mark II detector is in operation. It is found that the Mark II will considerably improve upon existing λ exclusion limits.

The Computer-Generated Event

One possible mechanism for the electroproduction of an e^+e^- pair is the QED bremsstrahlung process shown in the top two diagrams Fig. 1a. Another way to produce lepton pairs is the production and decay of a hypothesized λ particle (Fig. 1b). It is the latter process which is our potential "signal" using the Mark II, while the QED bremsstrahlung process will be the background.

Another possible QED background is the "two-photon" diagram (Fig. 1a, bottom diagram). This process may be neglected when one measure 3-lepton ("trident") final states, *e.g.* $e'e^+e^-$ or $e'\mu^+\mu^-$. This is so because this process is overwhelmingly dominated by the scattered electron going down the beam pipe and not being detected.

Figure 2 is a schematic of the primary ($e^- + p \rightarrow e^- + p + \lambda$) and secondary ($\lambda \rightarrow e^+ + e^-$) reactions. The electron (or positron) comes from a circulating bunch in the PEP ring and the target is hydrogen. Note that for a given simulated event:

1) E_1, E_λ and θ_λ are fixed.

2) θ_p is set to 0 (*i.e.*, the proton moves along the z-axis). This simplification is reasonable, since when one demands to see the complete final state, the kinematics are dominated by $\overrightarrow{p_e}$ and $\overrightarrow{p_\lambda}$ balancing the transverse momentum.

3) The four-momentum transfer to the proton is minimized in order to maximize the cross section. This is accomplished by choosing the smaller value of $|\overrightarrow{p_p}|$ in the quadratic equation which results from conditions 1) and 2) above.

4) E_e and θ_e are then calculated.

5) ϕ_λ is random; this fixes $\phi_e = \phi_\lambda + \pi$ so that $\overrightarrow{p_1}$, $\overrightarrow{p_e}$, $\overrightarrow{p_p}$ and $\overrightarrow{p_\lambda}$ are coplanar.

6) The decay $\lambda \rightarrow e^+ + e^-$ is isotropic in the λ rest frame, so both ϕ and $\cos(\theta)$ for the e^+ are random. These angles are then fixed for the e^- since its momentum is equal and opposite to that of the e^+. The e^+e^- pair is then taken through a Lorentz boost and two rotations to regain the lab frame.

Some of these assumptions were made to enable rapid and extensive acceptance studies. A Monte-Carlo model which more precisely reproduces the cross section formula of Tsai and has better detector modeling is planned.

Geometry of the Mark II Detector

The lifetime of the λ is assumed to be short enough that the e^+e^- pair emerges essentially from the interaction point. Figure 3 depicts a typical event in the Mark II detector. As shown in the figure, the interaction point (IP) is assumed to be at the upstream face of the central drift chamber (CDC). It is true that interactions can occur anywhere along the length of the gas target, which would tend to reduce the rate because of the steeper angles needed for the particle to be accepted, but this is offset by the expectation that we will also be getting positrons interacting at the opposite end of the target, which improves the rate by a factor of two.

Acceptance Conditions

Three tracks are generated for each event (Fig. 3): the outgoing e^- plus the e^+e^- pair generated by the decaying λ. An event is only accepted if the following conditions are satisfied:

(1) Two of the three tracks must pass through at least 3.5 "superlayers" of the CDC and pass completely through the endcap calorimeter (ECC).

(2) The third track must pass completely through the ECC or the small angle monitor (SAM).

In the above conditions, "pass completely through" means crossing both the upstream and downstream faces of the detector; in other words, the track cannot merely clip the corner of the detector.

Cross Section for λ Production

Tsai (Tsa89) has calculated the differential cross section $d\sigma/(dxd\theta_\lambda)$, where $x \equiv E_\lambda/E_1$, for the process $e^- + p \rightarrow e^- + p + \lambda$ for both a spin-0 λ and a spin-1 λ, and for many values of $m_\lambda, \theta_\lambda$ and x. Figure 4 displays $d\sigma/(dxd\theta_\lambda)$ vs. θ_λ for three different x values; in this graph, λ is spin-0 and m_λ= 0.1 GeV/c^2. Note the semilog scale: $d\sigma/(dxd\theta_\lambda)$ drops by many orders of magnitude with increasing θ_λ. In Tsai's calculations, it is assumed that the unknown λ coupling constant $\alpha_\lambda = 1$.

Mass Resolution

For each event, there is a mass resolution associated with the λ which can be calculated by examining the momenta of the e^+e^- pair:

$$\frac{\Delta m_\lambda}{m_\lambda} = \frac{1}{2}\left[\left(\frac{\Delta p_1}{p_1}\right)^2 + \left(\frac{\Delta p_2}{p_2}\right)^2 + \left(\frac{sin\theta_{12}\Delta\theta_{12}}{1-cos\theta_{12}}\right)^2\right]^{\frac{1}{2}}$$

where $\Delta p_i/p_i$ is the momentum resolution for the i^{th} track and θ_{12} is the angle between the two tracks. The third term in this equation is fixed for a given event, but the first two terms are optimized by using the better of the CDC or the ECC resolutions. Typical values for $\Delta m/m$ were 2% to 7%.

Sensitivity to α_λ

For each set of 1000 events run, the acceptance and average mass resolution $(\overline{\Delta m/m})$ were obtained. A weighted differential cross section $[d\sigma/(dxd\theta_\lambda)]_w$ was now calculated at each θ_λ by multiplying $d\sigma/(dxd\theta_\lambda)$ by the corresponding acceptance at that value of θ_λ (Fig. 5). This was usually done at 0.25° intervals.

After the data points $(\theta_\lambda, [d\sigma/(dxd\theta_\lambda)]_w)$ were generated, they were fit to a cubic polynomial, which was then integrated to yield the total cross section weighted by acceptance. For a fixed m_λ,

$$\sigma_w = \int\int \left(\frac{d\sigma}{dxd\theta}\right)_w d\theta dx$$

Meanwhile, a mass resolution weighted by the cross section was calculated for each m_λ:

$$\left(\frac{\Delta m}{m}\right)_w = \frac{\sum_i \overline{\left(\frac{\Delta m}{m}\right)}_i \left[\left(\frac{d\sigma}{dxd\theta}\right)_w\right]_i}{\sum_i \left[\left(\frac{d\sigma}{dxd\theta}\right)_w\right]_i}$$

where i denotes the i^{th} set of 1000 events.

Using Tsai's results [Tsa89], the cross section for the QED background (Fig. 1a) is

$$\sigma_{bkgd}(m_\lambda) = 1.13 \times 10^{-5} \left(\frac{\Delta m}{m}\right)_w \sigma_{w,v}(m_\lambda)$$

where $\sigma_{w,v}$ is the weighted cross section for vector λ production. The number of expected background counts is then

$$N_{bkgd}(m_\lambda) = \sigma_{bkgd}(m_\lambda) \int L dt$$

We demand a signal that is large enough that we are 99% confident that such a signal could not have been a background fluctuation in any of the ~200 mass bins from m_λ =0.02 to 2.0 GeV/c^2. Thus,

$$1 - CL < \frac{1\%}{200} = 5 \times 10^{-5}$$

where CL is the confidence level. For each N_{bkgd}, a Poisson distribution was used to calculate the N_{signal} needed to satisfy the above conditions. The minimum coupling constant $\alpha_\lambda (\equiv g_\alpha^2/4\pi)$ is then

$$\alpha_\lambda(m_\lambda) = \frac{N_{signal}}{N_{signal}(\alpha_\lambda = 1)} = \frac{N_{signal}}{\sigma_w(m_\lambda) \int L dt},$$

because σ_w was calculated based on the assumption that $\alpha_\lambda = 1$.

Results

Figure 6 shows α_λ vs. m_λ for a vector λ (spin-1). Clearly, the PEGASYS/Mark II detector will improve upon existing exclusion limits by up to two orders of magnitude if the λ is not found. Only the case of $m_\lambda = 2.0$ GeV/c^2 falls inside a region already covered by previous experiments. Work on the pseudoscalar λ (spin-0) case is still in progress.

References

(Haw89) C. A. Hawkins and M. L. Perl, Phys. Rev. **D40**, 823 (1989).

(PEG88) PEGASYS Proposal, December 1988.

(Tsa89) Y. S. Tsai, Phys. Rev. **D40**, 760 (1989).

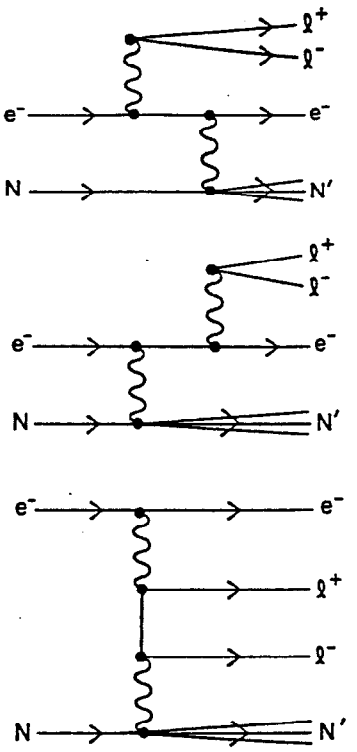

Figure 1a. The QED background. Particle "l" (lepton) can be either an electron or a muon. Only the top two diagrams are significant for trident final states.

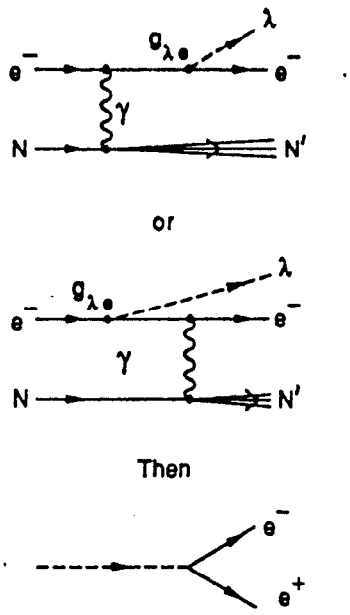

Figure 1b: Production of a λ followed by its decay.

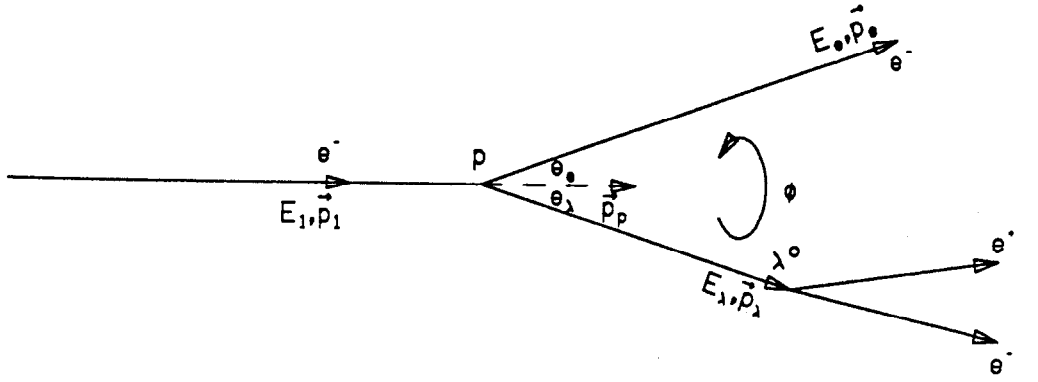

Figure 2. Definition of the geometry for production and decay of the λ.

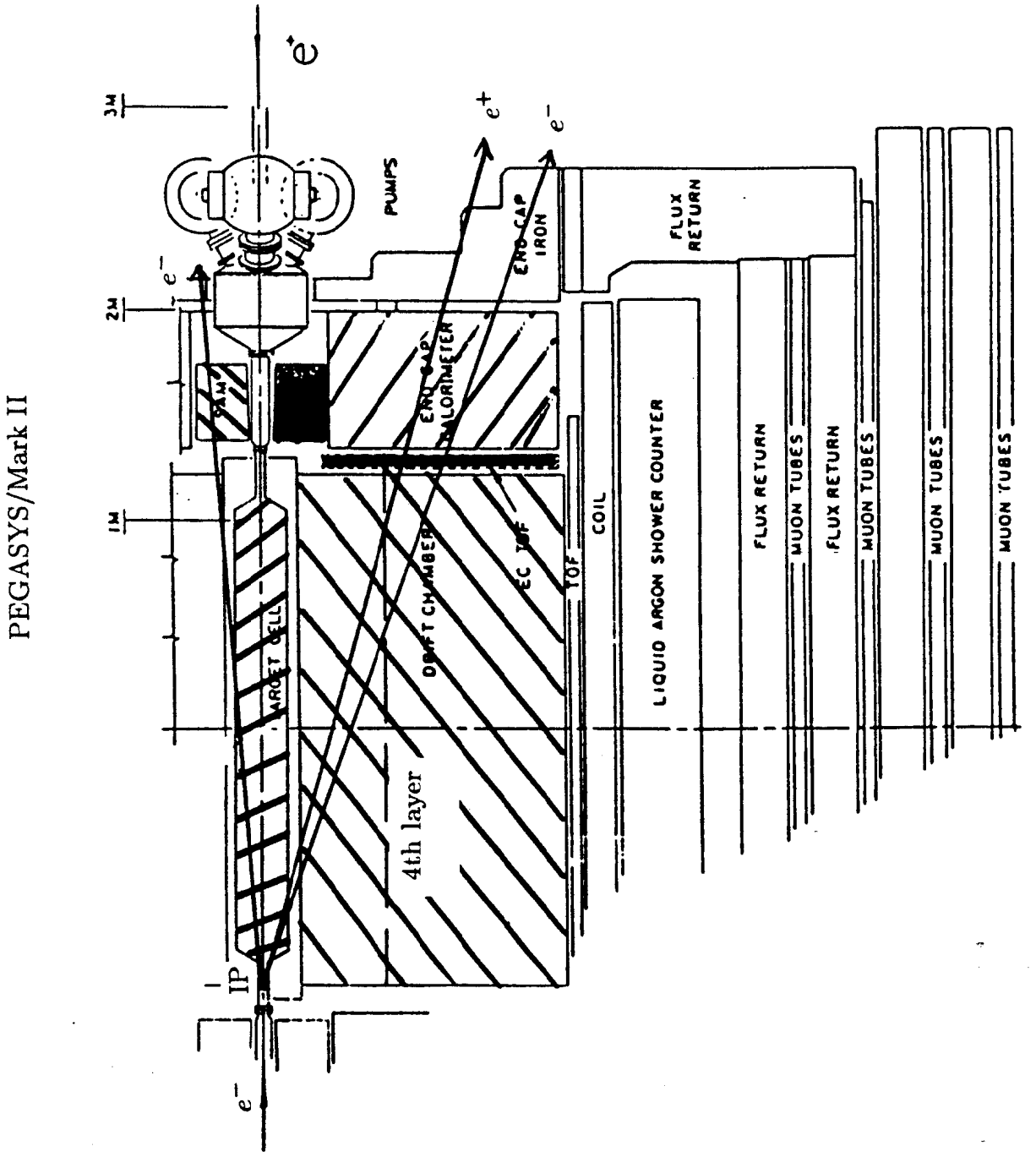

Figure 3: A sample accepted event in the PEGASYS/Mark II detector.

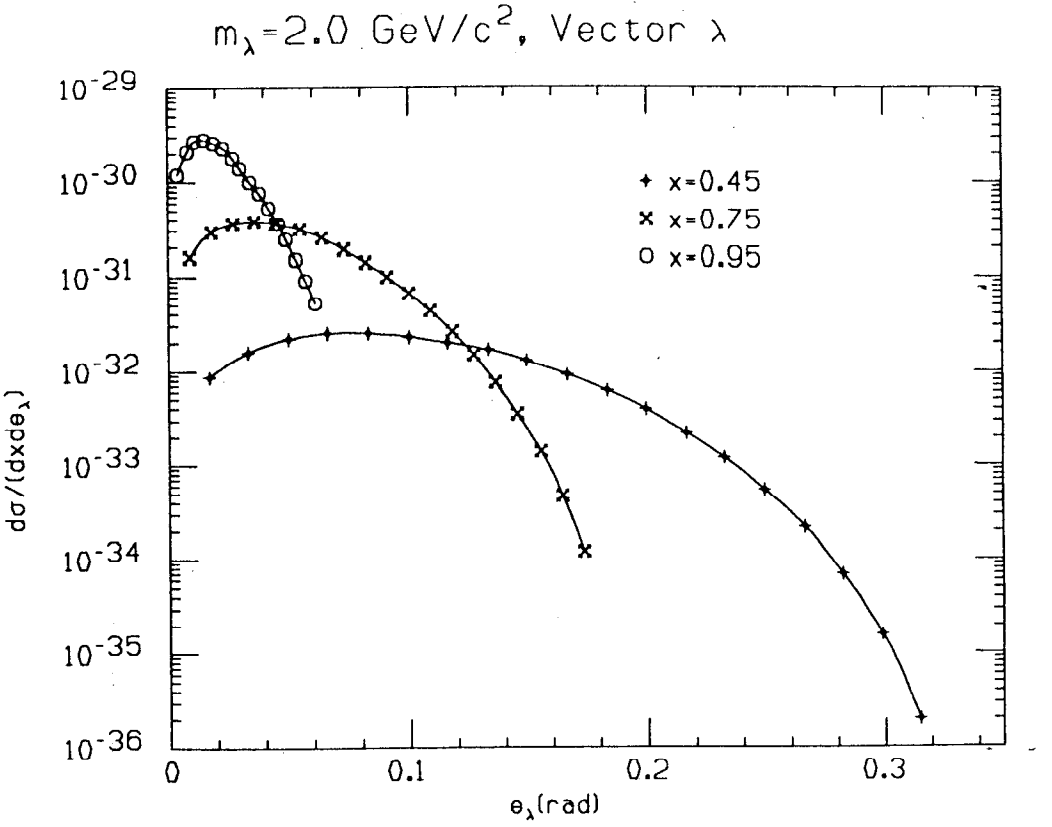

Figure 4: Differential cross section for 3 different x values ($x \equiv E_\lambda/E_1$).

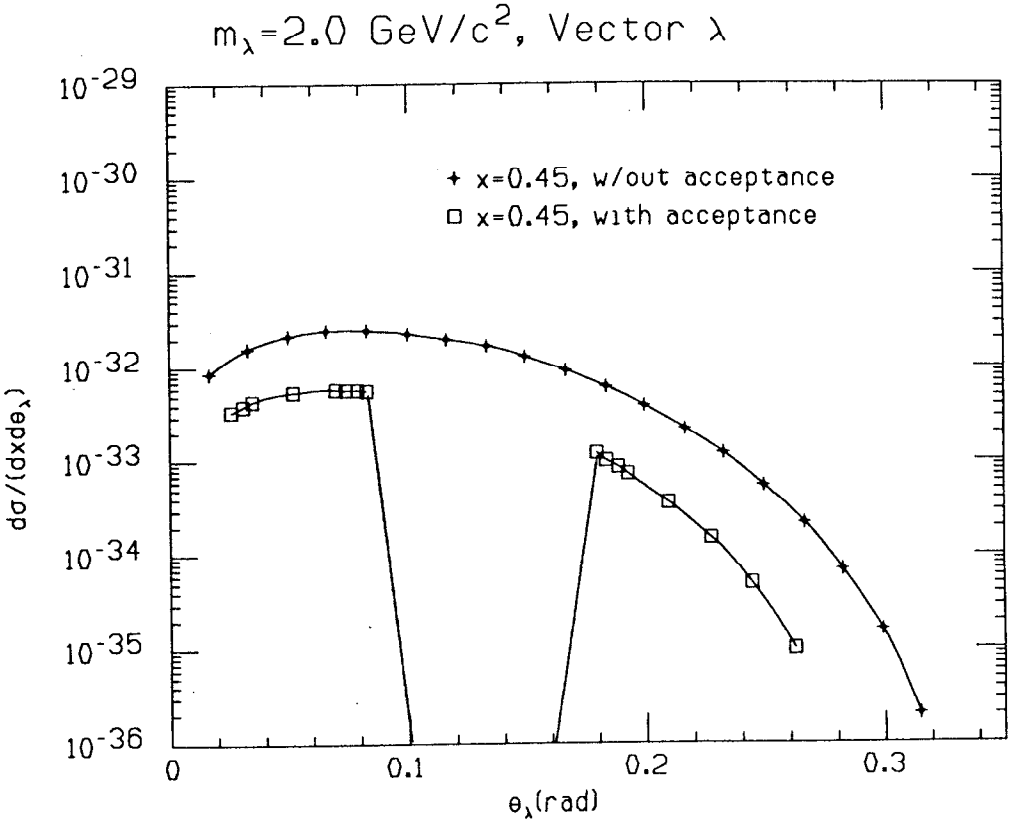

Figure 5: Differential cross section with and without acceptance.

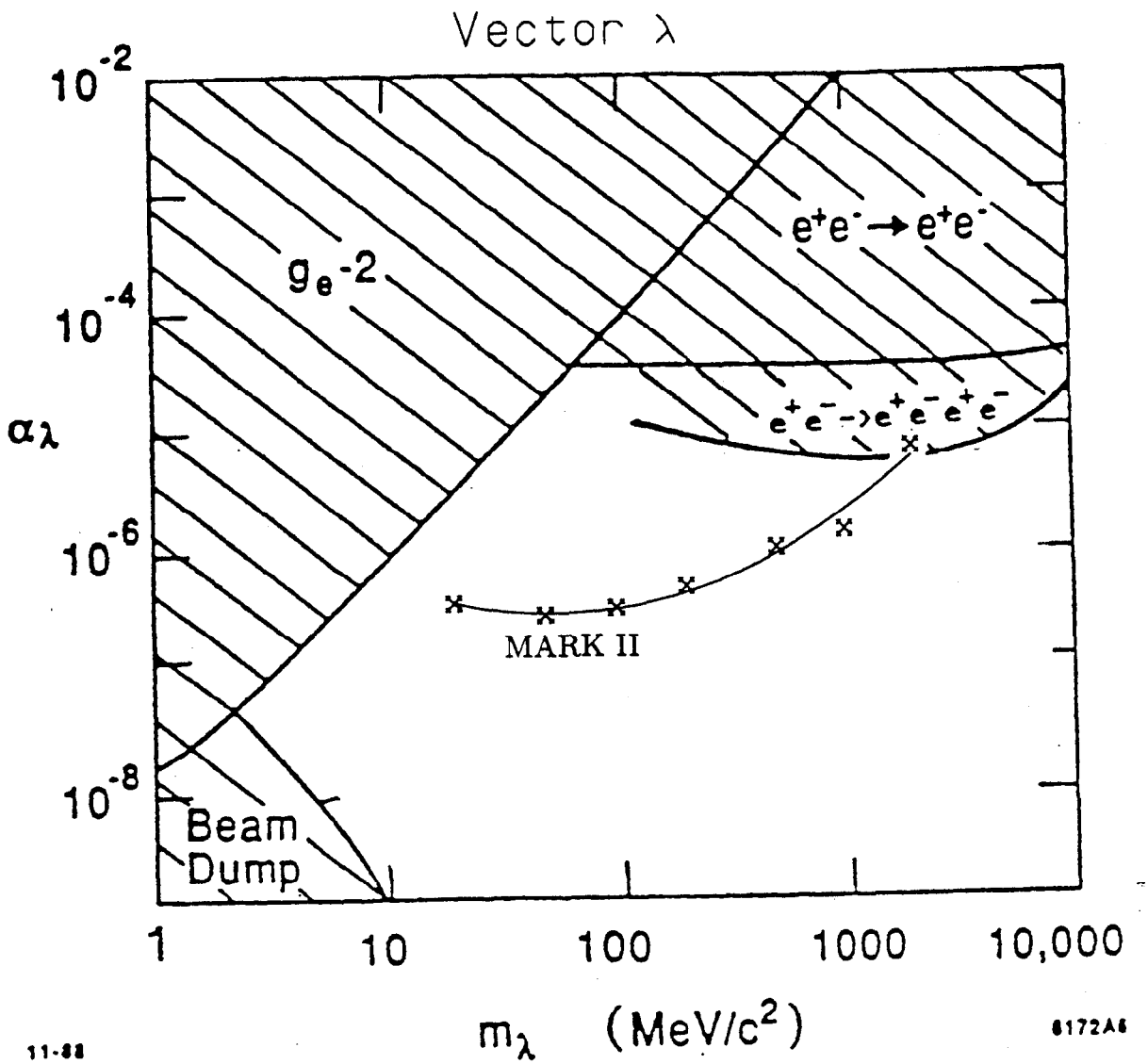

Figure 6: α_λ ($\equiv g_\lambda^2/4\pi$) vs. m_λ for previous experiments and the Mark II.

III.O. Bose-Einstein Correlations in $(e, A) \rightarrow (e', \pi^{\pm}\pi^{\mp}, X)$

Correlations between identical particles have received much attention in recent years as a way to study the size of the hadronization region and the dynamical processes involved in hadronization. Comparing the correlations of like-charged pions to those of unlike-charged pions produced during the hadronization process shows decisive differences. These correlations of pions with like charges are often referred to as Bose-Einstein correlations due to the quantum statistical properties used to explain the effects seen. One of the interesting points of such studies is that measurements of these correlations can be interpreted to give information on the size of the source producing the identical particles.

The large solid-angle MARK II detector provides the necessary momentum resolution and particle identification to study Bose-Einstein correlations. In fact, such studies of identical particle correlations have been done in e^+e^- experiments at the PEP ring (Gol86), as shown in Figure 1. The feasibility of using a large solid-angle detector with a gas target to study identical particle correlations in inelastic lepton scattering has already been established by the ITEP collaboration using the ARGUS detector with 5 GeV e^+e^- beams (Deg90), as shown in Figure 2. The events in Figure 2 are from interactions with the background gas (mostly oxygen). The PEGASYS/MARK II experiment will extend such studies over a broad range of A of the target nucleus and will look for possible effects of the nuclear medium on the hadronization process. The electron tag will identify the Q^2 and ν associated with the events. There are a great many studies of identical particle correlations from colliding beam experiments (Gol86), but at present there are only a few data points from deep inelastic lepton scattering, mostly at higher energies (Ant90). PEGASYS/MARK II will therefore make a valuable contribution to the existing data base.

Of great interest is the use of the Bose-Einstein correlation technique to measure the longitudinal extension of the hadronization region along the direction of the 3-momentum transfer (Yan78,Osb88). The measurement of this dimension of the source size provides unique insight into the dynamics of the hadronization region but as yet has only been studied in a few experiments. This analysis requires a good knowledge of the 4-momentum transfer vector which the PEGASYS/MARK II can provide, and in particular good measurements of the transverse and longitudinal momenta. Further modeling will be done to study the degree to which transverse and longitudinal source sizes can be separately measured. In principle, the PEGASYS/MARK II provides a unique opportunity to study the longitudinal-transverse separation both as a function of the average x_F of the particle pairs and as a function of the target nucleus.

References

(Ant90) P. L. Anthony, Ph.D. Thesis, Massachusetts Institute of Technology, Cambridge, MA, 1990.

(Deg90) P. B. Degtyarenko *et al.*, Z. Phys. **A335**, 231 (1990).

(Gol86) G. Goldhaber and I. Juricic, Presented at LESIP II Workshop, Sante Fe, NM, 1986, and LBL-21531 (1986).

(Osb88) L. S. Osborne, Phys. Rev. Lett. **60**, 987 (1988).

(Yan78) F. B. Yano and S. E. Koonin, Phys. Lett. **78B**, 566 (1978).

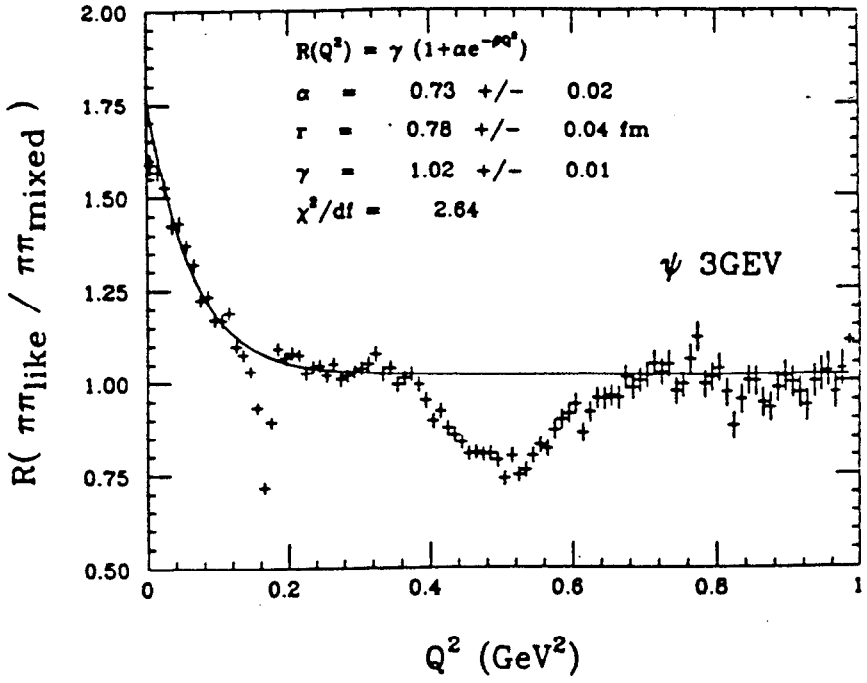

Figure 1. Ratio of the number of like-charged pion pairs to the number of unlike-charged pion pairs detected using MARK II on the PEP ring with e^+e^- collisions. The enhancement at low $Q^2 = |p_1 - p_2|^2$ (four vectors) demonstrates the identical particles correlation effect. The solid line is a fit to the function shown to extract the size of the source producing the pions.

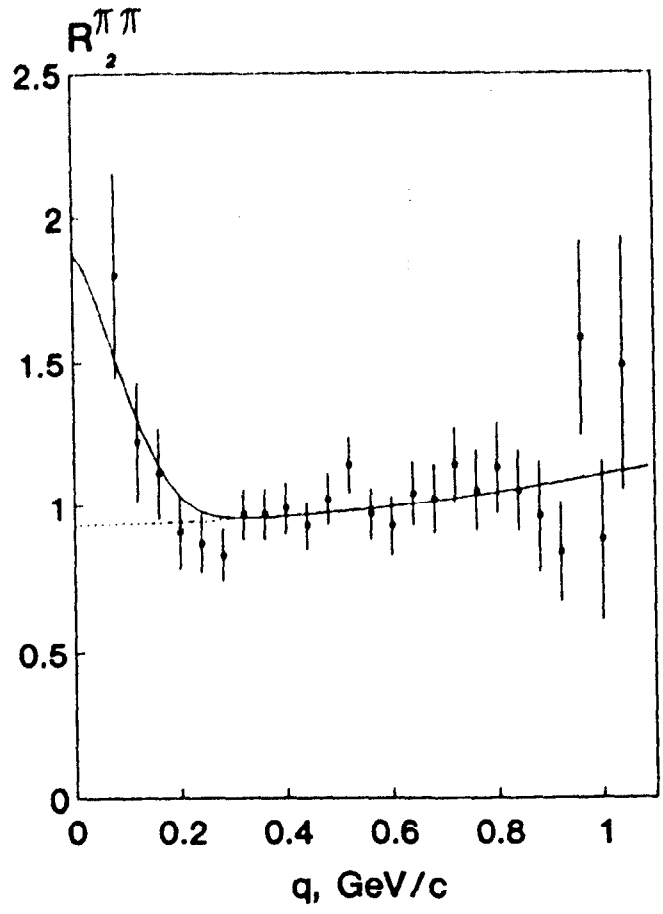

Figure 2. Ratio of like-charged pion pairs to unlike-charged pion pairs as a function of $q = |p_1 - p_2|$ (4-vectors) using the ARGUS detector. The solid line represents the fit to the data to extract the size of the source ($\simeq$ 1.8 fm) producing the pions; the dashed line represents the shape of the background.

Section IV. THE DETECTOR

The Mark II detector (see Figure 1) is well-known to the e^+e^- physics community, and therefore this section will not contain detailed descriptions of individual systems which are found in (Abr89) and references therein. Instead, we will focus on new components introduced into the facility for the purpose of doing internal target physics, and its expected performance in this mode.

We propose to take over the entire detector as it presently exists at the SLC, minus the DC and silicon vertex detectors, and the mini-SAM. In the place of the vertex detectors will be the conductance-limited target (*i.e.* a "bottle target"). The Møller (Bhabha) luminosity monitors to be constructed for this experiment will reside just in front of the Q1 quads. Scintillator hodoscopes will be added on both ends just in front of the End Cap Calorimeters. These will be segmented into 24 wedges, and read out by PMT's outside the detector through flexible light guides. The SAM's may also be covered with scintillator-PMT detectors. The principle purpose of the End Cap Hodoscopes are to assist in triggering (most of the triggers will require an electron or positron in either the ECC or SAM). They will also allow us to make a clean multiplicity trigger for large number charged-particle final states, which will be very useful for *e.g.* untagged associated production of charmed baryons. Finally, they will have some utility for a photon trigger.

A quarter-cut view of the PEGASYS/Mark II detector is shown in Figure 1. It is to be remembered that we are interested in doing physics with both $e^{\pm}$ beams; in the case of virtual Compton scattering, new physics is contained in the $e^+ - e^-$ asymmetry as described in Section III.G. The availability of simultaneous electrons and positrons with a symmetric detector is a unique opportunity for direct photon physics.

In Year I, we will use the detector as described above. During this time, the Collaboration will learn how to use the detector, solve unforseen problems, and take some analyzable data. In Year II, we plan to upgrade the detector (the options are described in Section IV.G) and do high luminosity running. In Year III, we will simply run, without any further modifications to the detector.

References

(Abr89) G. Abrams, *et al*, Nucl. Instr. and Meth. **A281**, 55 (1989)

PEGASYS/Mark II

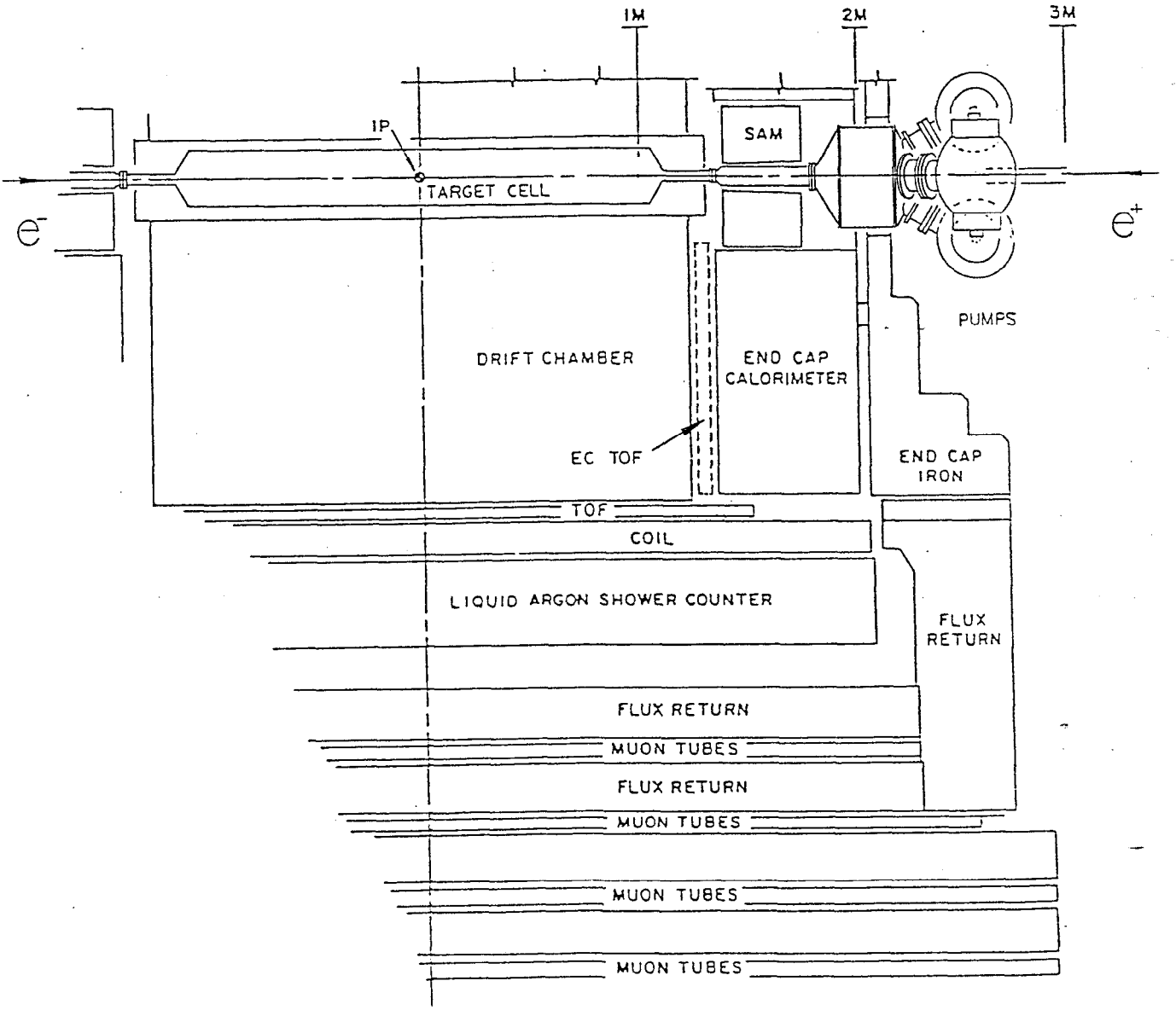

Figure 1. Quarter-cut view of the PEGASYS/Mark II detector.

IV.A. Target

The allowed target areal densities for species ${}^{A}Z$ are unchanged from those in the 1988 PEGASYS Draft Proposal, and are reproduced here as Figure 1. The densities (and corresponding luminosities per beam with a 20 mA current) shown here are for a beam storage lifetime of 2 hours. The lifetime depends inversely on the density, therefore the maximum allowable densities may be simply scaled. All rate estimates in this proposal are based on a 12-hour beam lifetime.

An approximately rectangular gas density profile along the beam line can be produced by means of a bottle target, with conductance restrictions on either end that are small in cross section compared to the main cell. In our target, gas will be bled into the center of the main cell through a small diameter tube. We anticipate using a relatively long target cell (approximately 2 meters), at least at the outset of our program. The areal densities of Figure 1 therefore correspond to the central pressures shown in Figure 2; for all species of interest molecular flow pertains.

This single-stage pumped design was modeled in the approximation of tubes in series, with step-function discontinuities in radii. The series impedance can then be calculated analytically, including expressions adequate for short-tube sections where molecular-beaming plays a significant role. The following parameters were examined in the optimization: *(i)* the main cell radius, *(ii)* the ratio of length to radius of the conductance-limiting tube attached to the target cell, and *(iii)* the total pumping speed. The design turned out to be relatively non-critical in all three of those parameters (Bre90). The density profile in the main cell is very flat, and is reduced by a factor of 10 within 40 cm of the end of the cell (see Fig. 3). A total pumping speed of approximately 10,000 liters/second (4 turbopumps of 2200 l/s each) on each end is completely adequate (see Fig. 4). Note that the use of Balzers turbopumps for use on the PEP beam line has been approved in principle by the SLAC vacuum group, during our work with them in the previous incarnation of the PEGASYS proposal. A target cell radius of 12.5 - 15 cm will be adequate; this will leave us some room between the cell and the inner wall of the CDC for an upgrade option of an inner drift chamber, for example.

The gas throughputs are modest, even at the very highest pressures, and gas recovery is not planned. For H_2, the throughput is 300 liters/day, and for Xe, about 0.1 liter/day. The Xe rate is so low because not only is less high-Z gas permitted for a given beam storage lifetime, but the conductance of the system goes down for heavier gases.

The procedure for establishing, monitoring and controlling the gas flow into the target cell to achieve a particular luminosity is a problem that was solved already 5 years ago at PEP, during the LLNL pilot study of a gas bump target in

the beampipe of the TPC/2γ detector (Mel87). Figure 5 shows the gas panel that was developed, tested and approved by the SLAC vacuum group, and used in this first experiment of internal target physics at PEP (Eri86). A particular target gas in a high pressure storage bottle is transferred to a low pressure control volume by two successive expansions. The valve V-9 is opened, presenting the gas at low pressure to a precision sapphire-seat needle valve, with a large dynamic range in conductance. The gas thereafter flowed through 1/4" SS pipe approximately 60' to the IR hall and the PEP ring. The purity of the gas was monitored by residual gas analyzers both on the PEP ring and on the gas panel itself. The gas handling system for PEGASYS/Mark II will be almost identical, except that most of the valves will need to be automatically actuated, and the whole gas system controlled by computer. This is necessary because we want to frequently cycle different gases to control systematic errors for the many A-dependence experiments.

References

(Bre90) J. Brereton, "Optimization of Target Design for PEGASYS," PEGASYS Technical Memorandum, August, 1990

(Mel87) S.O. Melnikoff, "Nuclear Physics at PEP: Recent Results Using the Time Projection Chamber," in "Workshop on Electronuclear Physics with Internal Targets," SLAC, January 5-8, 1987, p. 111, R.G. Arnold, R.C. Minehart, ed. (SLAC-316).

(Eri86) E.D. Ericson, "Operating Procedures for the Gas Injection System (PEP IR-2)," LLNL protocol, November 26, 1985, rev. January 20, 1986.

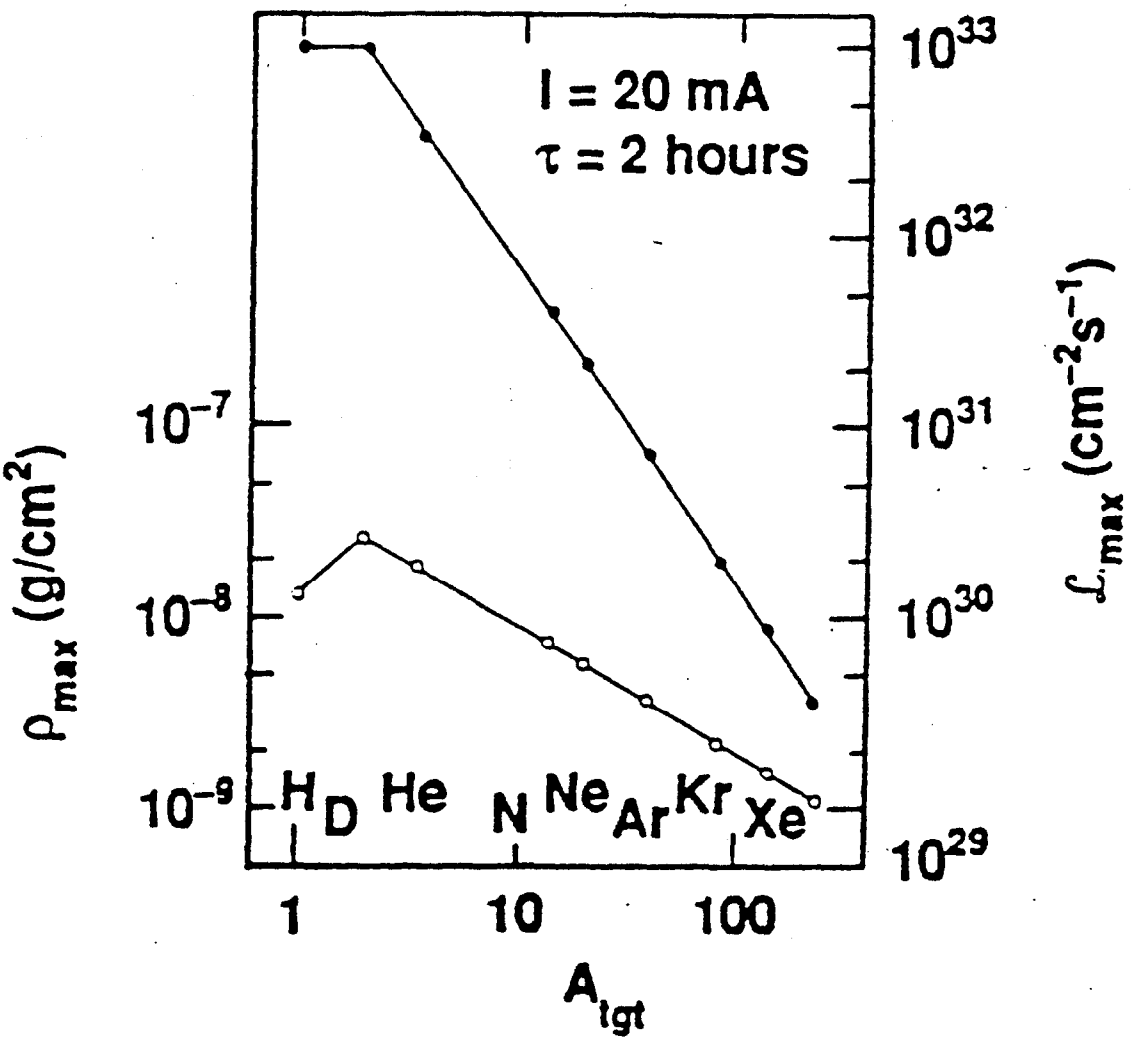

Figure 1. Maximum gas density and corresponding luminosity per beam for PEP as a function of target gas. The results are based on 14.5 GeV electrons, a 2-hour storage lifetime, and a beam current of 20 mA.

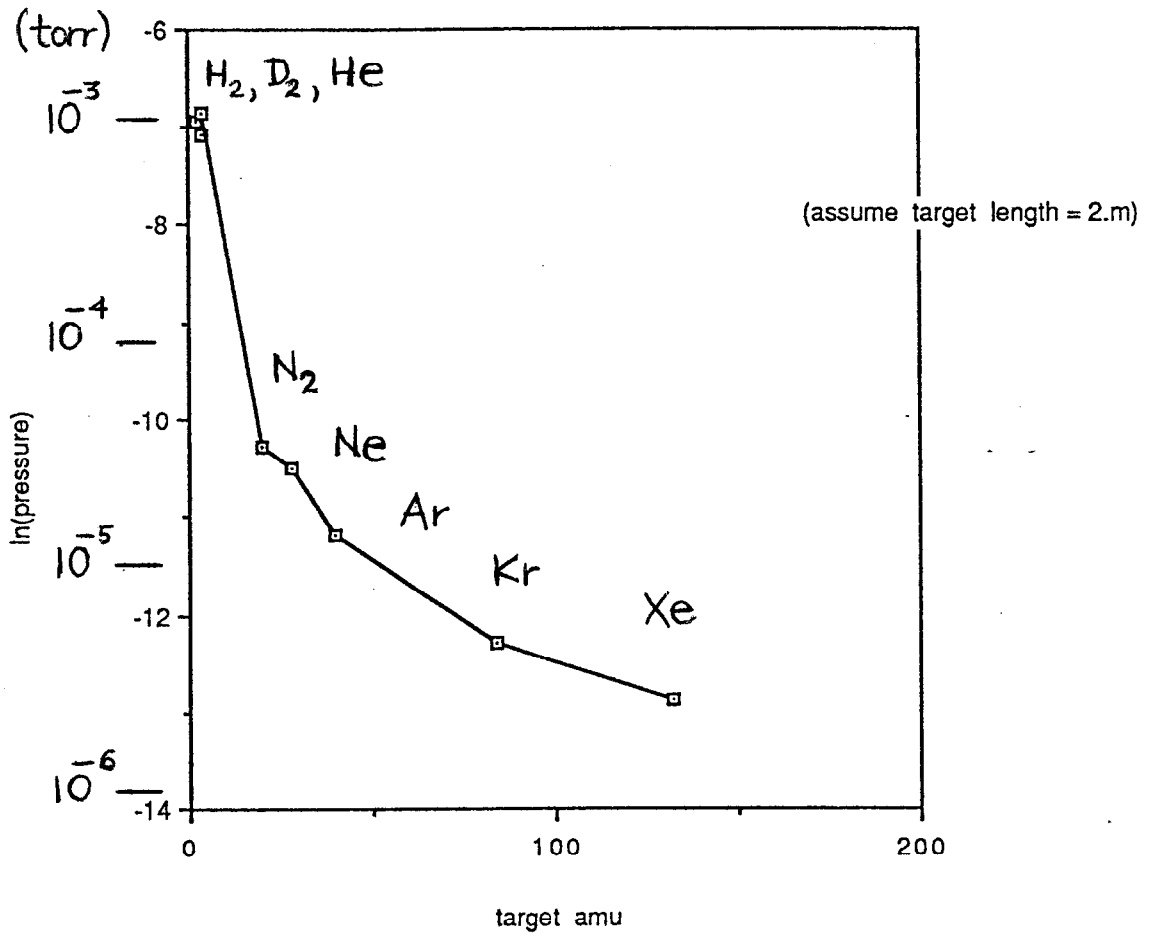

Figure 2. The pressure in a target cell of length 2 meters, corresponding to the densities of Figure 1.

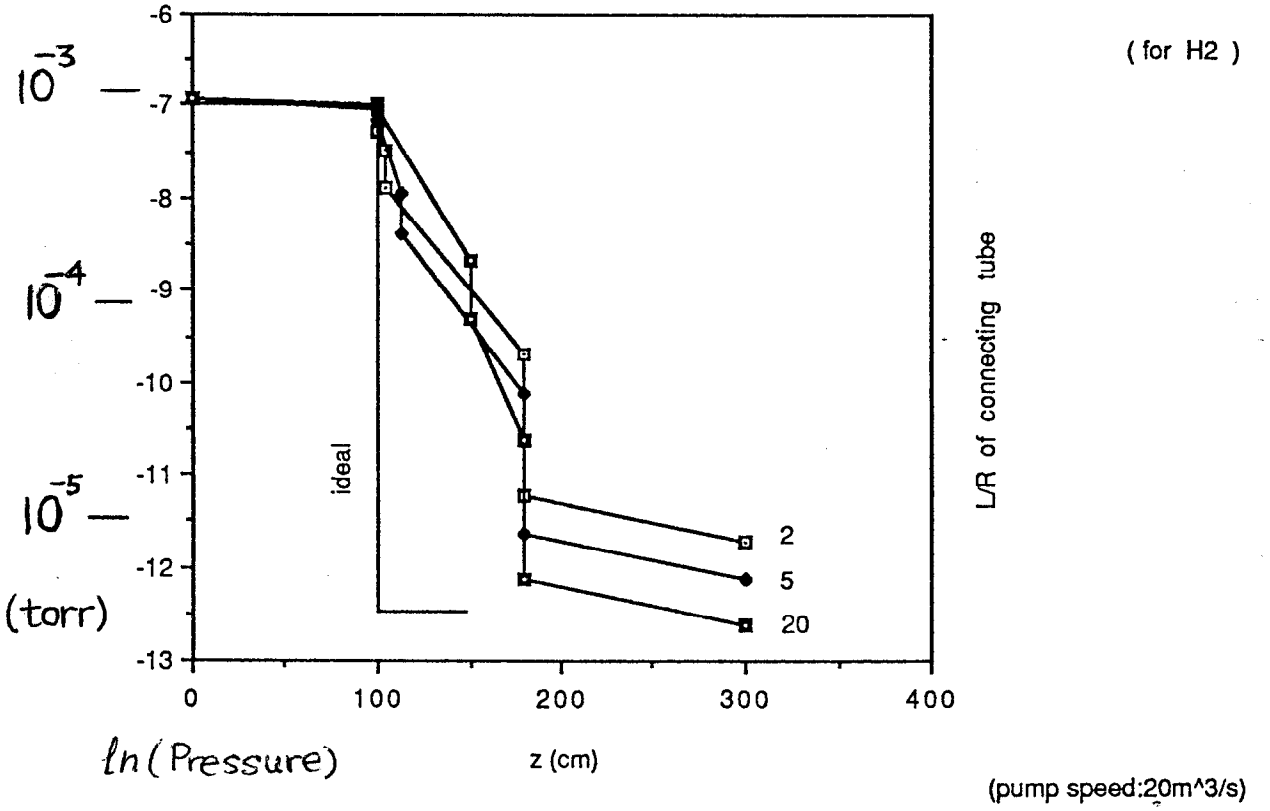

Figure 3. Pressure profile in the PEGASYS/Mark II target, as a function of the length-to-radius of the conductance-limiting pipe to target cell. The gas was hydrogen, with a total pumping speed of 10,000 liters/second at each end.

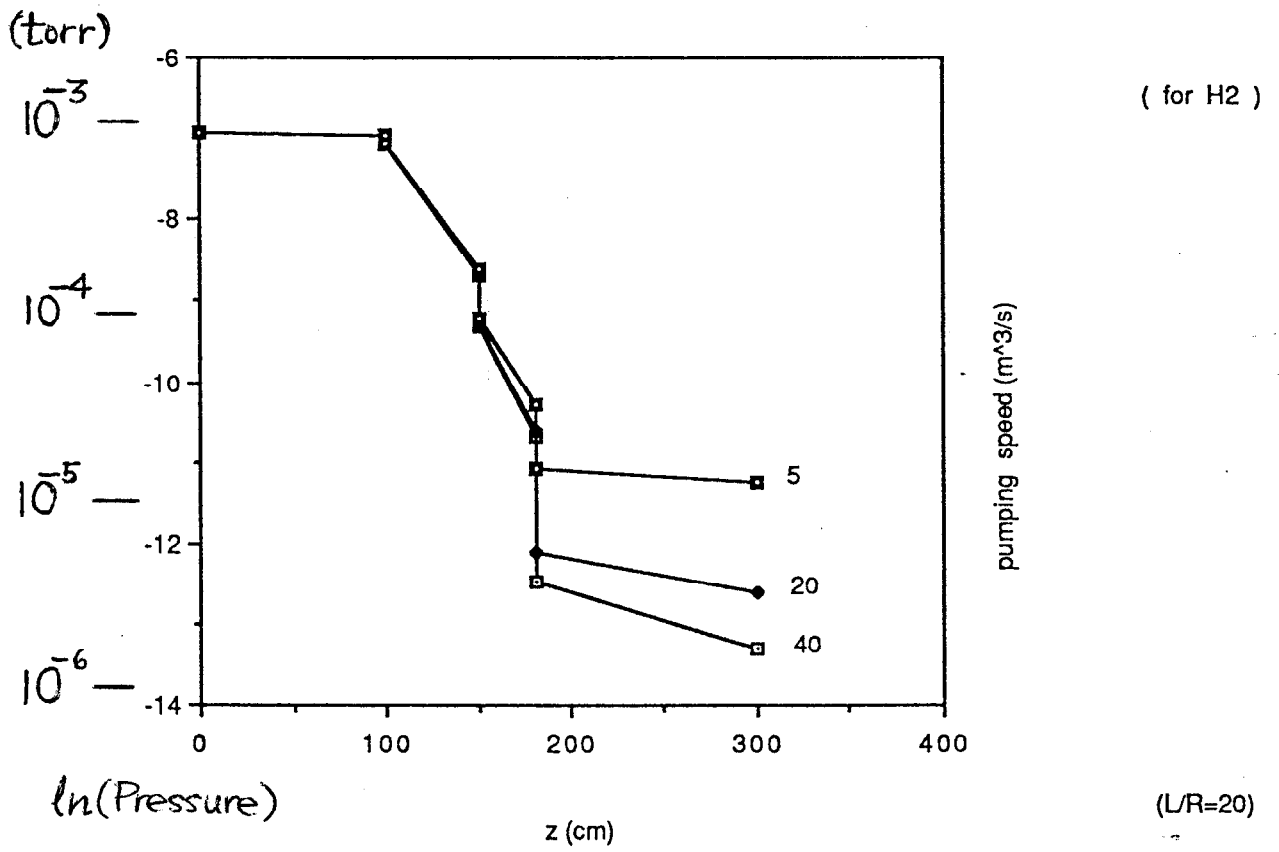

Figure 4. As in Figure 13, except as a function of pumping speed. Here the conductance-limiting pipe's aspect ratio is chosen to be 20.

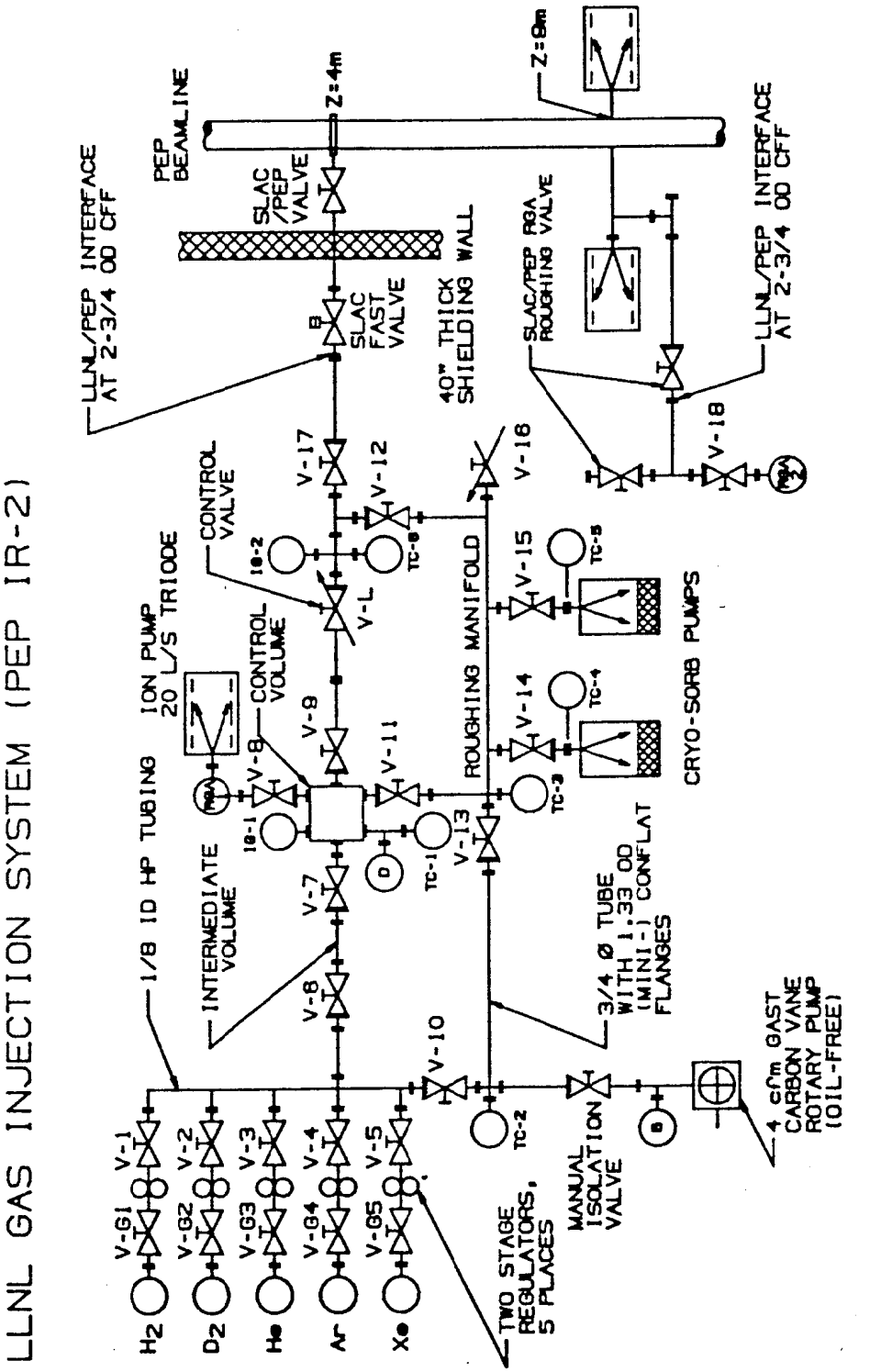

Figure 5. Gas handling system for the LLNL gas injection test with the TPC/2γ detector (Eri86).

IV.B. The Endcap Hodoscope

The most important triggers will involve at least one electron (or positron) in the Endcap Calorimeter (ECC). For these to be relatively clean, it is vital to reduce the number of competing triggers from "background" photons. Thus we plan to install a simple Endcap scintillator array on the inner surface of each ECC, in a plane perpendicular to the central axis of the Mark II. The sectors will serve to provide rough positional information for any charged particle(s), to veto events with neutrals that subsequently interact in the ECC, and to give some time-of-flight discrimination (especially for low-momentum particles originating in the "upstream" portion of the target cell).

The Endcap Hodoscope (ECH) will consist of 24 (or perhaps 48) scintillators, each a wedge-shaped sector 15° (or 7.5°) in azimuth. These scintillators will be as thick as space permits (perhaps up to 1-in.), and will extend from just inside the 13.5-in. inner radius to the 58-in. outer radius of the ECC. Light pipes attached at a 90° angle to the scintillator sectors, with a 45° reflecting surface or a small-radius bend, will serve to transmit light from both ends of each sector. (For optimal position and time information, 48 scintillator sectors are preferable; but space limitations would probably require the joining of adjacent sectors to a single light pipe at the inside radius.)

As shown in Fig. IV.B.1, the Small-Angle Monitor (SAM) which will be positioned inside each ECC will limit the radial clearance (to about 1.7 in. between the SAM and the ECC). This space should be adequate, however, for at least 3/4-in.-thick light pipes (connecting perhaps to flexible fiber-optics pipes) to be extended through the central hole of the endcap iron, between the beam-pipe pumping chamber and the iron. Connections can be made externally to well-shielded conventional photomultipliers. Alternatively, if light-pipe space is limited by existing electrical connections - even after removal of the present Mark II vertex detector - special Hamamatsu phototubes (R2490) that can function in an axial magnetic field of 5 kG or greater could be employed just upstream of the SAM, inside the inner radius of the ECC; in this case, only HV and signal cables would be brought out through the central hole in the endcap iron.

It is desirable, for better light collection as well as better time definition, to provide light pipes at the outer periphery of the ECH scintillator sectors. Although there is only about 1-in. radial space between the ECC and the outer cylindrical shell that extends upstream from the

central drift chamber (CDC), it may be possible - though with substantial loss of light-transmitting area - to bring out thin light pipes that taper to mate with flexible light pipes of 1/2- to 3/4-in. diameter. Because connections (HV and signal) to the CDC and also light pipes attached to the present barrel-stave TOF scintillators take up most of the space in the cutouts of the stationary flux-return iron (at a radius just outside the movable endcap iron), it is more likely that these flexible light pipes will be passed through the holes (over 5-in. dia.) in the endcap iron through which gas and electrical connections are made to the ECC. Once the electronics "boxes" for the present vertex chambers are removed, it is believed likely (from consultations with B. Denton) that there will sufficient clearance in the fourteen 5-in. holes for the ECH outer-radius light pipes to be extended through these holes to external photomultipliers. Thus, both the inner-radius light pipes and phototubes and the outer-radius light pipes and tubes would be attached to the movable ECC and the endcap iron that supports it.

The time resolution that may be expected from each of the ECH sectors will be perhaps 1 nsec. For particle flight paths of 2 meters (from the upstream part of the target), some discrimination between pions and protons will be possible up to 1.7 GeV/c; but discrimination between pions and kaons will be poor unless they are below 1.0 GeV/c. The table below gives time-of-flight differences for particles of a given momentum.

Momentum (GeV/c)	$t_p - t_\pi$ (ns)	$t_K - t_\pi$ (ns)
0.5	7.4	2.5
1.0	2.5	0.74
2.0	0.69	0.19

We are presently also studying the possibility of installing scintillators to cover the inner surface of each SAM (Small-Angle Monitor).

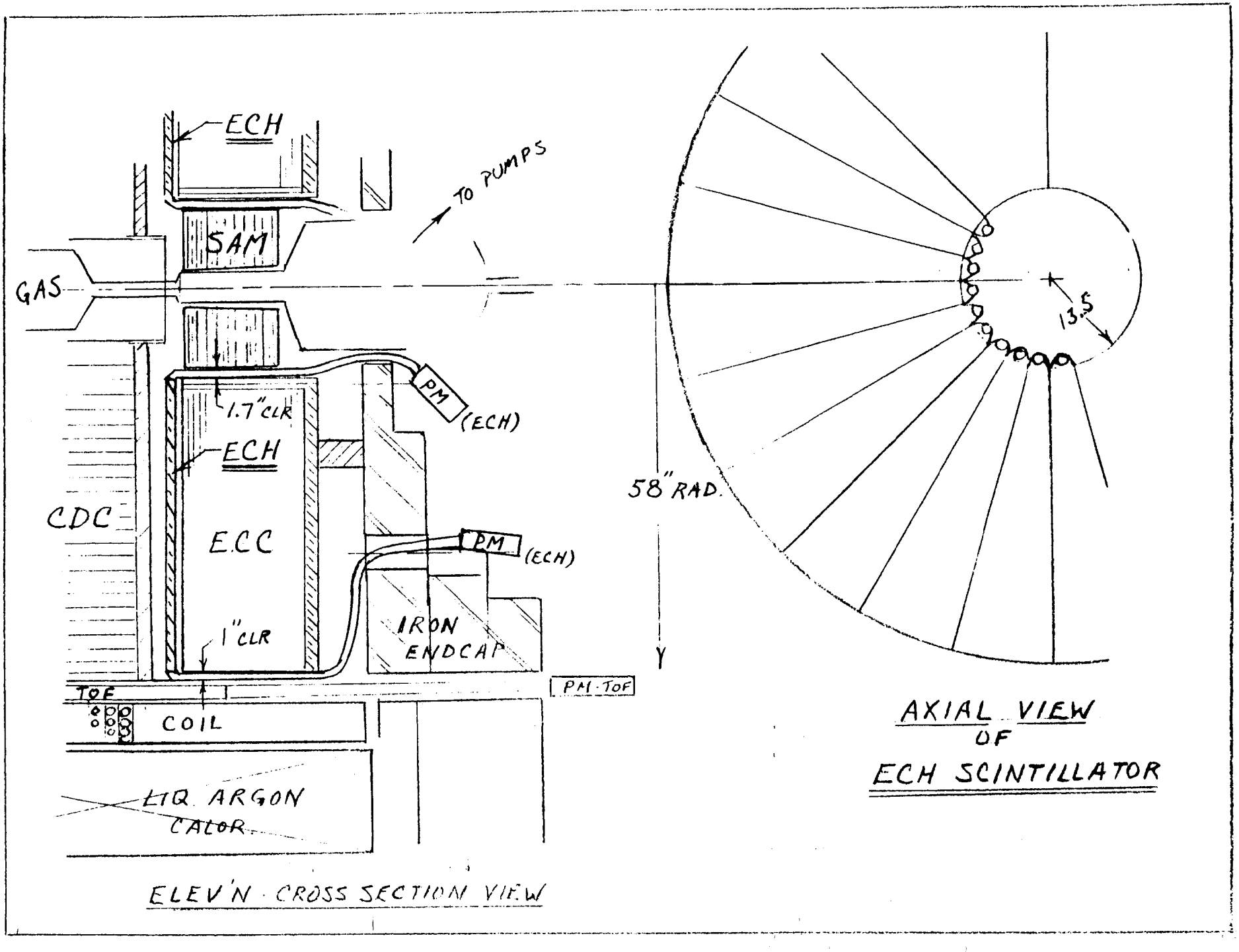
ECH
TO PUMPS
SAM
GAS
PM
(ECH)
1.7" CLR
ECH
CDC
E.C.C
PM
(ECH)
1" CLR
IRON
ENDCAP
TOF
PM-TOF
COIL
LIQ. ARGON
CALOR.
ELEV'N · CROSS SECTION VIEW
58" RAD.
13.5
AXIAL VIEW
OF
ECH SCINTILLATOR

Fig. IV.B. - 1

IV.C. Møller Luminosity Monitor

Luminosity monitoring is vital to any accelerator-based experiment. For external beam, fixed target experiments, it is straightforward to integrate the beam current and measure the target density during the experiment. Internal target experiments with colliders pose a special challenge insofar as there is no known way to measure independently, to the required accuracy, the gas density and profile where it intersects the circulating beam. As in colliding beam physics, luminosity monitoring must be based on scattering processes of known cross section occurring simultaneously with the physics being studied. For e^+e^- collider physics, this process is Bhabha scattering $e^+e^- \rightarrow e^+e^-$ at small angles, where the electron and positron are observed in opposing quadrants by two small-angle calorimeters on either end of the detector.

For internal target physics, the channel of choice would be Møller (Bhabha) scattering of the electron (positron) beam with the atomic electrons of the target nucleus. (Ideally, of course, one wants redundancy, and measurement of the deep inelastic electrons in the spectrometer will provide such an additional luminosity monitor). The kinematics are such that for a scattering angle of 90° in the center of mass, the laboratory angle of each electron (positron) is 8.4 mr at 14.5 GeV beam energy, and 11.3 mr at 8 GeV. In the Mark II detector both the e^- and e^+ beams would be scattered by atomic electrons in the extended gas target. We will thus monitor the luminosity by detecting e^+e^- pairs (Bhabha scattering) at one end of the MARK II and the e^-e^- pairs (Møller scattering) at the other end. Like Bhabha scattering for collider physics, the strength of the technique is that it is a coincidence measurement with the pair energies summing to the total beam energy, and with a tight kinematic correlation between the pair. In the SLC the mini-SAM was used for luminosity monitoring, but it cannot be used here since it violates the Beam Stay Clear (BSC) of the PEP ring.

Our design is based substantially on the design of the Bhabha scattering monitor in the MAC detector at PEP (Hel83, All89). It consists of two sectors at one end of the MARK II to measure Møller scattering and two sectors at the other end to measure Bhabha scattering. All four sectors are identical. The target fiducial volume will be roughly 2 m long centered at the IP. The front face of the luminosity monitors will be about 5.5 m from the IP. The target is being designed to produce as flat a bump as possible in that region, which also maximizes the gas inside the target cell relative to that upstream and downstream. The exact profile will be maximal at the IP, and decrease slightly toward either aperture. With the luminosity monitors we would determine in real time the luminosity (and therefore the gas density) as a function of distance z along the beam axis.

The luminosity monitors each consist of two halves on either side of the beam pipe, with a Pb-scintillator shower counter in back, and a 'ladder' hodoscope of scintillators in front to define the polar angle of the electrons within bins. The "beam's eye" and side views for the monitor are shown in Figs. 1 and 2, respectively. The luminosity monitors are not azimuthally symmetric since the Beam Stay Clear is elliptical at that point (z between 5.5 and 6 m), with the major axis vertical, and the minor axis horizontal.

The beam-defining scintillators are all $1/4''$ thick and consist of a "loose" solid angle-defining scintillator that subtends an azimuthial angle of $\pm$ 45° to the horizontal. For c.m. scattering at 90°, pairs are accepted over the whole range from 8.0 to 14.5 GeV beam energies. The scintillator has a minimum and maximum radius of 35 and 90 mm, respectively. A $1/4''$ thick antiphoton splashback scintillator is located next to the shower counter. In front of the luminosity monitor is a "ladder" hodoscope of $1/4''$ thick scintillators to define the polar angle of the hits within bins which are segments of circles viewed head-on. There are six segments that are 42.3 mm wide and overlap their neighbors by 1/3 to make logical bins 14.1 mm wide. The segments subtend slightly smaller angles than the "loose" scintillator.

The shower counters identify an electron pair, and insure that the pair energy is crudely consistent with the beam energy. The shower counter consists of 15 pairs of $1/4''$ Pb followed by $1/2''$ of scintillator which is 15 radiation lengths thick. A BBQ wavelength shifter transmits the light to the phototubes. The shower counter is housed in a stainless steel box. The luminosity monitor is shielded from the beam by 5 mm of Pb.

The scintillators are BC414 and the wavelength shifter is BC484. These scintillators are all PVT-based since PVT is more radiation resistant than acrylics or lucite. The light pipes will be made of PVT into which a material has been added to quench scintillation. The scintillators will be connected by light pipes to $2''$ phototubes except for the hodoscope, which will be read out by $1''$ phototubes.

Before the complete luminosity monitor is built, one sector will be constructed to act as a prototype. Design, student labor, and material to build the prototype were provided by a research award from the Ames Laboratory at Iowa State University. The prototype will be built by the Iowa State group and will be modeled by the Pennsylvania group. Together we will test the completed prototype using a separated $e - \pi$ beam and a photon beam. Such beams, if not available at SLAC, are available at BNL and in Europe.

The goals of the prototype will be to:

1. Optimize construction techniques and materials selection.
2. Determine the relationship between measured energy and incident energy, as a function of position and energy, particularly near the boundaries of the device (i.e., test the shower containment and light collection efficiency).
3. Measure the energy resolution of the shower counter as a function of position and incident electron energy, and compare with Monte Carlo simulations.
4. Test the e/π discrimination of the shower counter.
5. Test the efficiency of the photon-splashback veto scintillator, and compare with Monte Carlo simulations.
6. Test (if possible) the light output as a function of radiation dose.

References

(All89) J. V. Allaby, Nucl. Instr. and Meth. **281,** 291 (1989).

(Hel83) "Measurement of the Total Cross Section and Energy-Energy Correlations for Electron-Positron Annihilation into Hadrons at 29 GeV," B. K. Heltsley, Thesis, University of Wisconsin, 1983. [MAC detector].

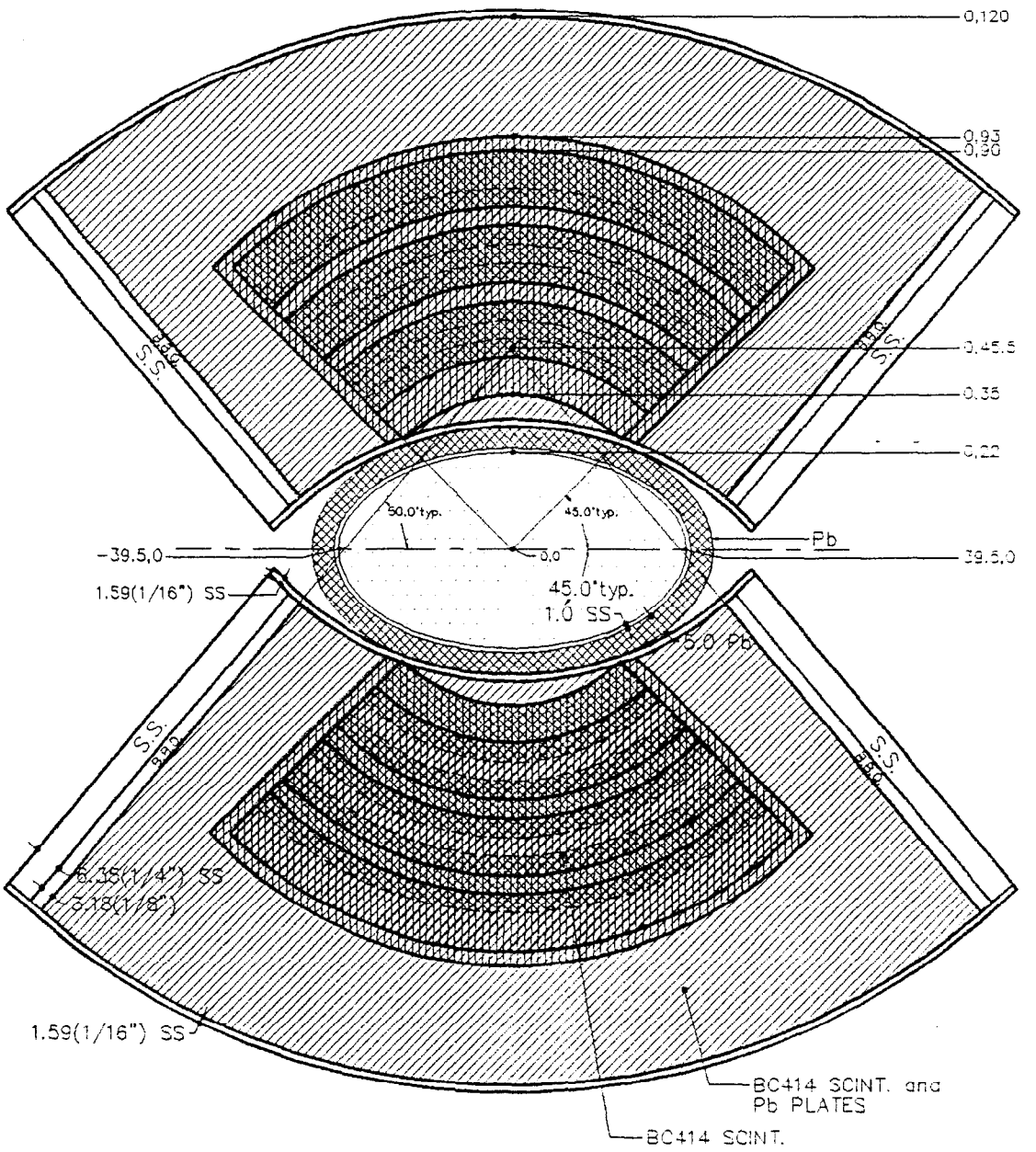

Figure 1. A "beams eye" of the luminosity monitor. Dimensions are given in mm and angles are in degrees. Up is to the right in this figure.

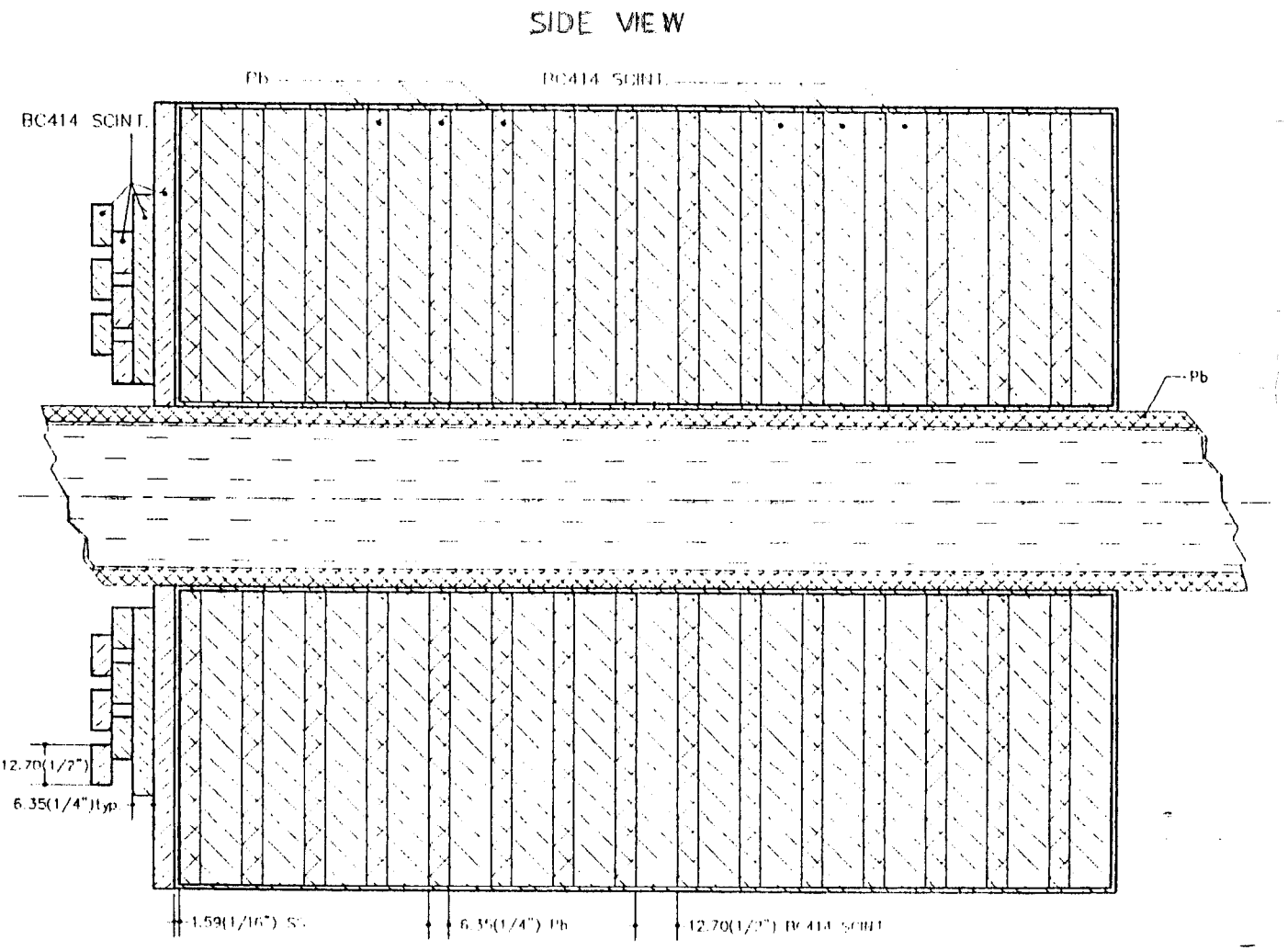

Figure 2. A side view of the luminosity monitor. Dimensions are given in mm and angles are in degrees.

IV.D. Triggering and Data Acquisition

The triggering of the PEGASYS experiment is designed to match the present capacity of the MARK II Data Acquisition and computer system. For the relatively small multiplicity and clean running conditions at PEP, we will probably be able to trigger at a rate of between 5 and 10 Hz. Future upgrades to the Data Acquisition system are feasible. With small costs in hardware and significant programing effort we would be able to buffer many complete events in FASTBUS and significantly reduce the overhead in the computer. We estimate that this would enable us to run at 30 Hz.

For now, the triggering system is designed to accept as many of the interesting events as possible, while staying within the limits of 5-10 events per second. The trigger is designed for a total luminosity of 1.7×10^{32} cm^{-2} sec^{-1} per nucleon. The major addition to the existing system are the hodoscopes in front of the End Cap Calorimeter and possibly the Small Angle Monitor. Additional electronics may be needed to form some of the triggers. The details of the triggering electronics is under study.

Trigger

We will use the existing signals from the front end electronics. Most of these are already used to form parts of the MARK II triggering system at SLC. We estimate that trigger decisions will be made in a few microseconds and result in rather small deadtimes.

Trigger Types

There are four general classes of triggers:

I) An electron in one of the shower counters, possibly accompanied by other particles into the rest of the detector. This will cover most of the physics discussed in this proposal. The minimum electron energy will be approximately 5 GeV to avoid pion contamination.

II) A multi-electron trigger for J/ψ Production and New Particle Searches.

III) A high multiplicity trigger for Open Charm Production.

IV) Special purpose triggers for monitoring, calibration and sampling of high rate processes. They include, but are not limited to, elastic scattering, backgrounds, single electrons, random triggers, and cosmic rays. These will be pre-scaled to reduce their summed rates to less than a few Hz.

Rates

TRIGGER CLASS I.

End Cap Calorimeter:

The expected single-arm electron rate into the ECC for electrons of energy $E' \geq 5$ GeV is approximately 0.5 Hz. Most of these events are at the minimum angle of 9^o and come from the upstream end of the extended target. The trigger will require a coincidence between the new hodoscope and large energy deposited into the front, middle, and back sections of the ECC. A coincidence with a charged or neutral particle in the rest of the detector may be necessary.

SAM (outer section):

The expected single arm electron rate into the outer part of the SAM (beyond a radius of 15 cm, with $\theta \geq 3.5^o$ and $E' \geq 5$ GeV) is 10 Hz. This will be reduced by a factor of 5 by also requiring a coincident photon of energy greater than 2 GeV either in the ECC or another part of the SAM. Electrons not in coincidence with a photon will be prescaled by a factor of approximately 5. A prescaled trigger of an electron in coincidence with one or more charged and neutral particles is also under consideration. The outer section of the SAM is defined by the outer 15 proportional or drift tubes on each plane of each module of the SAM. They are already electronically separated from the inner 15 tubes. An electron going into the outer section is detected by requiring a crude track through at least one set of planes of a given orientation (horizontal, $+30^o$, -30^o) of the tracking part of the SAM and large energy deposited in at least one set of planes of a given orientation in the calorimeter part of the SAM in the outer 15 tubes.

SAM (inner section):

The expected single arm electron rate into the inner part of the SAM (inside a radius of 15 cm, $\theta \geq 1.7^o$, and $E' \geq 5$ GeV) is 70 Hz. This will be reduced by a factor of approximately 5 by requiring a coincident photon of energy greater than 2 GeV and reduced by an additional factor of 10 by prescaling. Electrons not in coincidence with a photon will be prescaled by a factor of 70. A prescaled trigger of an electron in coincidence with one or more charged and neutral particles is

also under consideration. An electron into the inner section of the SAM requires a crude track in the tracking part of the SAM and energy greater than 5 GeV in the calorimeter part.

TRIGGER CLASS II.

QED background and New Particle Search

The expected tri-electron rate with two electrons in the ECC and one in the SAM due to QED is ≤ 0.1 Hz. At least one of the leptons will have an energy greater than 5 GeV and will be readily distinguishable from pions.

J/ψ production:

The expected rate from detecting lepton pairs from untagged J/ψ production is very small. The threshold is at $\nu = 8$ GeV and thus the J/ψ will have a high forward momentum. Thus the trigger will consist of a coincidence of two electron signals from any of the shower detectors, each with a threshold of about 3 GeV.

TRIGGER CLASS III.

Open charm:

The expected rate for untagged (no electron detected) open charm production is expected to be less than 0.2 Hz. The trigger will consist of a combination of high charged particle multiplicity as determined by the curvature modules for the central drift chamber and neutral particle multiplicity in the shower counter. The background rate has been calculated from real photoproduction data, muon scattering data and KNO scaling for scattered electrons which go down the beam pipe. Charged multiplicities of 7 or more are not uncommon, but a large fraction of the charged particles miss the central drift chamber because of the small P_t. In contrast decay products of charmed particles have a large P_t and a very high probability of entering the CDC. For example, a trigger requiring 7 charged tracks (such as from a decay mode of $\Sigma_c^{++} + D^-$) is expected to accept a background rate of less than 1 Hz. This trigger can be pre-scaled by a small factor if necessary.

Data Acquisition

We have searched through existing notes and publications describing the Mark II data acquisition system and have talked with Mark II collaboration specialists to understand capabilities and limitations of the system. Some relevant parameters of the data acquisition system as we understand them now are:

1. Event data size in bytes is related to a number of charged tracks in the detector by an equation $size = 3456 + 1952n$, where n is the number of tracks.

2. The data acquisition system was designed to handle a computer interrupt rate of the order of 1 Hz (presently the computer is interrupted for each event trigger). As we understand it, the system can not be interrupted at a rate higher than 15 Hz even when the event size is 0. This limit is due to operating system overheads incurred in handling computer interrupts and device IO's.

3. The event data is written to disk files on the local VAX computer. When an event data disk file is "full" a transfer of that data is initiated to the IBM complex for archiving and analysis. The data is transmitted over SLAC Ethernet and the transmission speed is limited to 110 Kbytes/sec by hardware. The data is written to 3480 cartridge tapes.

4. Data analysis on the IBM complex takes 0.5 second of CPU time for a 20 track event.

First Year

We envision using the Mark II detector and the data acquisition during the first year experiments without any major modification. Hence the data acquisition system limitations listed above will apply. We estimate that a typical event will have less than 4 charged tracks which corresponds to an event size of $\approx$11.3 Kbytes. The data acquisition system might be capable of handling up to 10 such events per second. The data rate at 10 Hz is 113 Kbytes/sec which just exceeds the maximum data transfer rate to the IBM complex. The Ethernet hardware will limit us to less than 10 events per second. Assuming conservatively that the time to reconstruct an event scales with number of tracks then analysis of a 4 track event on the IBM complex should take 0.1 sec of one-processor CPU time. Hence, one processor in the IBM complex should be able to analyze up to 10 typical events per second. We have an informal proposal from the French part of the collaboration to do part of the first pass analysis on an IBM 3090–600S computer (three times as many processors as the SLAC IBM complex) at the University Blaise Pascal, Clermont-Ferrand, France.

Subsequent Years

Some experiments that we propose to carry out as part of the PEGASYS program will benefit from collecting data at s higher event rate than the data acquisition system will now permit. It is possible to modify the system so that the CAMAC part of the electronics is accessed via the Fastbus (FB) interface.

This could be done by installing two FB CAMAC branch drivers in a FB crate which would then drive otherwise unmodified CAMAC branches. The cost for this modification would be on the order of $10,000 and the benefits would be considerable. First, all data would enter the VAX computer via the FB interface which can transfer data at five times the rate of the existing CAMAC to VAX interface. Second, all data from many events could be collected into one data buffer in FB. Hence, the computer would only need to be interrupted at a rate of $\approx$ 1 Hz to read many events worth of data in one DMA data transfer. This would allow us to increase the event rate to 30 Hz or even higher. The limiting factors in this case would be:

1. The CPU power of the VAX 8600 needed for data processing.
2. The volume of data that we could store and analyze. The problem here is that at an event rate of 30 Hz and a typical event size of 11 Kbytes the data rates are $\approx$330 Kbytes/sec. As discussed above we could not possibly store and analyze this volume of data on the IBM complex. Hence we would need to find an alternate solution. One such solution might be to write the data on 8 mm magnetic tapes and build a farm of RISC processors to analyze the data.

Conclusions

It is possible to trigger the MARK II detector for PEGASYS physics using the existing data acquisition system and computers. Trigger rates will be less than the 5-10 Hz limit set by the computers. Almost all the experiments in the proposal will receive a significant number of events. The data will be stored and analyzed on the SLAC IBM complex and at University Blaise Pascal. During the first year we will familiarize ourselves with the system, learn precisely its limitations, and will design modification to the system which would allow higher event rates for subsequent experiments.

IV.E. Acceptance of Final States from Deep Inelastic Scattering

This section describes some aspects of the response of the Mark II detector in Phase I to deep-inelastic events. This study illustrates some of the great strengths of the Mark II, but also suggest improvements that could be made for Phase II. Figure 1 shows the relative acceptance of Mark II for electrons scattered from a 2 m long target, centered on the interaction region, as a function of the variables Q^2 and ν of the scattered electron. The region on the upper right is the deep inelastic scattering region ($Q^2 > 2, W > 2$). The acceptance for electrons going into the ECC is determined by the fraction of the target length that can be "seen" by the ECC for given kinematics, while the low-Q^2 region seen by the SAM is further reduced by a factor 0.2 due to necessary prescaling in our trigger (trigger class I; see section IV.D). It can be seen that the overall acceptance is on the order of 0.2 at low Q^2, but climbs to near 1.0 at high Q^2, where the cross sections are the smallest. The remaining part of this section is devoted to the study of what happens to the hadrons produced in coincidence with the deep-inelastic scattered electron.

The event samples used were generated with the Lund jet-fragmentation model (And83) which proceeds by: 1) formation of the initial parton configuration, in the present case by deep-inelastic electron scattering from a nucleon, 2) formation of primary hadrons via the materialization of quark-antiquark pairs, and 3) decay of the primary hadrons into the observed mesons and baryons according to experimentally determined branching ratios. The specific implementation employed the jet-fragmentation routines JETSET (Sjo86) Version 6.2 and the leptoproduction generator LEPTO Version 4.3. We have tested the utility of the model as an event generator in the energy range of interest by fitting data on hadron production from DELCO and SLAC, and have found that the data are reproduced with reasonable accuracy with parameters that are close to those used in $e^+ - e^-$ annihilation, and μ-scattering experiments at higher energies (100-280 GeV) (Die86).

Five 1000-event samples were generated, corresponding to five kinematic regions of interest in the proposed experiments. The regions are defined in the bins in ν and Q^2 shown in the following Table, along with the corresponding typical values of electron scattering angle $\theta_{e'}$, invariant mass squared W^2, scaling variable x, and virtual photon direction θ_q. All spectra were generated with a beam energy of 14.5 GeV.

Sample	Q^2	ν	$\theta_{e'}$	W^2	x	θ_q
	$(\mathrm{GeV/c})^2$	(GeV)	(deg)	$(\mathrm{GeV})^2$		(deg)
1	5-6	5-6	10-12	4-7	0.5	17
2	1-2	5-6	5-7	8-11	0.1-0.2	10
3	10-11	10-11	22	8-11	0.5	9
4	5-6	10-11	16	13-16	0.25	7
5	1-2	10-11	10	17-20	0.05-0.1	4

Table 1. Kinematics of the five event samples used in the study.

Electrons were considered to be detected if they hit the SAM or endcap calorimeter, and their momentum was determined by the calorimeter resolutions. Other charged particles were considered to be detected if they passed through at least three superlayers in the drift chamber and hit either the endcap or barrel calorimeters. Their resolutions were determined by the drift chamber, with multiple scattering corresponding to a 0.03 r.l. beam pipe. For the momentum resolution we used the formula

$$\frac{\sigma_{p_\perp}}{p_\perp^2} = 0.004(\frac{133}{R})^{2.5},$$

where R is the radial distance in cm traversed by the particle in the drift chamber. This gives a resolution of $\sigma_p/p = 0.022p$ for particles at 20° passing through 4 of the 12 superlayers. Photons were considered detected if they hit the SAM or the endcap or barrel calorimeters. Their momentum and position resolution was chosen according to the hit detector. In order to increase the detection probabilities for the particles, which generally point along the direction of the virtual photon, the interaction point was taken to be at either end of a 1 m target centered in the Mark II.

Particle Reconstruction

The resolution and backgrounds for reconstructing parent particles which decay into two daughter particles is illustrated in Figure 2. In the mass spectrum for all detected $\gamma\gamma$ pairs, the π^0 peak is clearly visible above a relatively small combinatorial background, but the η does not stick out. However, if photon pairs which match to a π^0 are removed from the plot, the background is reduced and a distinct η peak emerges. In the $\pi^+\pi^-$ spectrum, the broad ρ^0 peak can be seen as well as a very narrow peak (about 5 MeV FWHM) from K^0 decays. In the $p\pi^-$ spectrum, the Λ peak is found to be quite narrow (about 6 MeV FWHM)

and background-free. The actual background would be quite a bit higher since pions and protons cannot be readily distinguished above 2 GeV/c, but the peak should still be visible. The study also showed that for the large W^2 samples the ϕ in the K^+K^- spectrum, the ρ^+ in the $\pi^+\pi^0$ spectrum, and the ω in the $\pi^+\pi^-\pi^0$ spectrum can all be seen. In the low W^2 samples, not enough of these particles were produced to distinguish them above the combinatorial backgrounds.

Particle Production and Detection Efficiency *vs.* z

Figure 3 shows the z-distributions of the most common stable particles (pion, kaon, and proton) for sample 4, where the fractional energy z is defined as $z = E_p/\nu$, where E_p is the particle energy. Note that pions are by far the most common stable charged particle produced, followed by protons and kaons. This holds true for the other event samples as well. There are generally about equal number of positive and negative pions and kaons produced. The hatched histograms indicate the z-distributions of detected particles. For sample 4, the virtual photon direction is only 7 degrees, so particles with large z values, which tend to travel along the virtual photon direction, tend to miss the drift chamber and are not detected. If the forward region were instrumented with a hadron identification system in Phase II, the efficiency at high z would increase to almost 100%. The efficiency for pions as a function of z is shown for the other four event samples in Figure 4. It can be seen that at low W^2 (or high x), where θ_q is larger than 10 degrees, the efficiency at large z is very good, as expected, since most of these particles now pass through the wire chamber and hit the endcap calorimeter. This shows that high-z studies of the nuclear dependence of hadronization can be done for selected kinematics even in Phase I.

The z-distributions for four of the most common particles reconstructed from their two decay products are shown in Figure 5, for events from sample 4. It can be seen that the efficiency at high z is quite good for π^0's and η's because photons at small angles are detected in the SAM, and are not required to go through the drift chamber. Thus, high-z studies using neutral pions can be made in Phase I for the full kinematic range. The efficiency for low-z pions drops due to the requirement of a minimum energy of 300 MeV for each of the decay photons. The efficiency for detecting neutral K's and ρ's extends to somewhat higher z than for their charged partners since the two-body decays spread the decay particles to somewhat larger angles than the parent, but the efficiencies at high z are not nearly as good as for neutral pions. The z distributions from the other 4 event samples are shown for ρ^0 in Figure 6, and show a similar trend as for the charged pions in Figure 4. Note that in both cases the total number of particles produced increases with W^2.

Efficiencies *vs.* $P_\perp$ and ϕ

One of the physics goals of PEGASYS is to study the high $P_\perp$ region, where higher twist effects may be important. The production probability and detection efficiency for charged pions is shown as a function of $P_\perp$ for four regions of z in Figure 7 for events from sample 2. It can be seen that at low z the efficiency is uniformly high, but at high z the efficiency peaks at high $P_\perp$, which is the region of greatest physics interest. A similar trend can be seen in Figure 8 for the production and efficiency versus the polar angle ϕ, where the efficiency at high z peaks at large ϕ, corresponding to larger scattering angles with respect to the beam axis. Similar trends can be seen in the other event samples after taking into account that the overall efficiency at large z drops with increasing W^2.

Event Multiplicities

A final topic examined in this study was the multiplicity of produced and detected particles. This is useful in designing the electronics trigger and judging if the granularity of the detectors will be adequate. Figure 9 shows for sample 4 the detected multiplicity distribution for initial multiplicities of 4, 7, 10, and 12 charged and neutral particles. It can be seen that the average number of produced particles is between 7 and 10 (it peaks at 8), while typically a little over 50% of the particles are detected, or an average of 4.5 detected particles per event. They are about equally divided between photons and charged particles. The average detected multiplicity increases weakly with Q^2, from four particles for sample 1 to five particles for sample 5. These multiplicities are low compared to the high particle rates that the Mark II is designed to measure at SLC, so that the granularity should be quite adequate.

References

(And83) B. Anderson *et al,* Phys. Rep. 97, 31 (1983).

(Die86) F. S. Dietrich, C. W. Johnson, Research Program at CEBAF, Vol. 2 (1986).

(Sjo86) T. Sjostrand, Comp. Phys. Comm. 39, 347 (1986).

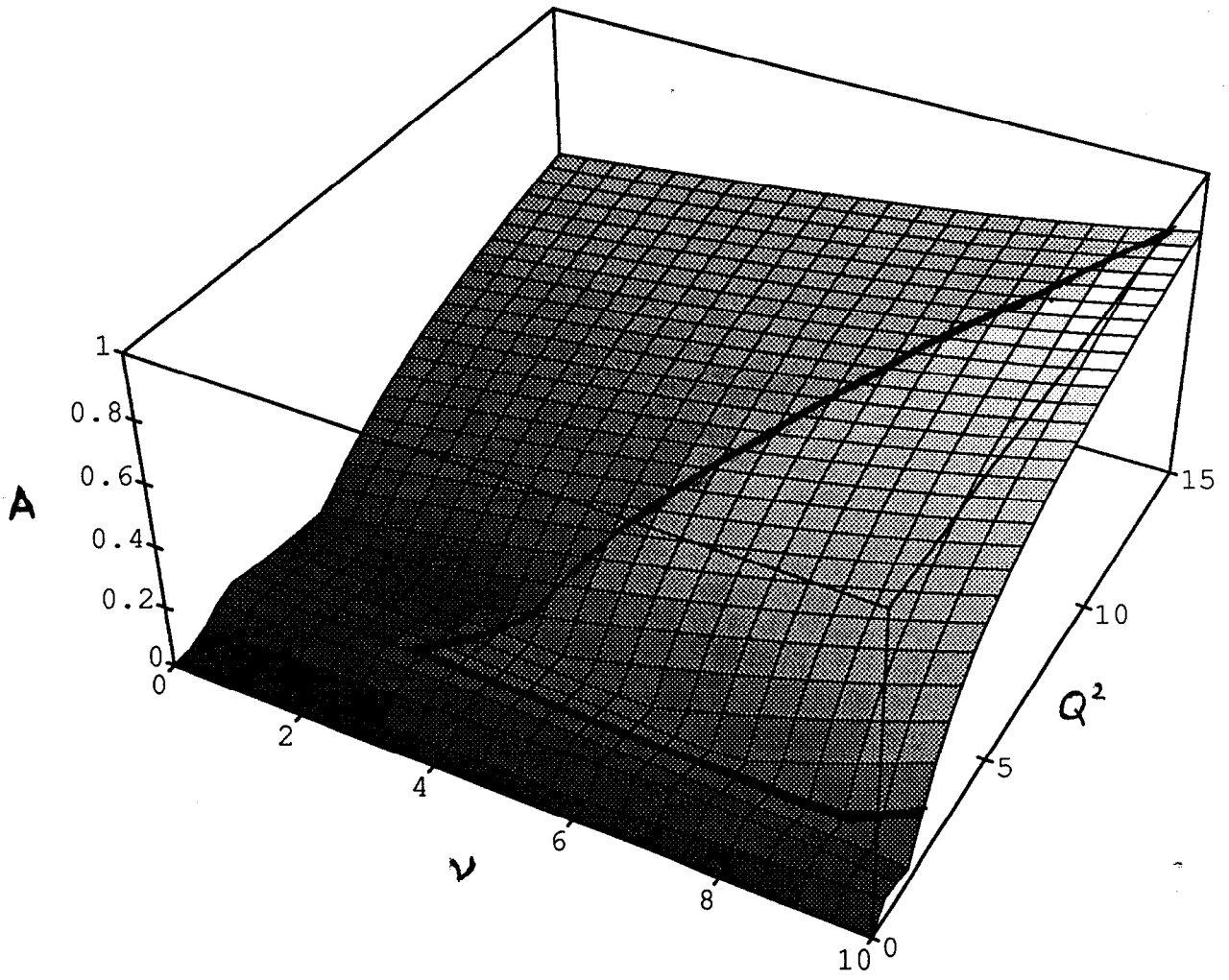

Figure 1. Acceptance of the Mark II detector for electrons scattered from the gas target as a function of energy loss ν (in GeV) and 4-momentum transfer Q^2 (in $(\mathrm{GeV/c})^2$). The acceptance for electrons that are detected in the SAM has been scaled down by 0.2 to keep the trigger rate low enough. The deep inelastic region is to the right of the heavy line.

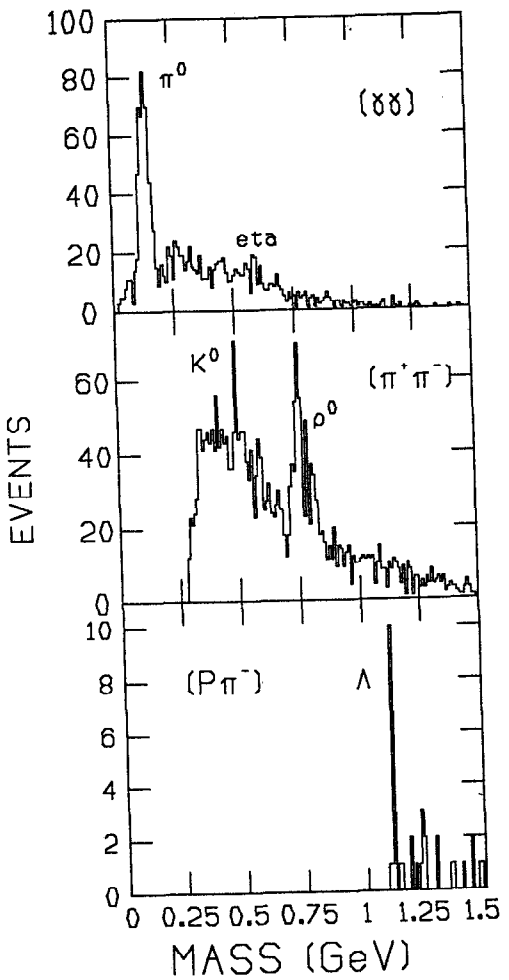

Figure 2. Mass spectra of detected $\gamma\gamma$, $\pi^+\pi^-$, and $p\pi^-$ pairs from sample 4. Resolution effects have been included. The π^0, K^0, ρ^0, and Λ peaks are clearly visible.

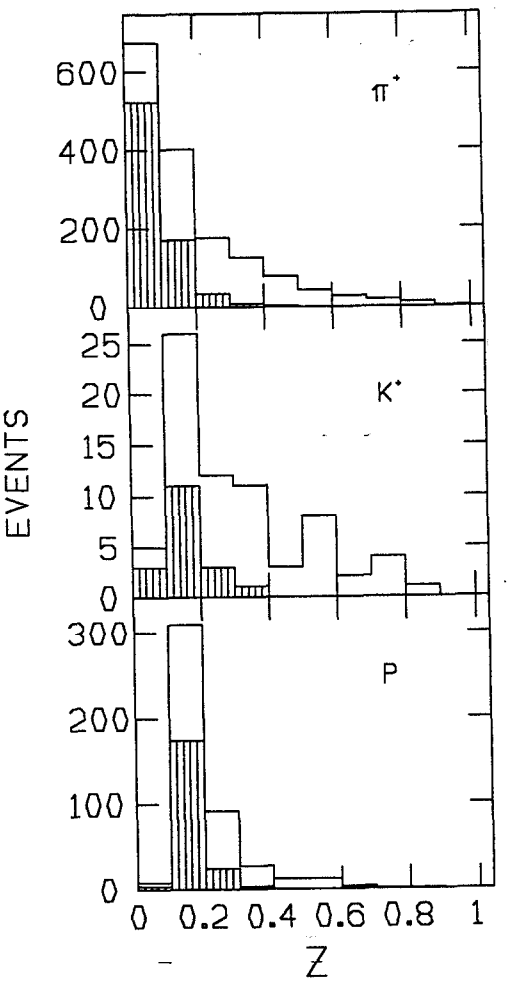

Figure 3. Spectra of generated (open histograms) and detected (shaded histograms) charged particles as a function of $z = E_p/\nu$ (E_p is the particle energy) for events from sample 4 ($E = 14.5$ GeV, $Q^2 = 5 - 6$ (GeV/c)^2, $\nu = 10 - 11$ GeV).

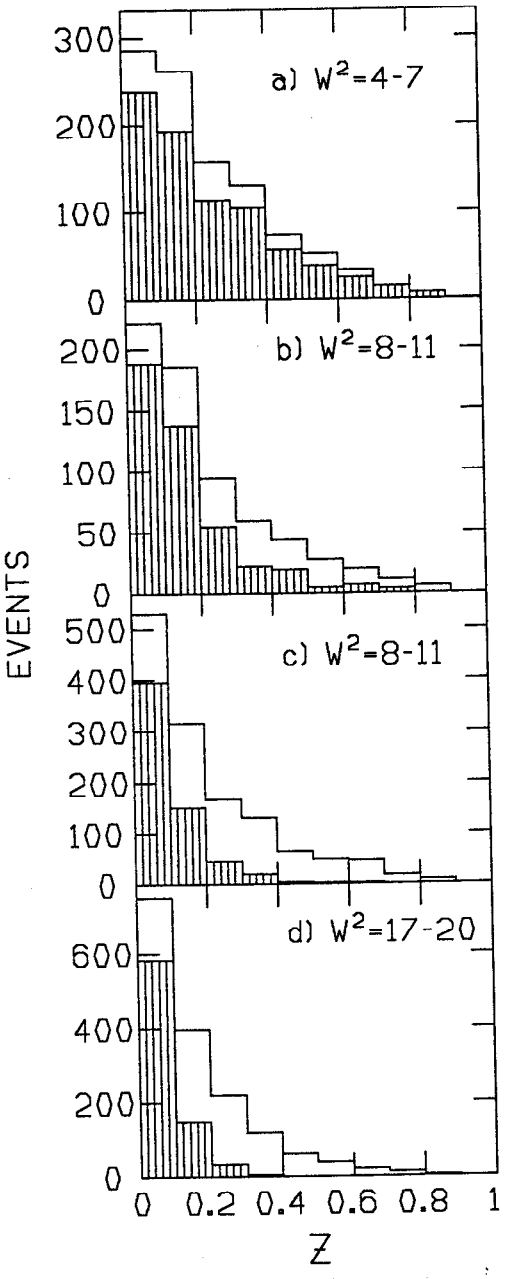

Figure 4. Spectra of generated (open histograms) and detected (shaded histograms) pions as a function of z for a) sample 1, b) sample 2, c) sample 4, and d) sample 5 (see Table 1).

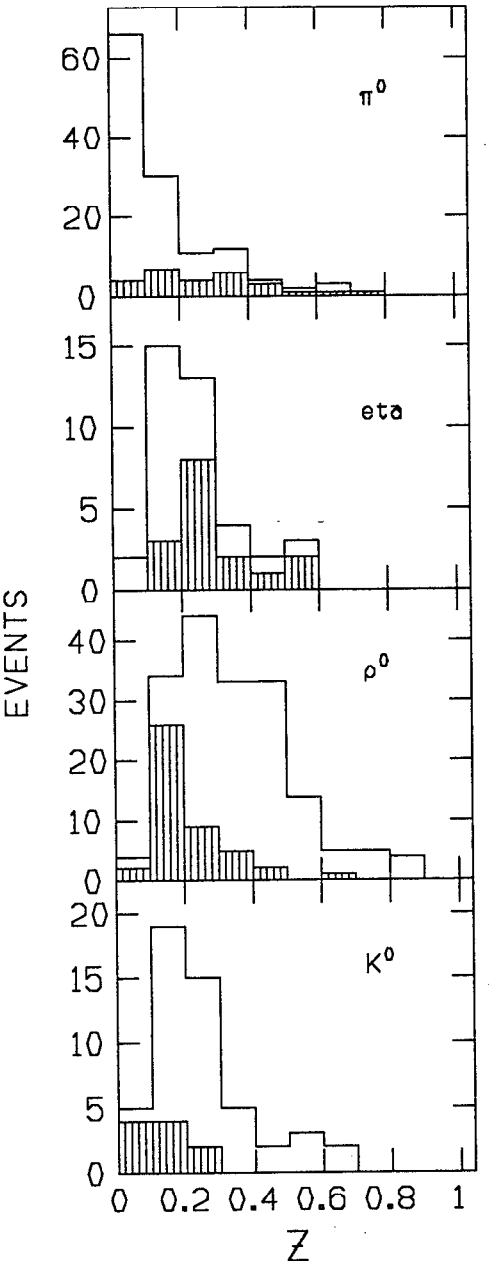

Figure 5. Same as Figure 3 except for particles detected by their two decay products.

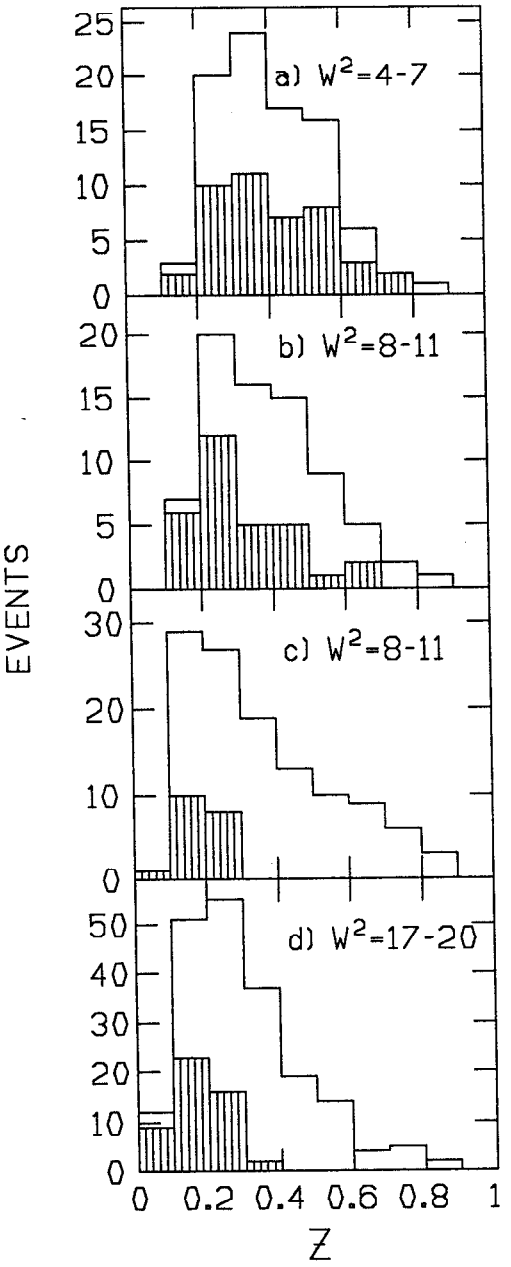

Figure 6. Same as Figure 4 except for ρ^0 particles.

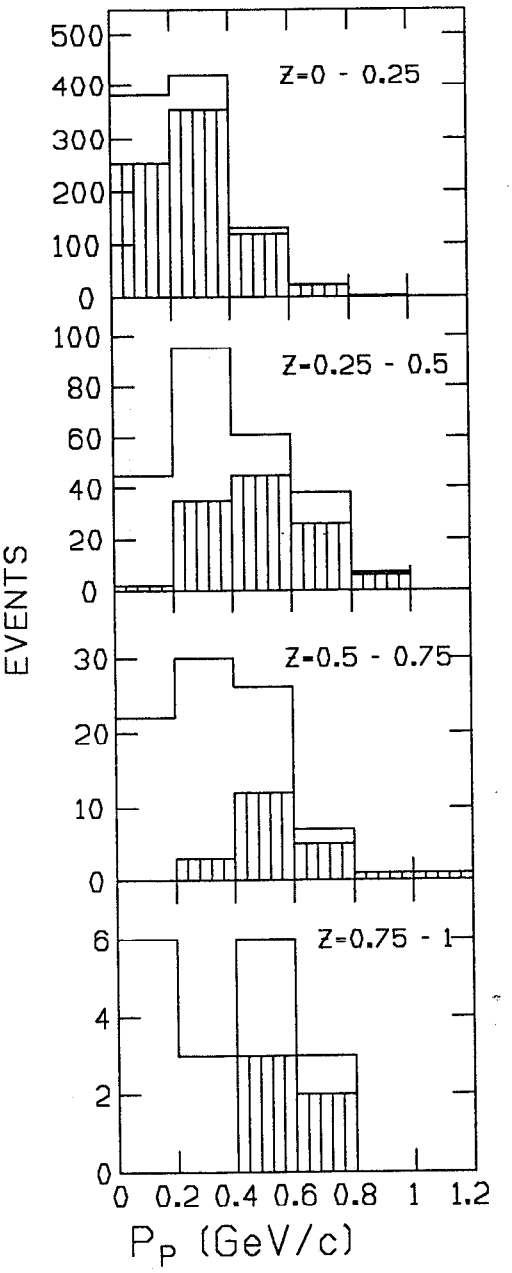

Figure 7. Spectra of generated (open histograms) and detected (shaded histograms) charged pions as a function of $P_\perp$ for events from sample 2 for four regions in z.

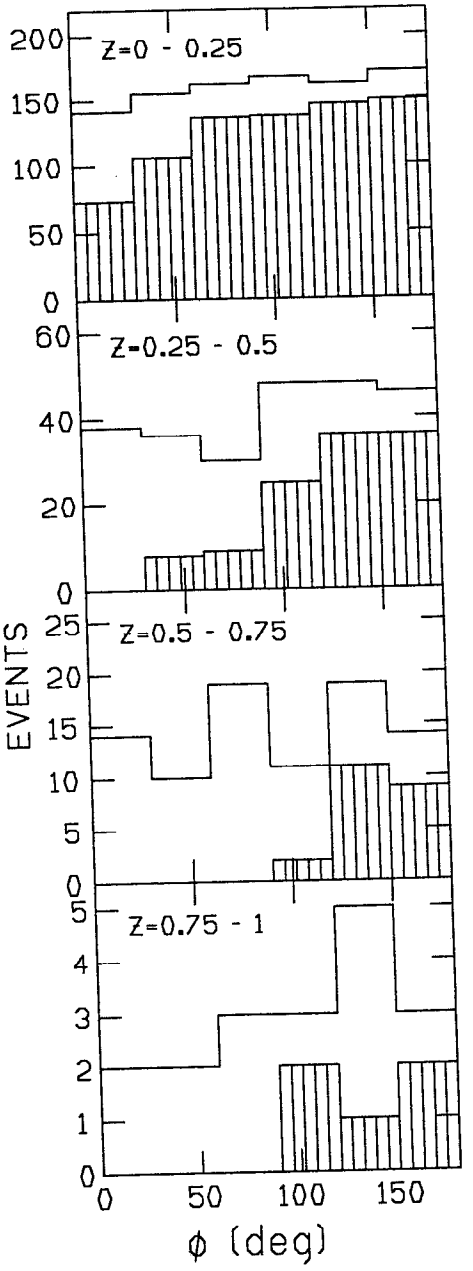

Figure 8. Spectra of generated (open histograms) and detected (shaded histograms) pions as a function of polar angle ϕ for events from sample 2 for four regions in z.

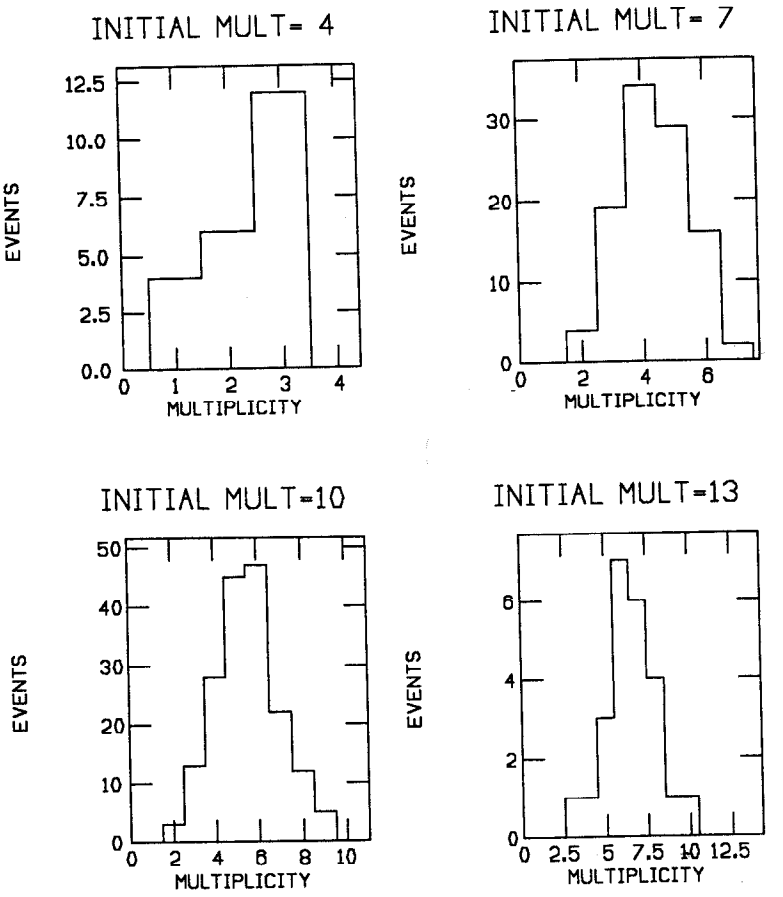

Figure 9. Detected multiplicity distribution for four initial multiplicity values for events from sample 4.

IV.F. Electromagnetic Background

There are three principal physics processes which potentially can introduce background into the Mark II detector, especially the Central Drift Chamber. These are (i) wide-angle bremsstrahlung; (ii) atomic X-rays resulting from K-shell knock-out; and (iii) radiative Møller scattering. These will be discussed in the sub-sections below.

Wide-Angle Bremsstrahlung

Useful analytic expressions for the angle and energy distribution for radiated photons are given in (Glu53). We have numerically evaluated the doubly-differential unpolarized cross section $d\sigma/(dkd\Omega)$ at $E = 14.5$ GeV. Here k is the photon energy, and Ω are its angular coordinates. The general features of the results are an approximately $1/k$ spectrum in photon energy, and a $\sin^{-4}(\theta)$ dependence on angle. Table 1 below gives some numerical values (for $Z = 1$), and Figure 1 shows the energy spectrum *vs.* k for three different lab angles. These results are in excellent agreement (within 3%) with the values calculated from other analytic expressions (Jac75).

As will be seen below, these cross sections are small in comparison with those of radiative Møller scattering.

k	θ	$d\sigma/(dkd\Omega)$
[MeV]	[radians]	[cm^2/MeV/sr]
0.001	1.0	5.2×10^{-32}
0.001	0.05	7.8×10^{-27}
0.010	0.05	7.1×10^{-28}

Table 1. Doubly-differential cross sections for wide-angle bremsstrahlung photons for selected kinematics.

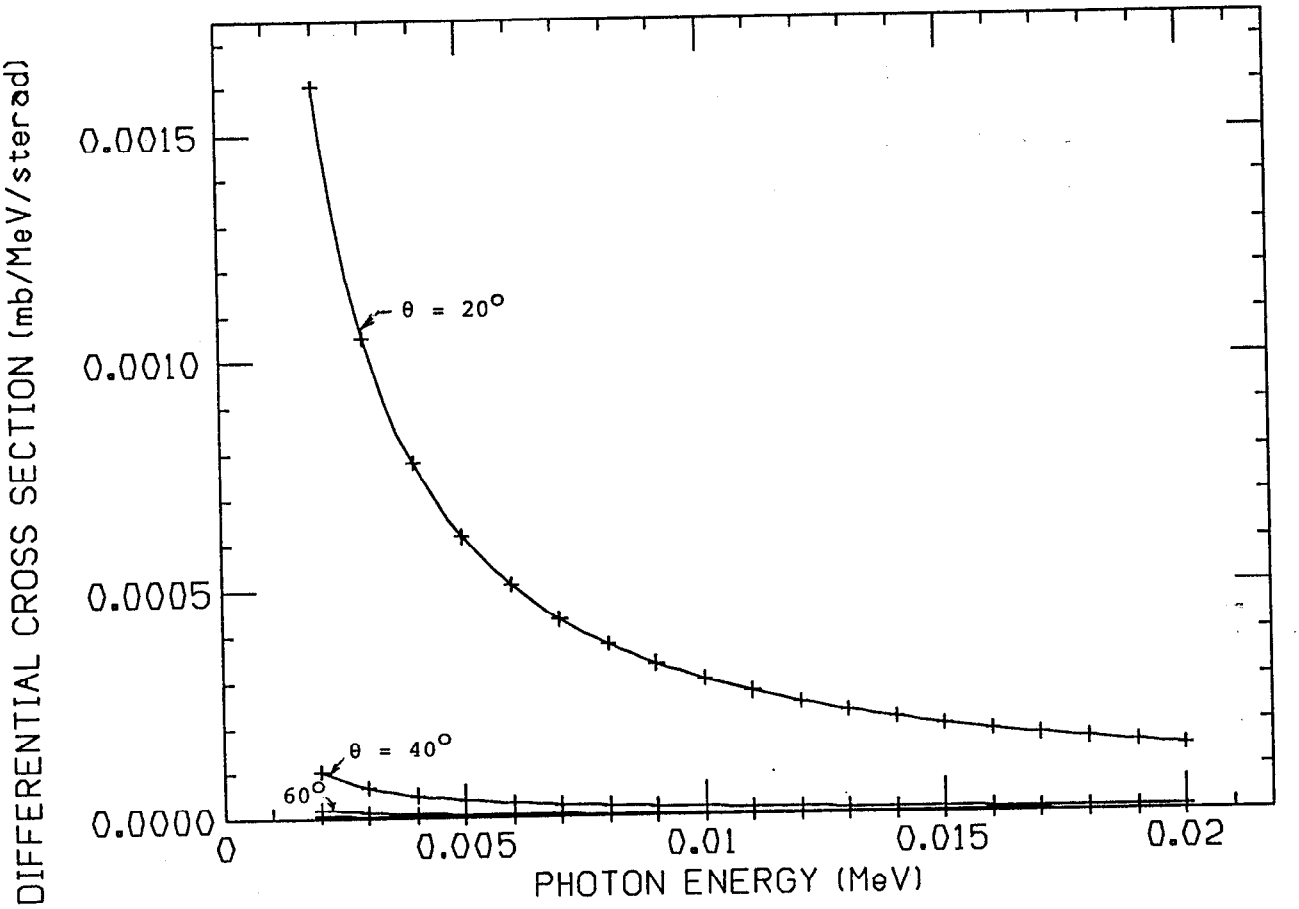

Figure 1. Differential cross section for wide-angle bremsstrahlung as a function of photon energy for three photon angles.

Atomic X-Rays

Another source of photon background for the PEGASYS/Mark II CDC will be atomic x-rays resulting from the knockout of K-shell electrons and subsequent atomic transitions, at least for the heavier gases to be used as targets.

Upper limits for this background may be set by estimating the total number of photons that are emitted and pass through the inner wall of the CDC without attenuation. The estimate is carried out by first calculating the number of K-shell vacancies that are created, by integrating the Møller cross section over the scattered electron energy starting from the K-shell ionization energy. (The ionization energies are 3.2, 14 and 35 keV for Ar, Kr and Xe respectively.) The transition of concern to us is the L-to-K transition, the energies being roughly 3, 12 and 30 keV in order for the atomic species above. Atomic transition frequencies are taken from (Man74). Thus we find, for example, that with a luminosity of 3.0×10^{29} for Xe (the maximum luminosity per beam consistent with a 12-hour beam lifetime, and 20 mA current), the rate of 30 keV X-rays will be 2000 sec^{-1} total, of which 1000 could be seen by the CDC, averaging over the geometry of the target and tracking chamber.

Finally, we estimate the number that are not attenuated in the beam pipe (at least 1 mm Be, or 2 mm Al), and the 2 mm thick Be wall of the CDC. In the worst case of 90° incidence, transmission is only significant for the Xe X-rays, where 80% of the photons would pass through to the CDC.

Again, this is insignificant compared to the rate that will be seen from the radiative Møller background.

Radiative Møller Scattering

Radiative Møller scattering might be expected to cause background problems for the PEGASYS/Mark II detector. The background results from a collision between the electron beam and stationary electrons in the gas target. This is a new source of background not encountered when Mark II was previously run on PEP. The central drift chamber (CDC) and the small angle monitor (SAM) will be the detectors most sensitive to this background. The CDC, for example, could have some random wires firing each beam crossing due to this background. The following discussion attempts to quantify the background signals from Møller scattering; it demonstrates that the radiated photon rate, though greater than that of wide-angle bremsstrahlung, is tolerable.

The cross section for Møller scattering is very forward peaked. The cross section can be shown (to good approximation for angles greater than 1°) in the lab frame to reduce to:

$$\sigma_M \simeq (r_0)^2 / \cos^3(\theta)$$

where $r_0 = 2.8$ fm is the classical electron radius. For PEGASYS/Mark II, we are mainly concerned with scattering angles greater than 5°. The Møller cross section and the electron kinetic energy $T_{e'}$ (Jau76, Das73) are given in Table 2 for an incident electron energy of 13.7 GeV.

θ (deg)	$T_{e'}$ (MeV)	$d\sigma/d\Omega$ (mb/sr)	$d^2\sigma/d\Omega dk$ (mb/sr/MeV)
1	2690.	85.	1.9/k
5	132.	79.	1.8/k
30	3.07	121.	2.8/k
45	1.02	222.	5.0/k
60	0.34	627.	14.2/k

Table 2. The differential cross section and scattered electron kinetic energy for Møller scattering at various outgoing electron angles (all values for the lab system). Shown in the last column are the doubly differential cross sections for the radiated photons (see below).

The scattered electron rate from Møller scattering is considerable (about 50 MHz for a luminosity of 10^{32}), but very little of this rate affects the CDC. This is because the hundred-MeV electrons (at small angles) have small $p_\perp$ and will spiral

out along the beam pipe in the 4.5 kG axial magnetic field. Since the CDC has an inner radius of 19 cm, the maximum spiral radius that will cause background is 9.5 cm, which requires a $p_\perp$ of at least 14 MeV/c. The large-angle electrons have even less $p_\perp$, so the Møller electrons should not be a source of background (ignoring rescattering processes).

Of greater concern are the photons generated from radiative Møller scattering. This cross sections is down by about a factor of α (the fine structure constant) due to the extra vertex. The exact formula is given by Tsai (Mo69)

$$\frac{d^2\sigma}{d\Omega dk} = \frac{\alpha}{\pi k}[\ln(\frac{Q^2}{m^2}) - 1]\sigma_M$$

where σ_M is the Møller (differential) cross section given above, and k is the momentum (energy) of the photon. Q^2 is the usual 4-momentum transfer, given by $4EE'\sin^2(\theta/2)$ where E is the incoming electron energy. The $1/k$ distribution of the photon energy has a cutoff at a maximum value equal to the scattered electron energy E'.

To estimate the number of hits per second in the CDC, we coupled a radiative Møller event generator to the GEANT simulation code with a model of the detector. The geometry input consists of: a beam pipe with 2 mm thickness and outer radius 15 cm, the entrance wall to the CDC of 2 mm thick Be (radius 19 cm), and the CDC volume assumed to be pure Ar gas extending to an outer radius of 152 cm and 230 cm long. Next we need a photon generator, which must have a $1/k$ distribution and an angular distribution given by the Møller cross section. The vertex (origin) of the photon is randomly distributed along 2 m on the beam axis. GEANT simulates all the electromagnetic interactions automatically, so no more input is needed.

The results from the GEANT simulations (see Table 3) are that about 1-2% of the photons interact in the CDC volume, with the probability slowly increasing as the minimum electron and photon energies considered are lowered. The rate in the CDC for the smallest cutoff values considered is 57.6 kHz, which should be quite tolerable since the beam crossing rate is approximately 400 kHz.

E_γ^{min} (MeV)	$E_{e^-}^{min}$ (MeV)	PAIR	COMP	ALL	$L\sigma$ (MHz)	Rate (kHz)
1.0	1.0	13	63	75	0.95	7.1
1.0	0.5	24	124	124	0.95	11.8
1.0	0.2	27	154	148	0.95	14.1
1.0	0.1	21	166	170	0.95	16.2
0.5	0.5	8	46	81	1.9	15.4
0.5	0.2	12	118	137	1.9	26.0
0.5	0.1	12	163	166	1.9	31.5
0.2	0.2	1	34	38	4.4	16.7
0.2	0.1	1	74	74	4.4	32.6
0.2	0.05	2	135	131	4.4	57.6

Table 3. Estimated rates for Møller scattering background in the PEGASYS/Mark II detector. E_γ^{min} is the lower cutoff for the photon generator, and $E_{e^-}^{min}$ is the lower cutoff for the particle tracking (GEANT ignores electrons or photons below this energy). PAIR, COMP, and ALL are the contributions to the background from pair production, Compton scattering, and all processes. *Note: these values represent the number of interactions out of 10,000 incident photons.* The integrated rate $L\sigma$ for radiative Møller scattering for a luminosity $L = 1.7 \times 10^{32}$ is given in MHz, and the final background rate is determined from $L\sigma\cdot$(ALL/10000).

References

(Das 73) T. Das, *Relativistic Quantum Mechanics of Electrons*, (1973), p. 146.

(Glu53) R.L. Gluckstern and M.H. Hull, Phys. Rev. **90**, 1030 (1953).

(Jac75) J.D. Jackson, *Classical Electrodynamics*, 1975 (John Wiley & Sons).

(Jau76) J. M. Jauch and F. Rohrlich, *The Theory of Photons and Electrons*, (2nd edition, 1976), p. 368.

(Man74) S.T. Manson, D.J. Kennedy, At. Dat. and Nucl. Dat. Tables **14**, 112 (1974)

(Mo69) L.W. Mo and Y.S. Tsai, Rev. Mod. Phys. **41**, 205 (1969).

IV.G. Possible Upgrades

The first year of operation of the Mark II will utilize the detector "as is" to the extent possible. However, there are several ideas already under study towards improving the detector for Year II.

There is general consensus that at some point, the small polar angle regions of the detector must be improved. Two concepts have been put forward towards this end.

1.) Pb-Glass Electromagnetic Calorimeter. The first concept for upgrading the polar caps aims solely at improving the electron identification and energy resolution, and thus the measurement of the kinematical quantities ν, Q^2, x. We are looking into the possibility of replacing the six layers of thick Pb in the sampling calorimeter of the SAM (1.32 cm each, or 2.35 r.l., making a total of 14.3 r.l.) with thinner Pb layers (perhaps 0.28 cm each, or 0.5 r.l., making a total of 3 r.l.). Behind the SAM we would mount 4 by 4 cm blocks of Pb-Glass, thus making a high-quality calorimeter (10-12%/$\sqrt{(E)}$), longitudinally segmented into Pre-Radiator and Total Absorber sections, and preserving the good tracking characteristics of the SAM drift tube array. The U.S.S.R. PEGASYS group has agreed to provide the lead glass blocks, photomultiplier tubes, and mechanical support for this upgrade, should the collaboration opt for it.

2.) A design for endcap mini-toroid spectrometer magnets has been worked out; this option aims at both improving the hadron as well as electron coverage at small polar angles. The design calls for two 8-sector warm copper toroid magnets of less than 3 m length, and the weight of each being less than 10 tons. The angle coverage would go from 3.6° to 7.8° for interactions at the IP (implying $Q^2 \leq 3.5$ $(\mathrm{GeV/c})^2$ for electrons); for interactions occurring 0.5 m downstream of the IP in an extended target, the upper end of the angular range becomes 13.4° (implying $Q^2 < 8$). The peak magnetic field is 0.31 T, and the $\int Bdl$ would be between 0.3 and 0.6 T-m, depending on angle. Resolutions on the order of $\delta p/p^2 \approx$ 2-4 $\times 10^{-3}$ $(\mathrm{GeV/c})^{-1}$ are expected conservatively, depending on angle. The instrumentation of the spectrometer magnets has not been worked out in detail at this point.

There is also some dissatisfaction with the charged particle tracking at low angles. The momentum resolution gets progressively worse as the track angle becomes smaller; furthermore, if a particle does not cross 3 or 4 superlayers, it is essentially not tracked at all. This low-angle cutoff is deleterious to many experiments. Two other upgrade possibilities which aim to improve this situation are also under discussion:

3.) As the main target cell need not be so large as to fill up the entire bore of the CDC, we may consider installing a full length drift chamber between the target beam pipe and the CDC inner wall. Such a chamber would supplement the tracking in the first few superlayers of the CDC itself, and help with the determination of the position of the vertex along the beam axis, either by use of stereo layers, or charge-division on each wire. As an alternative to drift wire chambers, we have considered developing a scintillating fiber tracking detector to operate as a vertex chamber. It would be designed along the lines of the CERN's UA2 fiber chamber, but with 1/4 to 1/3 the number of layers, (Ans89), and with a similar readout system. The University of Virginia collaborators are at present working on a neutron detector based on waveshifting fibers, and the vertex chamber would be a natural extension of their current work.

4.) A few layers of planar end cap drift chambers could be mounted between the ECC and the CDC, based on the design of the AMY forward tracking chambers (Sil90).

Finally, a suggestion has been made to improve the data acquisition system:

5.) The upper limit for data-taking rate for the Mark II "as is" with our event topologies will be approximately 10 Hz. This will surely be deemed unacceptable after our first year of running. A solution to this is to pipeline the data acquisition by reading out the CAMAC by FASTBUS, and thus reduce the computer interrupts by a factor of 10. The cost is very modest (approximately $10K), and the data rate may be increased to 30 Hz. This will require however, a non-trivial investment in software development. It is also strongly suggested that we add 8 mm tape drives for local data storage.

References

(Ans89) E. Ansorge *et al.*, Nucl. Instrum. Meth. A265 (1989) 33.

(Sil90) A. Sill, private communication, 1990.

Section V. TIMELINE AND MANPOWER

V.A. Timeline

The last SLC/Mark II run ended on November 21. By the end of December, the Mark II should be fully rolled out into the east end of the Collider Hall pit. We plan to have all necessary new equipment (*i.e.* the beampipe with gas target and Møller luminosity monitors and the end cap hodoscope) ready and integrated in the Mark II detector by the end of 1991. We would then roll Mark II into the IR to begin a run in March, 1992. The minimal experimental program plans for three years of running:

In Year I, (92) we will use the detector essentially "as is". The only major additions to the Mark II will be the gas target and everything associated with our beamline, and the End Cap Hodoscopes. In this year, the goal is to learn to use the detector, and collect some data, both for H_2, D_2, and heavy targets. This will establish the overall feasibility (rates, backgrounds, *etc.*) associated with each experiment in the program. We should collect some useful data, but perhaps not with large integrated luminosity.

Between Year I and Year II we will probably incorporate an upgrade. The possibilities for upgrades were listed in Section IV.G. Year II (93) should produce a high luminosity data sample, both for hydrogenic and heavy targets.

Year III (94) will concentrate exclusively on running, with no further upgrades planned at this time.

V.B. Collaborating Institutions and People

This section lists the collaborating institutions and people from these institutions at the senior or postdoctoral level. Graduate students are not listed.

R.G. Arnold, P.E. Bosted, S.E. Rock, Z. Szalata
American University

J. Berthot, P.Y. Bertin, V. Breton, H. Fonvieille, E. Voutier
University Blaise Pascal (IN2P3)

J. Lambert
Georgetown University

J.C. Hill, F.K. Wohn
Iowa State University

P.V. Degtyarenko, Yu. V. Efremenko, V.B. Gavrilov, S. Kuleshov, G.A. Leksin, N.A. Pivnyuk, S.M. Shuvalov
ITEP, Moscow

D.M. Moltz
Lawrence Berkeley Laboratory

P. Anthony, F.S. Dietrich, K. van Bibber (spokesman)
Lawrence Livermore National Laboratory

C.C. Chang, H.H. Holmgren
University of Maryland

J. Button-Shafer, R. Hicks, R. Miskimen, G. Peterson, K. Wang
University of Massachusetts

L. Dick
University of Milan

R. Finlay, K. Hicks
Ohio University

K. Griffioen
University of Pennsylvania

P.F. Yergin
Rensselaer Polytechnic Institute

M. Bernheim, H. Borel, G. Fournier, R. Lombard,
C. Marchand, J. Morgenstern, B. Saghai, F. Staley,
C. Vallet, P Vernin
C.E.N. Saclay(CEA/IRF)

R. Gearhart, W. Langeveld, M.L. Perl, R. Pitthan,
G.G. Petratos, S.H. Rokni, Y.S. Tsai
SLAC

S.E. Kuhn
Stanford University

J. Alster, E. Piasetzky, I. Navon
Tel Aviv University

O. Rondon
University of Virginia

M.B. Frodyma, C. Hyde-Wright
University of Washington

M.J. Amaryan, A. O. Gasparyan, K. Sh. Egiyan, H.G. Mkrtchyan,
Yu. G. Sharabyan, S. G. Stepanyan
Yerevan Physical Institute

V.C. Institutional Responsibilities

The Collaboration is fully aware that running and maintaining the Mark II is an enormous job. In discussions with the Mark II Collaboration, we discovered that the Mark II runs on the basis of having 20-25 people permanently on site whose sole scientific activity is the Mark II. There are an additional 20 people or so who spend a large fraction of their time on site, and can be called upon on short notice to work on the Mark II. "Systems Experts" need not be senior personnel, but must be undistracted by other research activities.

All institutions within the Collaboration have agreed to an "N/2" policy by which we will achieve critical mass between now and June, 1991. By the "N/2" rule we mean that if an institution commits N scientists to the project (including students and postdocs), we will expect a stable base presence of N/2 people on site at all times.

During the July-November '90 run, most PEGASYS collaborators attended Mark II shifts as their schedules permitted. While this was insufficient to develop a complete familiarity with any system, it was a helpful orientation towards the systems they would be responsible for.

While the institutional commitments to various systems is neither complete nor final at present, we list below our present understanding.

Central Drift Chamber. The University of Massachusetts group will take principle responsibility for the CDC. They have considerable expertise in drift chamber technology, and designed and prototyped the drift chamber system in the original PEGASYS proposal.

The End Cap Calorimeter. The University of Washington will take principle responsibility for the ECC, as it is directly relevant to their physics interest, namely, direct photon production. The University of Maryland group will help with this system.

The Liquid Argon Calorimeter. The Tel Aviv Group has expressed an interest in the LAC. This system should have another institution committed to it; and the combined French group (Saclay/Clermont-Ferrand) would be agreeable to take this on, as well as constructing and operating the End Cap Hodoscope.

Time-of-Flight. The Ohio University group will be responsible for the TOF.

The End Cap Hodoscope. This will be designed, constructed and operated by the combined French group (Saclay/Clermont-Ferrand).

The Small Angle Monitor. The U.S.S.R. PEGASYS group will take responsibility for the SAM, and have agreed to provide a lead glass upgrade should the collaboration opt for this (see section IV.G).

The Muon Identifier. The muon system will be the responsibility of SLAC Group E.

The Møller Luminosity Monitor. This will be the responsibility of Iowa State University and the University of Pennsylvania.

The Data Acquisition System & Computer. This will principally be the responsibility of American University, with help from Tel Aviv.

The Target & Beamline. This will be the responsibility of LLNL and SLAC EFD.

The Magnet. This will be the responsibility of Stanford University.